UNIVERSITY OF MODENA AND REGGIO EMILIA

Degree in Doctor of Philosophy in Molecular and Regenerative Medicine

XXXIV Cycle

Molecular characterization of degenerating rod photoreceptors after treatments with cGMP analogues and DDS

PhD student

Li Huang

Supervisor

Prof. Valeria Marigo

PhD school director

Prof. Michele De Luca

Table of Contents

Acknowledgments

During my PhD study, I would like to express my sincere gratitude to my supervisor, Prof. Valeria Marigo, for her continuous encouragement, support and patience. I would also like to acknowledge the helps from my colleagues in our lab, who always sincerely support me whenever I need. I am also grateful to all the members of the transMed project, to the supervisors and to the ESRs, they are truly beautiful people, and I am very happy to work with them. I wish to show my appreciation to this project, through which I gained a quantity of knowledge in different fields. Finally, I would like to extend my special thanks to my parents, for their love and support throughout all my studies.

This study is supported by transMed project, transMed receives funding from the European Union's Horizon 2020 research and innovation program under the Marie Sklodowska-Curie Grant Agreement No 765441.

List of publications

(1) **Li Huang**, Erico Himawan, Soumaya Belhadj, Raúl O. Pérez García, François Paquet Durand, Nicolaas Schipper, Matej Buzgo, Aiva Simaite, and Valeria Marigo. 2022. "Efficient Delivery of Hydrophilic Small Molecules to Retinal Cell Lines Using Gel Core-Containing Solid Lipid Nanoparticles" Pharmaceutics 2022, 14, 74. https://doi.org/10.3390/pharmaceutics14010074

(2) **Li Huang**, Meltem Kutluer, Elisa Adani, Antonella Comitato, and Valeria Marigo. 2021. "New In Vitro Cellular Model for Molecular Studies of Retinitis Pigmentosa" Int. J. Mol. Sci. 2021, 22, 6440. https://doi.org/10.3390/ijms22126440

(3) Meltem Kutluer, **Li Huang**, Valeria Marigo. Targeting molecular pathways for the treatment of inherited retinal degeneration. Neural Regen Res. 2020 Oct;15(10):1784-1791. https://doi: 10.4103/1673-5374.280303.

List of abbreviations

AAV	Adeno-associated virus
AIF	Apoptosis inducing factor
AIPL1	Aryl Hydrocarbon Receptor Interacting Protein Like 1
AMD	Age-related-macular degeneration
ANTS	8-aminonaphthalene-1,3,6-trisulfonic acid disodium salt
AURKA	Aurora kinase A
BAX	BCL2-associated X protein
BP	Biological process
BRB	Blood–retinal barrier
CAMK	Ca^{2+}-dependent kinase-calmodulin
cAMP	Cyclic 3′,5′-adenosine monophosphate
CC	Cellular compartment
cGMP	Guanosine-3',5'-cyclic monophosphate
Cnga1	Cyclic nucleotide gated channel subunit alpha 1
Cngb1	Cyclic nucleotide gated channel subunit beta 1
CNGC	cyclic nucleotide-gated channel
CON	Control
CREB	cAMP response element-binding protein
CRX	Cone–rod homeobox protein
CSA	Cyclosporin A
CSNB	Congenital stationary night blindness
CSNK1A1	Casein kinase 1 alpha 1
DAPI	4′,6-Diamidino-2-phenylindole dihydrochloride
DDS	Drug delivery system
DMEM	Dulbecco's Modified Eagle Medium
DMEM/F12	Dulbecco's modified Eagle's medium and Ham's F12 nutrient mixture
DPX	*p*-xylene-bis-pyridinium bromide

EE	Encapsulation efficiency
EIF58	Eukaryotic translation initiation factor 5B
ER	Endoplasmic reticulum
FBS	Fetal bovine serum
G3BP1	G3BP stress granule assembly factor 1
GC	Guanylyl cyclase
GCAPs	Guanylyl cyclase activating proteins
GCIP	Guanylyl cyclase inhibitory protein
GCL	Ganglion cell layer
Gnat1	G protein subunit alpha transducin 1
GO	Gene Ontology
GSH	Glutathione
GSH-PEG	Glutathione-targeted PEGylated
GTP	Glycerol tripalmitate
HBSS	Hank's balanced salt solution
HPLC	High-pressure liquid chromatography
IKBKB	Nuclear factor kappa B
IL	Interleukins
ILM	Inner limiting membrane
INL	Inner nuclear layer
IPL	Inner plexiform layer
IRBP	Interphotoreceptor retinol-binding protein
IRD	Inherited retinal degeneration
IRE1	Inositol-requiring enzyme1
IS	Inner segment
LCA	Leber's congenital amaurosis
LCT	Soybean lecithin
LRRK2	Leucine rich repeat kinase 2
MAP3K7	Mitogen-activated protein kinase 7
MAPK12	Mitogen-activated protein kinase 12
MARCKSL1	Myristoylated alanine-rich C kinase substrate-like 1
MF	Molecular function
MFI	Mean fluorescence intensity

MTT	3-(4,5-dimethylthiazol-2-yl)-2,5-diphenyl tetrazolium bromide
NCKX	$Na^{+}/Ca^{2+}/K^{+}$ exchanger
NFATc	Nuclear factor of activated T cells
NFKB2	Nuclear factor kappa b subunit 2
NFL	Nerve fiber layer
NP	Nanoparticle
NPs	Nanoparticles
NR2E3	Nuclear receptor subfamily 2, Group E, Member 3
NRL	Neural retina leucine zipper
OD	Optical density
OLM	Outer limiting membrane
ONL	Outer nuclear layer
OPL	Outer plexiform layer
OS	Outer segment
PARP	Poly (ADP-ribose) polymerase
PBS	Phosphate-buffered saline
PCA	Principal component analysis
PCL	Poly-ε-caprolactone
PDE	Phosphodiesterase
PDI	Polydispersity index
PEDF	Recombinant human pigmented epithelium derived factor
PERK	Endoplasmic reticulum kinase
PKG	cGMP-dependent protein kinase
PKM	Pyruvate kinase M1/2
PL	Photoreceptor layer
PLGA	Poly lactic-co-glycolic acid
PLK1	Polo like kinase 1
PN	Postnatal
PPI	Protein–protein interaction
PRKACB	Protein kinase CAMP-activated catalytic subunit beta
PRKCD	Protein kinase C delta
PRKCZ	Protein kinase C zeta
RAD23A	RAD23 homolog A, nucleotide excision repair protein

RAF1	Raf-1 proto-oncogene serine/threonine kinase
RD	Retinal degeneration
RhoA	Ras homolog family member A
RhoB	Rhodamine B
ROCK1	Rho associated coiled-coil containing protein kinase 1
RP	Retinitis pigmentosa
RPE	Retinal pigment epithelium
RPS6KA1	Ribosomal protein S6 kinase A1
RPS6KA3	Ribosomal protein S6 kinase A3
SA	Stearic acid
SLN	Solid lipid nanoparticle
SLNs	Solid lipid nanoparticles
SNAP23	Synaptosome associated protein 23
TBK1	TANK binding kinase 1
TEM	Transmission electron microscope
VASP	Vasodilation-stimulated phosphoprotein
VASP	Vasodilator-stimulated phosphoprotein
VEGF	Vascular endothelial growth factor
VGCC	Voltage gated Ca^{2+} channel
ZAP	Zaprinast

Abstract

Retinitis pigmentosa (RP) is an inherited form of retinal degeneration characterized by a primary degeneration of rod photoreceptors followed by the loss of cone photoreceptors. Mutations in several genes linked to the disease often cause increased levels of guanosine-3',5'-cyclic monophosphate (cGMP) and calcium ion influxes, which trigger a series of down-stream processes, eventually leading to photoreceptor cell death. The cGMP-signaling pathway has surfaced as a cell death mechanism in hereditary retina degeneration in the last decade and has provided new knowledge on degenerative pathways. However, the underlying down-stream cellular mechanism of this pathway is still not fully understood. The purpose of this project was, first, to develop a new *in vitro* photoreceptor degeneration model for molecular studies of retinitis pigmentosa. The model was based on the 661W cell line, a photoreceptor precursor cell line. Secondly, we aimed at testing the effects of cGMP inhibitory analogues in the novel retinal degeneration model. Thirdly, a new drug delivery system (DDS) based on nanoparticles for delivering hydrophilic cargoes, such as cGMP analogues, was developed and tested on cells.

661W cells were genetically modified to stably express the neural retina leucine zipper (NRL), a rod photoreceptor specific transcription factor. One clone (661W-A11) was selected based on NRL target genes expression. 661W-A11 showed a significant increase in expression of rod-specific genes, but not of cone-specific genes when compared to 661W cells. Western blot confirmed that the rod specific protein levels were increased on 661W-A11 compared to 661W. Based on the knowledge that *Phosphodiesterase 6* (*PDE6*) gene mutations were found in RP patients, a protocol to mimic rod degeneration *in vitro* by treatments with zaprinast was developed. Zaprinast is an inhibitor of phosphodiesterase (PDE), specifically PDE6 and, at less extend, PDE5. The blocking effect of PDE6 activity was demonstrated by decreased viability, increased cell death, increased intracellular cGMP and calcium level, as well as the activation of cGMP-dependent protein kinase (PKG) and calpains, calcium-dependent proteases. Based on this new *in vitro* system, the effects of previously published neuroprotective drugs were validated. To identify new cell death markers, phosphoproteomic analysis was performed to study the phosphorylated substrates alterations in this model. Potential markers were analyzed *in vitro* and verified in a retinal degeneration mouse model. This new *in vitro* system, 661W-A11 cells, will open new molecular systematic studies on RP and will serve for high-throughput drug screening. At last, a new drug delivery system (DDS) based on different formulations of nanoparticles was evaluated *in vitro*. Two different formulations of fluorescein

labeled nanoparticles were tested and found to be successfully uptaken by 661W cells and, also, by a retinal pigment epithelium cell line, the ARPE-19 cells. These studies allowed us to define the best nanoparticle formulation to facilitate the entrance of hydrophilic drugs into retinal cells.

Keywords: retina degeneration, 661W, rod photoreceptor, cGMP, drug delivery system.

1. INTRODUCTION

1.1 Retina

How do human eyes perceive vision? When light hits the eye, it passes through the cornea and the pupil, penetrating the whole lens, and focusing onto the retina, then the journey of light capture starts from here: with the light, the retina initiates its function by creating an electrochemical signal which travels through all the retina layers until to the optic nerve, where this electrical signal is conveyed to the brain. This complex process allows us to perceive the vision [1].

The retina is the essential part of the eye, it is a thin layered light-sensitive neural tissue that lines the innermost wall of the eye, with one side contacting the vitreous cavity and the other side facing the choroid [2]. It is composed by millions of cells that are responsible for sensing the light and producing visual output. To fulfill this function, the retina forms a complex structure and connecting network with specialized photosensitive neurons, intermediate neurons and glial cells that provide structural support [3].

1.1.1 The structure of retina

The intricate retina structure is essential for our vision. If we observe a healthy retina with an ocular fundus photograph, the retina blood vessels, optic disc, a macula (around 5-6mm diameter) and a fovea would be visible. If the retina is observed with a vertical section, it consists of two general components: The retinal pigment epithelium (RPE) and the neural retina. Although these two components are morphologically distinct, their relationship is crucial to our sight.

The RPE is a single monolayer of cuboidal epithelial cells situated at the interface between neural retina and choroid. These are pigmented cells and the layer exhibits a hexagonal shape from the *en face* view [4]. The RPE cells accomplish important functions: i) they form the blood retina barrier and control the transportation of nutrients, ions and water; ii) these cells contain melanin which could absorb light and provide photooxidation protection; iii) they are also involved in the visual cycle for the reisomerization of all-*trans*-retinal into 11-*cis*-retinal; iv) other crucial functions include the phagocytosis of shed photoreceptors and secretion of essential factors for the integrity of the retina [4-6].

The neural retina contains three types of glial cells: microglia, astrocytes and Müller cells, and six classes of neuron cells: rod and cone photoreceptors, bipolar cells, retinal ganglion cells,

horizontal cells and amacrine cells. These cells are wired together by interconnecting with synapses, and organized in different layers in the retina [7].

With RPE and neural retina together, the whole retina can be structurally subdivided into ten distinct layers, from the outermost to the innermost (from the posterior of the head towards the front anterior of the head), the layers are organized as follows (Figure 1.1):

(1). Retinal pigmented epithelium (RPE) monolayer

The RPE monolayer lies at the outmost space, adjacent to the choroid, and serves as a protecting barrier between the choroid capillaries and the neural retina. The apical membrane of the RPE forms microvilli that envelop the outer segments of photoreceptors, while its basolateral membrane faces the Bruch's membrane, which separates the RPE from the endothelium of the choriocapillaris [8].

(2). Photoreceptor layer (PL)

The photoreceptor layer contains the inner and outer segments of rod and cone photoreceptors. The outer segment consists of membrane-bound discs that are rich in light-sensitive pigments. The inner segment is part of the photoreceptor cell body abundant with mitochondria, endoplasmic reticulum and other organelles that are needed for metabolic demands of photoreceptors [9]. Histologically, photoreceptor nuclei are located in the outer nuclear layer (see below).

(2.1). Outer limiting membrane (OLM)

The outer limiting membrane forms a barrier for the diffusion of proteins. It is located at the level of rod and cone cell bodies (inner segment), and is based on adherent junctions between photoreceptors and Müller glia cells or between different Müller cells [10]. Müller cells are a type of radial glial cells that extend almost all the retina from the apical side to the basal side, providing the structural, metabolic and homeostatic support to the retina [11].

(2.2). Outer nuclear layer (ONL)

The outer nuclear layer contains the part of the cell bodies of rods and cones containing the nuclei.

(3). Outer plexiform layer (OPL)

The outer plexiform layer is a neuronal synapse layer that connects the axons of photoreceptors with the dendrites of bipolar or horizontal cells, the synaptic endings are called rod spherules or cone pedicles.

(4). Inner nuclear layer (INL)

Inner nuclear layer consists of the cell bodies of horizontal cells, bipolar cells, amacrine cells, and Müller glial cells. Horizontal cells modulate the feedback signals on rod and cone photoreceptors [12]. Bipolar cells transmit and encode the synaptic inputs from photoreceptor cells onto ganglion cells [13]. Amacrine cells modulate the connections of bipolar and ganglion cells by receiving the input from bipolar cells and transmitting it to ganglion cells [14].

(5). Inner plexiform layer (IPL)

The inner plexiform layer contains the synaptic connections between the dendrites of ganglion cells and axons of bipolar cells, as well as processes of amacrine cells.

(6). Ganglion cell layer (GCL)

This layer contains the cell bodies of retinal ganglion cells and displaced amacrine cells. Retinal ganglion cells are the neurons forming the optic nerve that connects and conveys the visual signal from the retina to the brain.

(7). Nerve fiber layer (NFL)

This is the second innermost layer of retina close to the vitreous and is composed of the axons of ganglion cells and the processes of the Müller cells. In this layer ganglion cells converge and form the optic nerve.

(8). Inner limiting membrane (ILM)

The ILM borders between the vitreous humor and the retina, thus serves as a barrier between the neural retina and the vitreous. It is also the innermost layer of the retina and formed by the endfeet of Müller cells. It is separated from the vitreous body by a basal lamina [15].

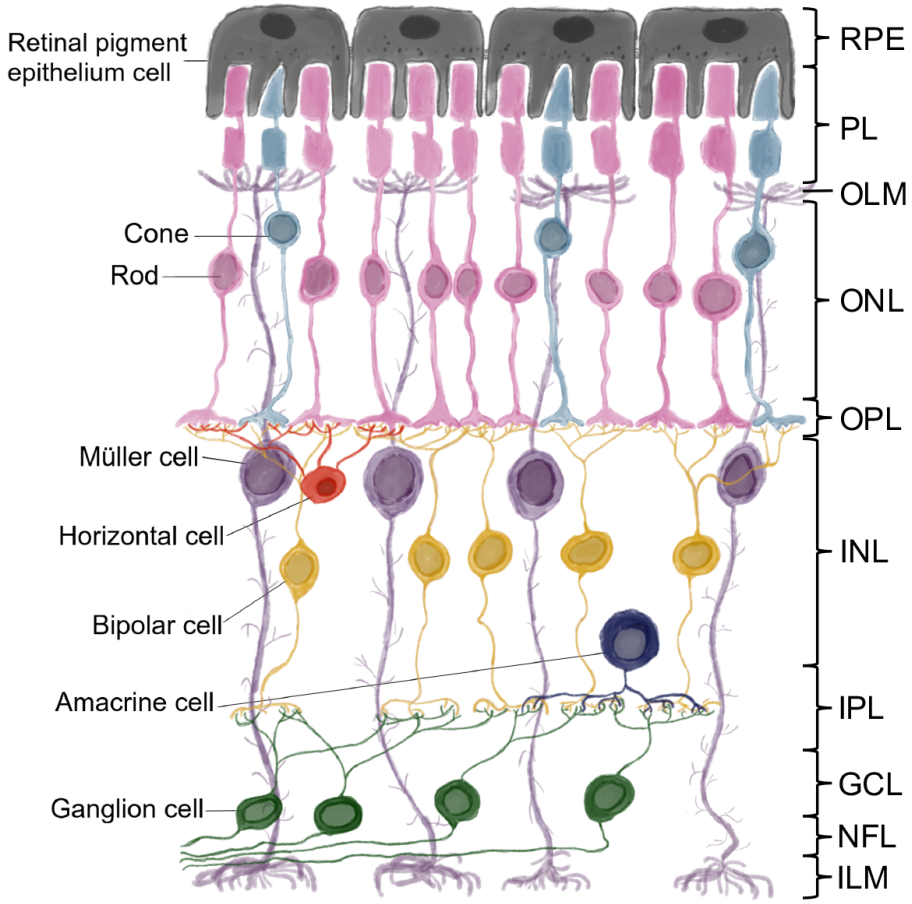

Figure 1.1 Structure of the retina. The retina is divided into 10 layers (from the outermost to the innermost): Retinal pigmented epithelium (RPE), Photoreceptor layer (PL), Outer limiting membrane (OLM), Outer nuclear layer (ONL), Outer plexiform layer (OPL), Inner nuclear layer (INL), Inner plexiform layer (IPL), Ganglion cell layer (GCL), Nerve fiber layer (NFL) and Inner limiting membrane (ILM). Eight types of cells are present in the structure: Retinal pigmented epithelium cells (grey), Cone photoreceptor (light blue), Rod photoreceptor (pink), Müller cell (purple), Horizontal cell (red), Bipolar cell (yellow), Amacrine cell (dark blue) and Ganglion cell (green).

1.2 Photoreceptors

Photoreceptors are highly specialized neurons capable of capturing photons and transducing them into electrochemical signals. Then the signal is relayed to the retina network via the synapses and eventually to the brain via the optic nerve. Two types of photoreceptors are present in the retina: the rod and the cone, named after their physical morphologies. Vertebrate rods and cones bear similar structures, with five principal regions constituting the structure:

the outer segment (OS), the connecting cilium, the inner segment (IS), the nuclear region and the synaptic region [16].

OS is the place where the light is captured and converted into an electrical signal. Both rods and cones outer segments are composed of hundreds to thousands membrane discs that contain opsins, which are photoreceptive pigments. The OS in both rods and cones are continuously renewing themselves, with new discs produced at the base, older and more mature discs are displaced toward the RPE. The older discs near the OS tip are daily shed and phagocytized by RPE cells. This growth and shedding process helps maintain a considerably constant length of OS and controls its regeneration after the exposition to photooxidative stress [17, 18]. Down below the OS, the cilium is a bridge to connect OS to IS. It is a highly organized structure composed of microtubules which gates the transfer of different molecules to the OS. The IS consists of cellular organelles, such as endoplasmic reticulum, Golgi apparatus, mitochondria. The nuclear region contains the nucleus of cell. The synaptic region is located at the end part of the photoreceptors and acts as a transporter to send neurotransmitters such as glutamate from photoreceptor cells to secondary neurons [19] (Figure 1.2).

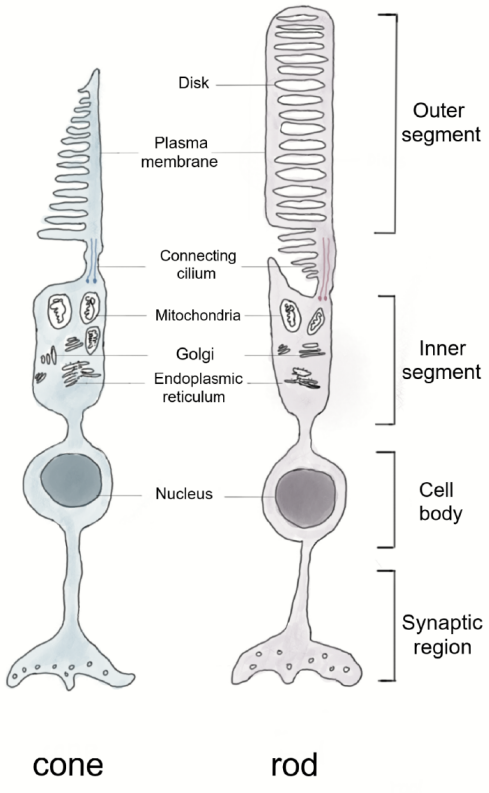

Figure 1.2 Basic structures of rod and cone photoreceptor. Rods and cones bear similar structures: outer segment, connecting cilium, inner segment, nuclear region, synaptic region.

Although rods and cones harbour similar structures, they exhibit distinct features and functions.

1.2.1 Rod photoreceptor

In the human retina, approximately 95% of the photoreceptors are rods, counting around 120 million cells [20]. They are located across the whole retina except at the central fovea (referred to as the foveola), and their density becomes denser from the fovea to the peripheral retina [21]. The rods are exquisitely sensitive to light and are able to sense a single photon of light, thus can detect photostimuli in dim light conditions, meaning that when the light is at lowest level, only rods can detect. Although our vision is benefiting from their high light sensitivity, the rods are relatively low functioned in spatial discrimination and are not able to distinguish different wavelengths of light, thus the rod system itself does not allow to detect different colors and has limited visual acuity [22].

The OS of rod is a cylindrical shaped structure composed of lobulated membranous pancake-like discs, this is the place where the visual pigments are stored. The pigments usually consist of proteins and opsins, and only one type of opsin called rhodopsin is present in human rod photoreceptors. There are about one thousand discs in one rod and each disc contains around 150,000 photopigment rhodopsin molecules, which comprise >85% of the disk membrane proteins. Apart from these, another distinct feature of the rod is that each membrane disc is completely enveloped in the plasma membrane [23] (Figure 1.2).

1.2.2 Cone photoreceptor

Compared to the considerable occupancy of rods in the retina, cones are in far fewer amount, numbering approximately 6 million. Like rods, they are located throughout the whole retina, but not evenly and they are particularly dense in the foveola, where only cones are present. The densely packed cones in the fovea produce the maximal vision resolution. The density of cones decreases with the distance moving outward from the fovea. Compared to rods, cones are much less sensitive to light, up to 100-fold less, thus they are active at high light level and responsible for the day light vision [24].

The OS of cones is generally shorter than that of rods, and is conical shaped. The discs are usually partially open to the extracellular space due to the fact that the cone discs are generated by evaginations of the ciliary membrane. Though the cones are not sensitive enough to be ideal

for the dim light vision, they possess some other advanced features: unlike rods that only have one type of opsin, the cones have 3 types of opsins: S-cones, M-cones, and L-cones, each expressing different opsins: blue in S-cones, green in M-cones, and red in L-cones, this feature allows the cones to detect a wide spectrum of light wavelengths, producing color discrimination [24, 25].

1.2.3 NRL in rod photoreceptor development

Retinal histogenesis is subject to a complex regulation by extrinsic signaling and intrinsic factors, the latter, which are specific transcription factors that control the initiation or suppression of specific genes, regulate the differentiation of individual cell types in retina [26, 27]. NRL, the basic motif–leucine zipper (bZIP) motif transcription factor, encoded by the *Nrl* (neural retina-specific leucine) gene, binds promoters and activates rod-specific genes. NRL is specifically expressed in rods and is critical for rod cell fate during retinal development [28]. It acts together with other two transcription factors, CRX (cone–rod homeobox protein) and NR2E3 (nuclear receptor subfamily 2, Group E, Member 3) for the transcription of rod genes, including rhodopsin and phosphodiesterase. CRX and NRL, synergistically, act on the rhodopsin promoter and stimulate its expression. Besides, CRX can directly bind to an enhancer of the *Nrl* gene and promote its expression. NRL, in turn, induces rod specific genes and suppresses cone specific genes by partially regulating the expression of *Nr2e3* gene [29]. While NR2E3 suppresses cone genes development in rods, it also directly interacts with CRX to enhance rhodopsin expression [30]. The importance of NRL in rod photoreceptor development is demonstrated by several studies: the ablation of *Nrl* gene in the mouse leads to photoreceptor precursors to acquire a cone state [31, 32]; mutations in NRL are linked to autosomal dominant retinitis pigmentosa in human [33, 34]. Altogether these data suggest that NRL can act as a master gene in the differentiation of rod photoreceptors.

1.3 Phototransduction

Phototransduction is the process of converting light into an electrical impulse in rod and cone photoreceptor outer segments, which are unique structures tightly packed with ciliary structured membrane discs rich of pigments (in rod it is rhodopsin) [35]. The phototransduction occurs at the similar way in rods and cones, thus I will take the rod as example. When the light hits the eye, the phototransduction in rod initiates with the absorption of photons by rhodopsin, which is a seven-helix structured protein, called opsin, member of the G-protein-coupled

receptor family, that binds a membrane embedded chromophore, 11-*cis*-retinal [36]. The 11-*cis*-retinal acts as an antagonist that keeps rhodopsin in an inactive form. When hit by light, 11-*cis*-retinal is isomerized to all-*trans*-retinal and triggers a conformational change that activates rhodopsin into rhodopsin R* (also known as metarhodopsin II). The all-*trans*-retinal detaches and is then transported to the RPE and in which it is converted back to 11-*cis*-retinal, a process called visual cycle [37].

The activated rhodopsin R* comes into contact with a G protein transducing (Gαβγ, comprising subunits α, β and γ) and is bound to it transiently. This binding promotes the release of a molecule GDP from the G-protein α subunit (Gα), allowing a molecule of GTP to substitute GDP. This process, named nucleotide exchange, activates the G-protein (from Gα-GDP to Gα-GTP), followed by its separation from rhodopsin R* and from Gβγ. Interestingly, the activated rhodopsin R* can continually contact G proteins transducin and start nucleotide exchange in one after the other Gα due to the fact that the rhodopsin R* is not altered by the first interaction. Thus, this process can repeat infinitely when rhodopsin R* remains active, and consequently activates numerous G proteins. The activated G protein (Gα-GTP) then binds to the two inhibitory γ-subunits of the enzyme called cyclic nucleotide phosphodiesterase (PDE), activating the PDE. The resultant activation of PDE hydrolyzes 3',5'-cyclic guanosine monophosphate (cGMP), dropping intracellular cGMP concentration. The decreasing level of free cGMP limits its chance to bind to the cyclic nucleotide-gated channels (CNG channels) on the OS membrane surface, leading to the channel closure. Due to the fact that the channel is permeable to Na^+ and Ca^{2+}, the opening CNG channel allows for an influx of Na^+ and Ca^{2+}, thus the closure decreases inner Ca^{2+} concentration. This is a crucial event that results in the reduction or even suppression of the electrical current that normally flows into the OS, ultimately causing the hyperpolarization of photoreceptors and slowdown of the release rate of neurotransmitter at the synapse. The change of signal is then captured by bipolar cells, relayed to ganglion cells and finally conveyed to the brain through the optic nerve. Noticeably, the electrical current reduction is largely dependent on the number of activated PDE molecules, which is in turn determined by the intensity of light, thus during darkness, the concentration of free cGMP remains at a relatively high level, and its binding to the CNG channel retains the channel in an open state, Na^+ and Ca^{2+} keep flowing inside, maintaining a relatively high concentration level of inner Na^{2+}, while K^+ and Ca^{2+} ions are extruded from a $Na^+/Ca^{2+}/K^+$ exchanger (NCKX) (Figure 1.3). The complex phototransduction cascade relies to a large extent on the interplay of two essential signaling molecules: cGMP and Ca^{2+} [38].

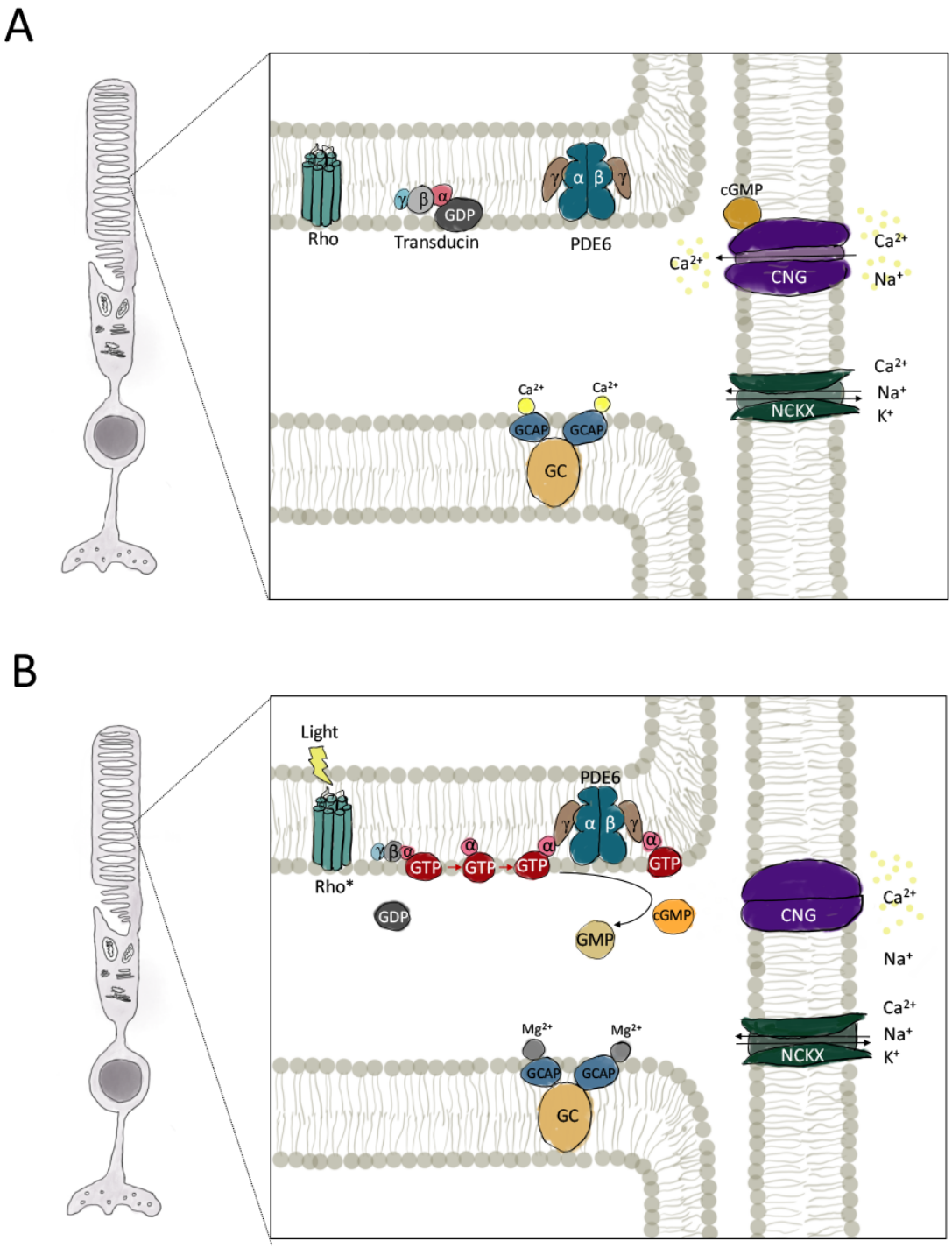

Figure 1.3 The phototransduction cascades in rods. (A) During darkness, cGMP is bound to the cyclic nucleotide-gated channel (CNG channel), which keeps the channel in an open state, allows for a steady influx of Ca^{2+} and Na^{+} into photoreceptor outer segment, thus intracellular Ca^{2+} level is relatively high. At the same time, K^{+} and Ca^{2+} ions are extruded from a $Na^{+}/Ca^{2+}/K^{+}$ exchanger (NCKX). With the high concentration of Ca^{2+}, the free Ca^{2+} binds guanylyl cyclase activating proteins (GCAPs), which inhibits the guanylyl cyclase (GC) activity and synthesis of cGMP. (B) With light stimulation, photon absorption triggers a conformational change in rhodopsin (Rho) and activated rhodopsin(R*) promotes

the GTP replacement of GDP in G protein transducing (Gαβγ), the activated G-protein (Gα-GTP) binds to phosphodiesterase-6 (PDE6), this activated PDE6 hydrolyses cGMP, resulting in CNG channel closure and a reduction of Ca^{2+} influx. This process causes the hyperpolarization of photoreceptors and generates the electrochemical signal. With the reducing level of Ca^{2+}, Mg^{2+} replaces the Ca^{2+} bound to GCAPs and activates the GC to synthesize cGMP.

1.4 3',5'-cyclic guanosine monophosphate (cGMP) in photoreceptors

The 3',5'-cyclic guanosine monophosphate, better known as cGMP or cyclic GMP, is a classical cyclic nucleotide that is employed as a second messenger in a variety of intracellular pathways, and is involved in transduction of extracellular signals into cellular responses in all eukaryotic cells [39]. cGMP regulates a number of physiological processes, including neuronal signaling and sensory transduction [40]. In photoreceptors, as in other types of cells, cGMP is a crucial second messenger that affects the physiology and function of the cell as well as the phototransduction cascade [40]. The first identification of cGMP was as early as in 1960s from rat urine [41], but it took quite a long time to shed light on its biological role from identifying and cloning the synthesis enzymes and elucidating the activation mechanisms. In the retina, cGMP was first discovered in 1970s when the presence of high phosphodiesterase activity against cGMP was exhibited from purified bovine rods outer segments [42]. Later it became clear that rod outer segment contained an unusually high concentration of cGMP, which had a rather critical function in the phototransduction cascade [43]. The metabolism of cGMP is regulated by the balance of its synthesis mediated by guanylyl cyclase, and its degradation, regulated by phosphodiesterase. Effects of cGMP occur through its binding targets and in photoreceptors, except phosphodiesterase and CNG channel that are targets in the phototransduction cascade, there are also other targets outside the cascade, notably, the cGMP dependent protein kinases (PKG) [44].

1.4.1 Membrane guanylyl cyclases (GCs)

Membrane guanylyl cyclases (GCs) catalyze the synthesis of cGMP from guanosine 5′-triphosphate (GTP) [45]. In photoreceptors, guanylyl cyclase activity is derived from two retinal membrane guanylyl cyclases (RetGCs): RetGC-1 and RetGC-2. Unlike other membrane GCs that usually have extracellular ligand binding domains where specific peptide ligands can bind to activate the enzymes, RetGCs handle this process in a distinct way: through a calcium-dependent manner mediated by guanylyl cyclase activating proteins (GCAPs). GCAPs are calcium-binding proteins that contain EF-hand motifs. When Ca^{2+} binds to EF-hand motifs,

GCAPs interfere with RetGCs activity and the production of cGMP will be inhibited [46]. During darkness, when intracellular Ca^{2+} level is high, the RetGC1 and RetGC2 are inhibited by GCAPs and cGMP is not synthesized. Conversely, under the light stimulation, the lower intracellular Ca^{2+} level leaves GCAPs motif sites empty, Mg^{2+} replaces Ca^{2+}, subsequently GCAPs can activate RetGCs, promoting the synthesis of cGMP and the recovery of photoreceptor from the light stimulus to dark-adapted state (Figure 1.3) [45, 46].

1.4.2 Phosphodiesterase 6 (PDE6)

In the visual transduction pathway, phosphodiesterase 6 (PDE6) is a central enzyme and, with its activation, it rapidly hydrolyzes cytoplasmic levels of cGMP, inducing the closure of CNG channel. PDE6, the key enzyme modulating the concentration of cGMP, comes from a large family of 11 Class I phosphodiesterases, and is highly expressed in the retina, and especially localized in photoreceptor outer segments [47].

Rod and cone PDE6 are comparatively unique throughout all other PDE families as they are the only PDEs which are directly activated by the binding of a G protein. In addition, unlike other PDE members, the predominant form of PDE6 in rod photoreceptor is present as a complex that contains one catalytic α subunit PDE6A, one catalytic β subunit PDE6B and two inhibitory γ subunits PDE6G. The α-subunit is farnesylated whereas the β subunit is geranylgeranylated [48]. Inside the complex, the α and β subunits form a heterodimer (Pαβ), while the 9.7-kDa inhibitory γ-subunit (Pγ) regulates the catalytic function of the complex by interacting with the domains of the catalytic subunits and forming a non-activated rod PDE6 holoenzyme (stoichiometry αβγγ) [49]. On the other hand, the cone PDE6 contains two identical catalytic α subunits and two distinct γ subunits (different genes encode rod and cone γ subunits). The catalytic subunits of cones are geranylgeranylated [50]. Inside the PDE6 structure, except the C-terminal catalytic domain, the catalytic subunits of PDE6 consist of two N-terminal regulatory GAF (regulatory domain found in certain PDEs, bacterial adenylyl cyclases, and the bacterial transcription factor FhlaA) domains (GAFa and GAFb) that are also present in four other PDE members of the family. These non-catalytic cGMP-binding GAF domains contain the biggest differences among PDE6 subunits [51]. In rods, the affinity of cGMP towards GAF domains is greater than that of cones [52].

During darkness, the γ-subunit binds to the two catalytic subunits, this binding suppresses the PDE6 activity. Upton light stimulation, rhodopsin activates the heterotrimeric G protein transducin, activated transducin α-subunit (Gtα) occupies and binds the space where γ-subunits

(Pγ) usually reside in PDE6, this displacement of γ-subunits results in the activation of PDE6 [47].

1.4.3 Cyclic nucleotide-gated channel (CNG channel)

Another cGMP key binding target is the cyclic nucleotide-gated (CNG) channel. It is a non-selective cation channel firstly identified in photoreceptors and olfactory sensory neurons. In photoreceptors, these ligand-gated ion channels control the flow of Ca^{2+} and Na^{+} in response to cGMP concentration [53].

In mammals, the CNG channels are classified into two subfamilies that comprise six homologous members: type A or α subunits (CNGA1-4) and type B or β subunits (CNGB1 and CNGB3). In all six CNG channel subunits, CNGA1, CNGA2 and CNGA3 are able to form functional homomeric channels in heterologous expression systems, while the remaining subunits (CNGA4, CNGB1 and CNGB3) do not give rise to functional homomeric channels [53]. In rods, the CNG channel is a heterotetramer composed of 3 CNGA1 and 1 CNGB1 subunits [54], while in cones, is composed by CNGA3 and CNGB3 in a 1:1 ratio [55]. For both rods and cones, the CNGA is the essential subunit for the channel functional activity whereas the CNGB acts as a modulatory protein [53].

The main function of the CNG channel in photoreceptors is to modulate the membrane potential and to control one of the major sources of intracellular Ca^{2+}. In the dark, with high concentration of cGMP, both channels are kept in an open state to allow the steady influx of Ca^{2+} and Na^{+} to depolarize the photoreceptors and stimulate synaptic transmission. With the light-induced hydrolysis of cGMP, the closure of the CNG channel results in the photoreceptor hyperpolarization and the turn off of the synaptic glutamate release [56].

Due to its unique function in phototransduction, naturally occurring mutations in CNG channel subunits have been linked to a variety of inherited retina disorders. For instance, mutations in CNGA1 and CNGB1 genes were identified in patients affected by retinitis pigmentosa [57, 58]. Loss function of CNGA3 or CNGB3 subunits could be found in the patients suffering achromatopsia, also known as total color blindness [59, 60].

1.4.4 cGMP-dependent protein kinase (PKG)

One of the targets of cGMP outside the phototransduction is PKG, a serine/threonine-specific protein kinase, that can phosphorylate diverse biological targets [61]. cGMP binding activates PKG, which phosphorylates serines and threonines in different proteins. Those modified

proteins then in turn get involved in many cellular functions including regulation of calcium homeostasis and gene expression, NO-signalling pathway and other processes [62].

Two different genes for PKG are expressed in mammals: the *PRKG1* gene, located on human chromosome 10, encodes for the isoforms PKGIα and PKGIβ; whereas the *PRKG2* gene, located on human chromosome 4, encodes PKG II [63]. The structure of PKG contains two functional domains: a regulatory domain and a catalytic domain. The regulatory domain can be subdivided into an N-terminal regulatory domain, an autoinhibitory sequence and two tandem cGMP-binding sites. In order to be activated by cGMP, PKG needs the binding of cGMP to the regulatory domain, inducing a conformational change in PKG that is required to liberate the catalytic site and release the inhibition of the catalytic core by the N-terminal autoinhibitory sequence [63].

Different PKG isoforms are also expressed with different sub-localizations in tissues. PKGIα and PKGIβ are usually localized in the cytosol, while PKGII is commonly associated to the plasma membrane. In the retina, a previous study based on immunohistochemical analysis of PKGI and PKGII reveals a predominant expression of PKGI in the photoreceptors ONL, while PKGII seems to be prevalent in the inner nuclear layer (INL) and the ganglion cell layer (GCL) [64].

In mammals, different PKG isoforms may exert different functions. PKGI could mediate the effects of NO/cGMP on vasodilation, vascular smooth muscle cell relaxation, proliferation, and apoptosis. On the other hand, PKGII could regulate homeostasis of Na^+, Cl^-, endochondral ossification of bones and various functions of the nervous system. Though not much is known in retina photoreceptors about the role of PKG, the manipulation of activity in PKG was shown to cause photoreceptor cell death and the activation was detected in different models of retinitis pigmentosa, which implies its key role in photoreceptors [65].

1.5 Ca^{2+} in photoreceptors

The Ca^{2+} ion is an important messenger for coordinating activity in many types of cells. It is widely distributed in diverse ranges of eukaryote cell types from different species and functions as a second messenger in several pathways [66]. Due to the ability of Ca^{2+} signaling in maintaining a large concentration variance between the cytosol and the extracellular space, which could count as high as 10,000-fold difference, the Ca^{2+} influx through the plasma membrane and Ca^{2+} extrusion from intracellular stores can stimulate great fluctuations of free

intracellular Ca^{2+} [67]. Another important feature of Ca^{2+} is that it is able to regulate different functions in different parts of the cells, thus the Ca^{2+} signals are specific to different subcellular locations. This property is mainly facilitated by Ca^{2+} binding proteins, which are often localized at specific sites in different parts of the cells. Therefore, it is important to map the distribution of Ca^{2+} targets such as Ca^{2+} channels and Ca^{2+} stores. This is especially true for primary sensory neurons, such as photoreceptors and olfactory cells, that are composed of different functional compartments [68].

As mentioned in chapter 1.2, the photoreceptors have more than one intracellular compartment and the OS and IS are composed of different sets of lipids and proteins on the membrane, thus they differ with respect to Ca^{2+} regulation.

In photoreceptor OS, Ca^{2+} regulation lies at the heart of modulating phototransduction cascades to shape the photo responses and the adaption to light. Maintaining Ca^{2+} homeostasis is, thus, critical for the survival of photoreceptors. The OS possesses a single plasma membrane Ca^{2+} entry pathway (CNG channel) and a Ca^{2+} clearance pathway, the $Na^{+}/K^{+}/Ca^{2+}$ exchanger (NKCX) (in rod NKCX1; in cone NKCX2) [69]. During darkness, the photoreceptor is continually depolarized due to an influx of Ca^{2+} and Na^{+} via the open CNG channel and Ca^{2+} maintains a relatively high level. This is regulated by the increasing level of cGMP via the dynamic equilibrium between cGMP synthesis (GC) and hydrolysis (PDE6). Conversely, with the light stimulation, the decreasing cGMP level leads to the closure of CNG channel, and the Ca^{2+} influx is blocked, however, the remaining Ca^{2+} continues to be extruded from the OS through NKCX, resulting in the drop of Ca^{2+} concentration [70]. By time, the extrusion of Ca^{2+} gradually decreases and comes into a balance with the influx, this results in a steady state of Ca^{2+} that determines the functions of the cells.

Ca^{2+} has a direct role in suppressing the cGMP synthesis through GCAP-RetGC, and cation influx through CNG channel. Notably, at high Ca^{2+} level, GC is additionally suppressed by a guanylyl cyclase inhibitory protein (GCIP). When the photoreceptors are exposed to light and Ca^{2+} level in the OS declines during sustained illumination, Ca^{2+} is released from GCAPs and replaced by Mg^{2+}, which activates GCAPs and stimulate the RetGCs to accelerate the synthesis of cGMP [71]. Increased cGMP synthesis promotes the rapid reopen of CNG channels, this in turn, drives the recovery of the dark current after a transient light stimulation.

Ca^{2+} regulation in phototransduction also involves the activity of rhodopsin kinases modulated by recoverin [72]. In darkness, when Ca^{2+} is high, recoverin exerts an inhibition effect on rhodopsin kinase, resulting in a delayed visual pigment phosphorylation [73]. With the

declining of Ca^{2+} level, the inhibition of rhodopsin kinase by recoverin is relieved, promoting the phosphorylation and inactivation of visual pigment.

In addition to its effects on cGMP, there is another mechanism of Ca^{2+} modulating the function of photoreceptors, which involves the CNG channel. Ca^{2+} exerts a direct control over the cation influx through the CNG channel. The CNGB1 subunit in rod photoreceptor contains a binding site for Ca^{2+}-calmodulin [74], when Ca^{2+} level is high in OS, it is bound. With the release of calmodulin from the channel in low Ca^{2+} condition, it enhances the affinity of cGMP to the channel, creating the potential for increasing the dark current. However, the contribution of this mechanism in rod appears to be minor as some studies pointed out that only a small portion of direct modulation on the channels can be observed under light stimulation [75]. Moreover, mutant CNGB1 without the calmodulin binding site in rod failed to show any effect on the response kinetics or on light adaptation in rods [74]. Nevertheless, this mechanism seems to be more prominent in cones.

Compared to the OS, the Ca^{2+} regulation in other cell compartments is paid much less attention. In the cilium, where itself functions as a barrier between OS and IS compartments, the diffusion of Ca^{2+}, as well as H^{+} and cGMP is hindered [76]. For example in the ellipsoid, the ellipsoid mitochondria function as gatekeepers for Ca^{2+} diffusion across the cilium [77]. Besides, these organelles possess a fairly capacity for Ca^{2+} sequestration which could help to control the interference from the Ca^{2+} influx in the IS to the OS. In the IS the endoplasmic reticulum (ER) is as multifunctional organelle containing the highest intracellular Ca^{2+} in photoreceptors and functions as a Ca^{2+} reservoir. Concurrently, the Ca^{2+} influx in the IS is governed by voltage-gated Ca^{2+} channels [67]. L-type channels are highly present in photoreceptor synapsis region, where they facilitate the release of neurotransmitter and mediate the visual information processing at the early stage [78].

1.6 Inherited retinal degeneration (IRD)

Inherited retinal degenerations (IRDs) represent a phenotypically and genotypically diverse group of debilitating retina degeneration (RD) diseases that can potentially lead to blindness with critical retinal dysfunction [79]. IRDs generally display a great heterogeneity with mutations in over 300 genes having been identified up to date (https://sph.uth.edu/retnet/), resulting in different visual impairments. The disease phenotype involves the degeneration and dysfunction of photoreceptors, of the retinal pigment epithelium, or of the choroid. The prevalence of IRDs is approximately 1 in 2000 individuals [80].

IRDs can be progressive, as for pretinitis pigmentosa (RP), Leber's congenital amaurosis (LCA) and Stargardt disease, or in some cases can be stationary, like congenital stationary night blindness and achromatopsia. The causative mutations in IRDs typically cause a primary degeneration of rod photoreceptors, with a subsequent secondary loss of cone photoreceptors, resulting in a complete loss of outer nuclear layer and outer plexiform layer, while the inner retina remains apparently intact, at least initially (Figure 1.4) [81].

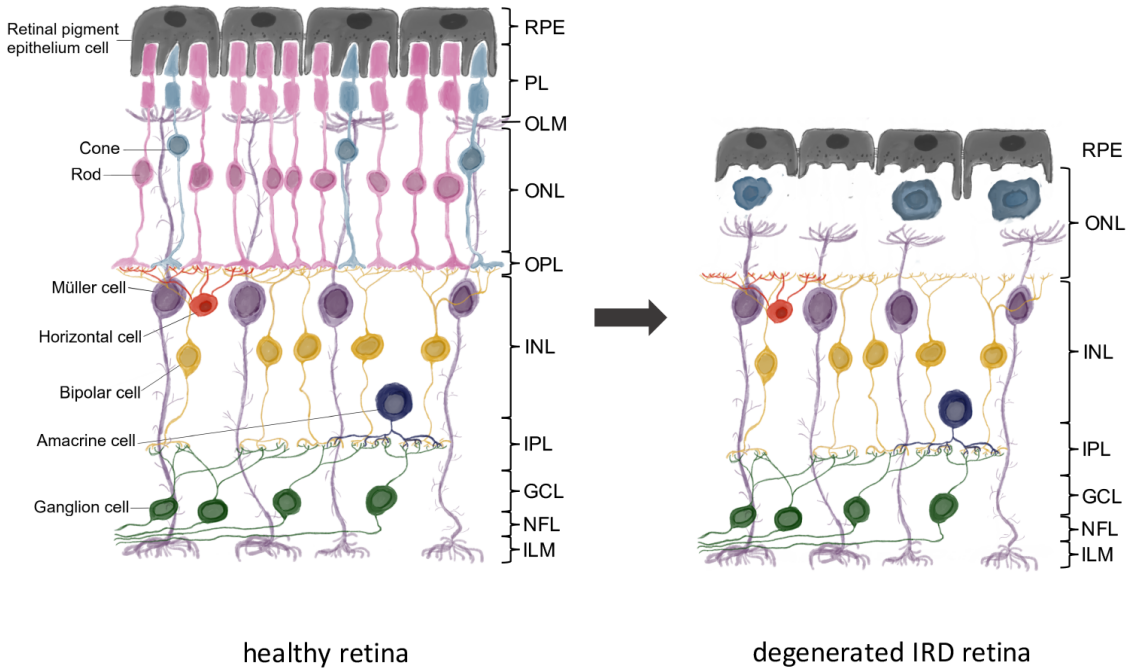

Figure 1.4 Schematic drawings of a healthy retina (left panel) and an inherited retinal degeneration (IRD) retina (right panel). RPE: Retinal pigmented epithelium; PL: Photoreceptor layer; OLM: Outer limiting membrane; ONL: Outer nuclear layer; OPL: Outer plexiform layer; INL: Inner nuclear layer; IPL: Inner plexiform layer; GCL: Ganglion cell layer; NFL: Nerve fiber layer; ILM: Inner limiting membrane.

Due to the great heterogeneity, some patients have similar clinical phenotypes but with different genetic diagnoses, this requires for specific gene therapies or gene-editing treatments. Most mutations behind many IRDs are still unknown, thus it is rather difficult to establish a gene specific treatment, so far only one gene therapy treatment is on the market for Leber congenital amaurosis (LCA2) based on *RPE65* gene, with some other gene therapies in developing or in clinical trials [82, 83]. This new era of gene therapy research into IRDs is rather enthralling due to the monogenic nature of the disease and opens new therapeutic window for the patients. However, considering the fact that developing gene therapy strategies

for each mutated gene or even more specific mutations in one gene, will require highly personalized strategies and relatively high expenses and only few patients would benefit from this [84]. Other possible treatments include cell therapy, which is based on the photoreceptor transplantation and it attracts great interests in treating IRDs, or neuroprotective agents or optogenetics. Several of these therapeutic strategies have entered into clinical trials [85].

1.7 Retinitis pigmentosa (RP)

As the most common type of the IRDs, RP is termed as a set of hereditary retinal disorders which leading to progressive vision loss and blindness, due to the loss of photoreceptors. It is characterized by the initial impairment of rod photoreceptors followed by the involvement of cone photoreceptors. RP approximately affects 1 in every 4000 people [86].

1.7.1 Symptoms

The symptoms usually start with nyctalopia or night blindness, along with a gradual visual field deficiency, tunnel vision or complete vision loss could be the final results, depending on the severity and progression of the disease. The symptoms can also be highly variable: as someone develops symptomatic visual loss since a young age, whereas others remain asymptomatic until adulthood. A classic symptom pattern includes the difficulties in dark adaptation and night blindness in adolescence followed by the loss of mid-peripheral visual field in young adulthood. With the disease advancing patients lose peripheral vision, develop tunnel vision, and eventually lose central vision [87].

At cellular level, the predominantly affected rod photoreceptors at first hand could explain the occurrence of night blindness and a gradual diminution of peripheral vision at the early stage of the disease as the rods are mainly responsible for the dim light vision. With the disease advancing, large numbers of rods are deteriorated which also affect the RPE and the cones are gradually affected. Rods appear to be more affected than cones. The involvement of gradual loss of rod and cone photoreceptors results into the severe damage of outer nuclear layer which consists of rods and cones nuclei, while the cells composing the other layers are fairly well preserved, however, many of them will also degenerate in the late stage of the disease [88].

RP can be "non-syndromic" or "syndromic". In terms of non-syndromic, the disease only involves vision loss and is confined to the eye, the majority of RP, falls into non-syndromic form [89]. As for syndromic RP, which is much less common, it refers to the conjunction with systemic diseases such as Usher syndrome and Bardet-Biedl syndrome, the former includes

not only vision impairment, but is also accompanied by hearing loss. The latter, Bardet-Biedl syndrome, is associated with cognitive impairment and obesity [88, 90].

1.7.2 Inheritance

As RP is an inherited disease, its genetics are quite varied. Firstly is the genetic heterogeneity: with the discovery of the first gene mutation responsible for RP in 1990 [91], till now over 85 genes have been identified, with 70 genes are linked to non-syndromic RP, 13 genes mutations to Usher syndrome and 17 genes to Bardet-Biedl syndrome. In addition to the genetic heterogeneity, allelic heterogeneity, which stands for different variants mutations in the same gene can cause same or similar diseases (symptoms of different diseases may overlap). Clinical heterogeneity has also been reported and refers to different clinical conditions even among different individuals who share the same mutation. RP can be inherited in an autosomal recessive (account for 50-60%), autosomal dominant (30-40%), or X-linked recessive (5-15%) manner, in which the autosomal recessive is the most prevalent form [92]. Such intricate features cause multiple patterns of inheritance and expressions in RP, making RP as one of the most complicated single gene inherited diseases.

1.7.3 PDE6B mutation

For non-syndromic RP, most of the genes mutations are found in the genes encoding phototransduction cascade components and one of them is the rod cGMP phosphodiesterase 6 (PDE6) complex [93]. As stated in the phototransduction chapter, this complex is responsible for regulating the intracellular cGMP levels thus each subunit is essential for rod photoreceptor functions and maintenance [94]. Mutations in *PDE6A* and *PDE6B* genes are the second most common mutations that cause autosomal recessive RP, just below the *USH2A* gene. PDE6 defects could account for around 8% of all autosomal recessive RP. Remarkably, mutations in *PDE6B* could lead to either progressive retinal disease, such as RP, or stationary disease, such as congenital stationary night blindness (CSNB). In autosomal recessive RP, 5-8% of patients are known to have defects in rod PDE6B [95].

The human *PDE6B* gene is located on chromosome 4p16.3 (OMIM *180072), comprising 22 coding exons, spanning approximately 45 kb, and 854 amino acid residues are encoded [96]. A mutation causing dysfunction of PDE6B could result in an elevated concentration of cGMP and increasing Ca^{2+} influx in rod photoreceptors, promoting cell death. There are mouse models bearing mutations in the *Pde6b* gene, such as *rd1* and *rd10*, which map on chromosome 5 and exon 13, respectively. The *rd1* mouse model is a well characterized animal model of RP and it was first discovered in 1924 among the rod-less mice [97]. *rd10* is a model of autosomal

recessive RP, with rod degeneration being not as fast as in *rd1* and starting at around postnatal day (PN)18 [98].

1.7.4 Treatment and management

No standard treatment is available for RP patients yet, supplementation with vitamin A is widely used as a recommended treatment for slowing the rate of degeneration according to some studies [99]. Recently, novel treatments are being developed based on the further understanding of the genetic causes of RP, for example gene augmentation therapy has been widely studied to restore normal gene expression in photoreceptors, such as the previously mentioned gene therapy for LCA2. Other therapies include cell therapy, a technique based on the transplantation retinal of progenitor cells into the eye to repopulate the photoreceptors [100]. While these approaches might only be efficient in relatively early stage of RP, as for the patients in late stage of disease progress, different types of electronic retinal implants have shown great promise in restoring partial function of the retina [101].

1.8 Cell death mechanism in inherited photoreceptor degeneration

Several mechanisms are associated with triggering photoreceptor cell death, including the dysregulation of cGMP, calcium overload, ER stress, inflammatory responses and oxidative stress.

1.8.1 Apoptosis

In last 40 years various concepts have been introduced to characterize the photoreceptor cell death mechanism caused by IRDs. Apoptosis, necrosis, programmed cell death and autophagy are commonly used terms to define the forms of cell death. Initially, apoptosis was often regarded as the cell death mechanism in photoreceptor degeneration. However, later it proved that the apoptotic pathways engaging executioner caspases in photoreceptor degeneration were quite controversial. Several studies have detected the activated caspase 3 and caspase 7 in transgenic rats and mice with a mutation in the *Rhodopsin (Rho)* gene [102-104]. However, other data have shown that a caspase-independent mechanism is activated in photoreceptor degeneration with different disease models, comprising degeneration caused by dominant mutations in *Rho* [104-106]. In *rd1* mice, knock-out of caspase 3 only provided transient photoreceptor protection effect suggesting that activation of caspase 3 plays a marginal role in IRDs [107]. Similarly, *in vivo* administration of a pan-caspase inhibitor, for instance Z-VAD-FMK, only offered scarce neuroprotection in murine models of IRDs [104, 108]. It should be noted that the activation of BCL2-associated X protein (BAX), a key player in caspase-

dependent apoptosis, in degenerating retinas of different IRD animal models built up the base for focusing on caspases. Indeed, the study from our lab evaluated the activation of BAX in different RP models: the *rd1* mouse model with a recessive mutation in the *Pde6b* gene, a transgenic mouse expressing the P23H mutation in *Rho*, and a *Rho* knock-out mouse, found that the activation was mainly associated to the efflux of the apoptosis inducing factor (AIF) rather than to caspase activation [109]. In fact, the pore formed by BAX is required for AIF to exit mitochondria and to translocate to the nucleus. Altogether these studies indicate that the activated caspases might not be crucial during the retinal degeneration process.

1.8.2 cGMP dependent cell death mechanism

The link between high concentration of cGMP and photoreceptor degeneration has already been established as early as in 1970s [110]. Later with the discovery of first disease-causing mutations in the *Pde6b* in the *rd1* mouse, an explanation of how IRD mutations lead to excessive photoreceptor cGMP levels could be forwarded [111, 112]. Nowadays, many forms of inherited retinal dystrophies, including RP, LCA and cone-rod dystrophy, are known to be associated with cGMP-dependent photoreceptor cell death [113-115]. Excessive accumulation of cGMP in photoreceptors observed in various IRD mutations suggests that cGMP may act as a common trigger for non-apoptotic cell death mechanisms in IRD. A critical question needs to be addressed is how exactly the high concentration of cGMP exerts its toxic effect on the cells. Recently it becomes more and more evident that excessive cGMP could target CNG channel and PKGs, causing excessive Ca^{2+} influx and specific protein phosphorylation, respectively (Figure 1.5).

1.8.2.1 CNG channel, Ca^{2+} influx and cell death

Ca^{2+} has long been known for its detrimental effect in cell survival and function [116]. Excessive Ca^{2+} influx is a major harmful condition in photoreceptor degeneration [117]. It is hypothesized that high levels of cGMP lead to Ca^{2+} influx through the CNG channel and that excessive Ca^{2+} triggers photoreceptor cell death [118]. However, how Ca^{2+} influx manipulates the cell death mechanism is still under debate. There are two major ways for Ca^{2+} to enter into photoreceptors: through the CNG channel localized in the outer segment, and through the voltage gated Ca^{2+} channel (VGCC) localized in the synaptic terminal. Under normal conditions, Ca^{2+} influx mediates the inhibition of cGMP synthesis via a feedback loop that guarantees cGMP and Ca^{2+} levels to be kept at a normal range. Once this feedback loop is

broken, unfitting changes in cGMP and Ca^{2+} concentrations happen. The hypothesis that elevated cGMP level increases Ca^{2+} influx is supported by the fact that loss-of-function mutations in PDE6 genes could cause an elevation of photoreceptor cGMP levels, Ca^{2+} influx and photoreceptor cell death [119]. A combined mutant mouse supported this hypothesis, in fact knockout of *Cngb1* gene, which affects CNG channel functionality, in *Pde6b* mutant background, could significantly delay photoreceptor degeneration [120].

On the other hand, the voltage gated Ca^{2+} channels (L-type channels) in the photoreceptor cell body and synapse region will open in response to the photoreceptor depolarization state initiated by the activity of CNG channel, and this event will further promote Ca^{2+} influx [121]. This might again activate downstream calpains, leading to cell death. The significant role of elevated Ca^{2+} influx has encouraged many studies to focus on blocking the CNG channel or L-type channel in order to save photoreceptors. Though these studies yielded contradictory results.

1.8.2.2 cGMP and PKG pathway in photoreceptor degeneration

The concept of PKG activity playing a role in cell death has been widely accepted. Some studies reported PKG activation as a protective event to promote cell survival, especially in certain neural cells [122]. On the other hand, activation of PKG can also induce cell death. For instance, PKG activation was used to induce apoptosis in different cancer cell lines [123, 124]. Nevertheless, PKG activation can have opposite effects in different types of cancers possibly because different activated isoforms of PKG may exert distinct functions. The activation of PKGIα was reported to promote cancer progression [125], while PKGIβ activity could induce apoptosis in certain cell lines such as human breast cancer cell lines and colon cell lines [123, 126]. The activation of the PKGII isoform could induce apoptosis and delay of tumor growth [127]. The PKG kinases are also associated with the NO-sGC-cGMP pathway, which is known as an important target for protection against ischaemia/reperfusion injury and heart failure [128].

Several studies pointed to a central role of the cGMP/PKG-dependent cell death mechanism in photoreceptor degeneration. In fact, triggering PKG by exposing the wild type retina to PKG activators induced photoreceptor degeneration [65]; Conversely, using PKG inhibitory compounds protected the degenerating photoreceptors in several RD models [129]. Similarly, knockout of *Prkg1* gene in mice helped rod photoreceptor survival and *Prkg2* gene knockout was found to protect the cone photoreceptors in a cone degeneration mouse model [130]. Although the degenerative process was not fully stopped when the PKG inhibitors were applied, possible explanations could be an insufficient effect of PKG inhibition or the existence of

different PKG isoforms activated during photoreceptor degeneration that could not be blocked by a compound preferentially targeting one PKG isoform.

1.8.2.3 Targeting downstream of PKG: the protein phosphorylation

cGMP activates PKG by binding its regulatory sites and initiating the kinase activity. PKG activation, will have several target proteins in photoreceptors. An open question is whether the PKG related phosphorylation can be associated to photoreceptor cell death. The post-translational modifications, including phosphorylation, acetylation, hydroxylation and methylation, affect a wide range of protein behaviors and characteristics, thus are important in controlling cell live and death [131]. PKG phosphorylates the components of different signaling pathways, such as G proteins, ion channels, cytoskeleton-associated proteins [61]. Phosphorylation, in particular, could be directly involved in apoptosis with a variety of distinct mechanisms. In addition, phosphorylation associated with apoptosis could influence neuronal cell death related to neurodegenerative diseases [132].

Due to the prominent role of cGMP-PKG pathway in photoreceptor degeneration, targeting PKG would provide a potential common treatment for patients if downstream targets are common in different forms of the disease. Therefore, the identification of PKG targets and the characterization of downstream signaling pathways are needed. Recently a study based on multiplex peptide microarray with human recombinant PKGs in combination with PKG activity modulators identified PKG substrates in photoreceptor cells. This study confirmed previously known PKG targets, such as vasodilation-stimulated phosphoprotein (VASP), but also some other novel substrates were identified [133]. Future studies will be needed to characterize the cGMP/PKG-dependent cell death mechanisms, thus the application of inhibitors or activators targeting PKG with a very high selectivity for the different isoforms would be beneficial to a better understanding of cell death mechanism and potential therapeutic approaches.

1.8.3 Ca^{2+} overload and cell death

A second effect consequent to increased cGMP is Ca^{2+} overload, which has been identified as a harmful event during photoreceptor degeneration. The discovery of increased intracellular Ca^{2+} level in different retinal degeneration animal models caused by mutations in different genes introduced the hypothesis that high intracellular Ca^{2+} concentration can be regarded as a common cell death mechanism during retinal degeneration [134].

1.8.3.1 Ca^{2+} and ER stress

As cellular Ca^{2+} reservoirs, endoplasmic reticulum (ER) and mitochondria are considered as major points of integration of cell death signals. They contribute to the unbalanced Ca^{2+} influx, which triggers cell demise. In several photoreceptor cell death models, the underlying pathways behind Ca^{2+} overload are differed from classical caspase mediated apoptosis and ER stress may be one of them [104, 108, 135]. ER stress can result from the unbalance between the demand of protein synthesis and ER capacity for protein folding. In dominant forms of RP, mutations in the Rhodopsin can account for 20–25%, and most of the mutations cause the misfolding of protein and retention in ER [136]. Mutations leading to Rhodopsin protein misfolding have been considered to be related to the increased intracellular Ca^{2+} in rod photoreceptors [137].

The role of ER stress contribution to cell death in photoreceptor degeneration is controversial. In retinas bearing the P23H dominant mutation, the activation of ER resident sensors, such as phosphorylated inositol-requiring enzyme1 (IRE1) and ER transmembrane protein kinase R-like endoplasmic reticulum kinase (PERK), could be detected, though it seems that this activation may be linked to ER-associated protein degradation and unfolded protein response but not to cell death [104]. While in the mouse with *Rho* gene knockout, high Ca^{2+} level could be found but not ER stress [138]. Otherwise, in retinas bearing other dominant mutations in Rhodopsin, such as the T17M mutation, ER stress response was involved [139].

1.8.3.2 Ca^{2+} and calpain activation

Calpains are a group of Ca^{2+}-activated cytosolic cysteine proteases, the first identified calpain was calpain 2, discovered and purified in 1976 [140]. In mammals, 15 different calpain isoforms have been discovered so far that can be subdivided into two groups based on the domain IV structure: typical calpains (calpain 1, 2, 3, 8, 9, 11, 12 and 14) have an EF hand domain that can bind Ca^{2+} , calpastatin or the calpain small subunit; atypical calpains (calpain 5, 6, 7, 8b, 10a, 13,and 15) lack a EF hand domain, thus are unable to bind calpastatin or the calpain small subunit [141]. Calpains contain 6 structural domains, domain I is cleaved after Ca^{2+} activation, domain II contains an active site, domain III consists of two Ca^{2+}-binding sites and a phospholipid binding motif. Domain IV contains a penta-EF hand that can bind Ca^{2+} and calpastatin. The penta-EF hand is one of the most important features of calpain activation [142]. The small regulatory calpain subunit, that dimerizes with typical calpains, consists of domain V and VI, and the function of domain V is to bind to the C-terminus region of domain IV in

large calpain subunits. Domain VI is identical to domain IV, it also has a penta-EF hand region for Ca^{2+} binding and heterodimer formation. Inactive calpains are heterodimers, composed of an 80 kDa proteolytic subunit (domains I-IV) and a 28 kDa regulatory subunit (domains V and VI). In the ER the calpains are inhibited by the highly specific and endogenous calpain inhibitor called calpastatin. The release of calpastatin together with Ca^{2+} stimulated dissociation of the regulatory subunit allow for a conformational change and autoproteolytic cleavage which activate the calpain enzymes [143]. Interestingly, increased expression of calpastatin had been correlated with reduced neural cell death [144].

In the retina, calpains, especially calpain 1 & 2, are distributed ubiquitously throughout the layers of retina [145]. Calpain activation had been well documented during retina neurodegeneration. For instance, the application of pharmacological inhibitors of calpains could block cell death in different experimental retina systems. Calpain inhibitor-2, Mu-F-hF-FMK was found to be able to provide neuroprotection of axonal degeneration in optic nerve fibers [146]; Calpeptin, a calpain-specific inhibitor, could also provide neuroprotection in retinal ganglion cells after Ca^{2+} influx [147].

Activation of calpains had been linked to photoreceptor cell death in IRDs and found specifically in the ONL [148]. Calpains 1 and 2 appear to be mostly activated and several inhibitors demonstrated to be effective in interfering with their activation, even if in some cases some toxicity was detected [108, 149]. Interestingly, calpains do not participate in chromatin condensation, instead they function via their specific cleavage sites in a broad spectrum of substrates, for instance, the AIF and BAX (Figure 1.5) [109]. AIF protein is a mitochondrial intermembrane space protein and is associated with non-apoptotic cell death. During the cell death process, AIF is released from mitochondria via BAX-formed pores, and subsequently translocates to the nucleus. Calpain 1 can regulate the cleavage and release of AIF from mitochondria [150]. The activation and nuclear translocation of AIF have been observed in retina degeneration [108, 138]. In several RD models, calcium overloads can be found behind the calpain activation, especially for calpain 1 and 2 [84, 149].

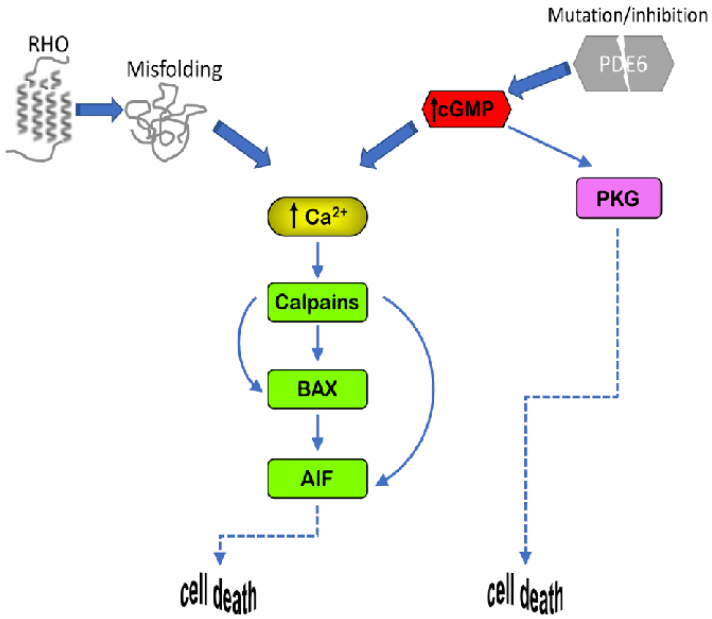

Figure 1.5 Cell death mechanism in photoreceptor degeneration. Image adapted from [84].

The complexity of the photoreceptor degenerative process, which involves cGMP, PKG and Ca^{2+}, requires a suitable and convenient system, such as a reliable *in vitro* model, to unravel the different contributions of these factors and for testing new compounds targeting these different pathways.

1.9 *In vitro* study of retinitis pigmentosa

Photoreceptors are differentiated, specialized neuronal cells, which means they are postmitotic cells. This results in the limited sources for photoreceptor cell lines as they cannot be derived from adult photoreceptor cells that cannot proliferate *in vitro*. Currently, several retinal cell lines exist for the study of inherited eye diseases. For instance, WERI-Rb1 [151] and Y-79 [152], are human cell lines derived from retinoblastomas tumors, and are highly transformed with limited characteristics of rod photoreceptors even if they express some rod specific genes. In fact, Y-79 cells show some rod-specific antigens, such as transducin, rod opsin, phosphodiesterase and recoverin [153]. Another method for retrieving photoreceptor cells is based on *in vitro* differentiation of retinal stem cells, which reside in the pigmented ciliary epithelium [154]. The differentiated cells from this procedure have been demonstrated to acquire several characteristics of rod photoreceptors, even the ability to respond to light stimuli, and are suitable for drug screening [129, 155]. However, the drawback of using this system is

the high variability intrinsic in primary cells that are isolated from ciliary epithelium, in fact not 100% of the primary cells can differentiate into photoreceptors [156].

1.9.1 661W cell

661W is a mouse photoreceptor cell line derived from retinal tumors generated in transgenic mice expressing simian virus (SV)40 T-antigen (T-ag) under the control of the human interphotoreceptor retinol-binding protein (IRBP) promoter [157]. This cell line expresses photoreceptor precursor genes, as well as some cone photoreceptor genes. In addition, 661W could be differentiated into retinal ganglion cells [158] or, by treatments with staurosporine, neuronal morphology could be induced [159]. It is also reported that 661W cell line is light sensitive and could undergo photo-oxidative stress [160]. All these features make 661W a promising tool for *in vitro* modelling photoreceptor degeneration diseases. Nevertheless, 661W does not significantly express rod photoreceptor markers and the demand of a cell line with higher expression of rod specific markers is needed for the study of rod photoreceptor degeneration and for *in vitro* high-throughput drug screening systems for the treatment of retinal degeneration. A genetic modification of the 661W retinal precursor with a rod-specific master gene might be promising to generate a cell line with rod characteristics.

1.10 cGMP analogues

In the last 40 years, a large variety of cyclic nucleotide analogues have been applied to study intracellular cyclic 3′,5′-adenosine monophosphate (cAMP) and cGMP pathways and to investigate biochemical and physiological signaling pathways, cyclic nucleotide binding partners like ion channel and protein phosphorylation [161, 162]. cGMP analogues are a class of second messenger compounds that could either inhibit or activate PKGs, and are widely used in different research areas. For instance, cGMP analogues that act as PKG activators have been found to significantly reduce cellular proliferation, migration and to increase cell death in melanoma cells [163], as well as decrease proliferation in different colon cancer cell lines [164]. In melanoma cells, the PKG activation was demonstrated to negatively target the EGF/EGFR pathway [165]. Moreover, specific cGMP analogues type can help to define the exact role of different PKG isoforms in specific cellular events. For example, the use of the activator 8-Br-PET-cGMP, prevalently targeting PKGIβ, resulted in the growth inhibition and apoptosis in human breast cancer cells [126].

cGMP analogues designed as PKG inhibitors contributed to the identification of cGMP dependent cell death mechanisms in different RD animal models. Based on this evidence, PKG can be considered an interesting target for the development of treatments for RD type diseases. Springing from this hypothesis, a number of cGMP analogues designed for PKG inhibition were synthetized to target PKGs as well as the CNG channel [129]. Those analogues carried a common motif of an Rp-configured phosphorothioate that could antagonize the activation of PKG and have the ability to bind to the cGMP binding sites in the regulatory domain, without evoking conformational changes of the enzyme required for activation of the catalytic site (Figure 1.6). According to the Cahn–Ingold–Prelog rules for chiral atoms, the prefix "Rp" is defined as the configuration of this moiety. Another feature, which deserves to be noted, is the resistance against hydrolysis by mammalian PDEs [166].

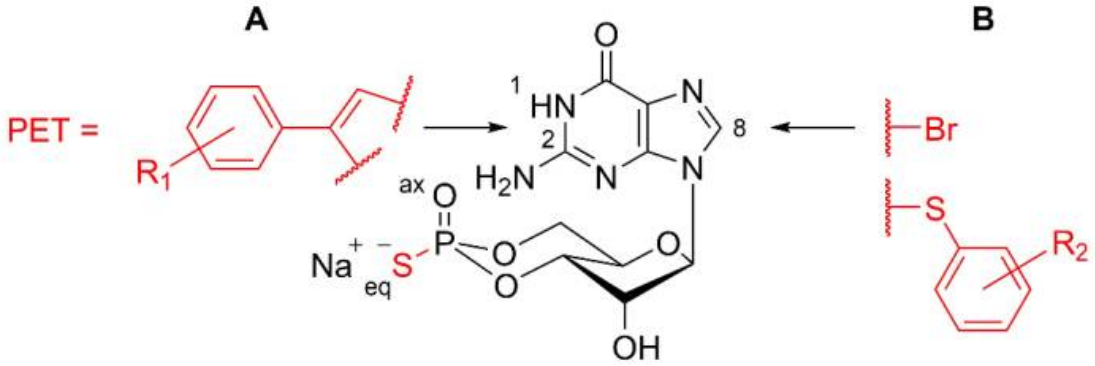

Figure 1.6 Structure of Rp-cGMP analogues. The two arrows depict the structural positions in Rp-cGMP for substituents to generate Rp-cGMPs analogues with improved inhibitory potency for PKGI or PKGII. (A) Position 1: Addition of β-phenyl-1, N^2-etheno-modifications (PET) with different substituents (R_1) to Rp-cGMPs. (B) Position 8: Addition of halogens, e.g., bromine (Br) or sulfur-connected aromatic ring systems with different substituents (R_2). Image adapted from [166].

In the study of testing cGMP analogues in IRD, 10 different cGMP analogues (CN1-10) were designed with the aim of blocking the two targets of cGMP: PKGs and CNG channel. Those analogues were tested in *rd1* derived rod-like cells and retina explants derived from *rd1* mice. Among the tested analogues, CN03 was the most promising one as it was proved to be acting on both PKGs and CNG channel [129]. Further study demonstrated that the CN03 was targeting the PKG rather than PKA, with the evidence showing that CN03 could reduce the phosphorylation VASP at site serine 239 instead of site serine 157, which are differently phosphorylated by PKG and PKA, respectively [167].

CN03 exhibited a reduction in intracellular Ca^{2+} level in photoreceptors, suggesting it could interfere with CNG channel. In addition, it also showed an effect in reducing calpain activation and nuclear localization of AIF. When it was applied to organ cultures, CN03 neuroprotective effects could be observed in retina explants from *rd2* and *rd10* mice [129].

Recently, a novel cGMP analogue called CN238 was identified with a strong protective effect in retina explants derived from *rd1* and *rd10* mice. Notably, this compound also showed an unexpected preservation in the demise of RGCs in long-term culture retina [168].

Due to the hydrophilic chemical features of the drug and the necessity to pass the blood retina barrier to reach the retina, the delivery of CN03 *in vivo* is quite challenging. To facilitate the delivery, CN03 was encapsulated in glutathione-targeted PEGylated (GSH-PEG) liposomes, which were proven to be able to deliver drugs to the retina upon systemic administration. The systemic intraperitoneal injection of encapsulated CN03 (LP-CN03) showed a protective effect in degenerating photoreceptors in *rd1*, *rd2* and *r10* mice. On the contrary, non-encapsulated CN03 didn't show any beneficial effects [129]. This suggests that evaluation of appropriate compounds combined with a drug delivery system is fundamental for *in vivo* treatment of the retina.

1.11 Delivery of compounds to photoreceptors

Compounds such as cGMP analogues might have strong therapeutic effects and at least partially, address the genetic heterogeneity of IRD. Nevertheless, to transform those compounds into successful treatments, appropriate delivery to the photoreceptor cells needs to be developed. This task can be quite challenging due to the fact that photoreceptor cells are not in directly contact with the blood vessels or with the vitreous.

The retina is protected from external agents (e.g., blood borne toxins and pathogens) by the blood–retinal barrier (BRB), which is composed of inner and outer components (inner BRB and outer BRB): The inner barrier is formed by endothelial cells (non-fenestrated vessels) in conjunction with pericytes, astrocytes and Müller glial cells, in which the Müller glial cells play an important function due to the fact that they form the outer and inner limiting membranes. The outer limiting membrane provides the shield between the neuroretina and RPE, while the inner one shields between neuroretina and vitreous humor. The outer BRB is formed by tight-junction-coupled RPE cells and endothelial cells lining the fenestrated choroidal vasculature

[169]. Though the BRB itself plays a fundamental role in the microenvironment and the protection of the retina, it also hampers the delivery of therapeutic compounds.

A variety of routes are available for drug administration to the retina, such as systematic administration, topical application, intravitreal injection [170], subretinal injection [171], suprachoroidal injection [172] and subtenon injection [173] (Figure 1.7). Each of these routes has its own specific advantages and disadvantages. Subretinal injection is the most frequently used technique in gene therapy to deliver the gene constructs with adeno-associated-virus (AAV), which is commonly used vehicle since the first approval gene therapy targeting RPE65 [174]. This procedure, however, will inevitably cause a detachment of the neuroretina form the RPE and this can be detrimental to the retina viability. Nevertheless, given that the gene therapy treatment will be needed only once in a lifetime, the benefit seems to be greater than the risk. Intravitreal injection is the most frequently used route and is widely accepted in treating age-related-macular degeneration (AMD) with the anti-vascular endothelial growth factor (VEGF) reagent. This application is easier to perform and the risk for retina damage is lower compared to subretinal injection. On the other hand, the intravitreal injection with anti-VEGF requires regular administration which will lead to an increased risk to the eye, especially related to intraocular infections [175]. A systematic administration can also be envisaged if using a drug delivery system able to target the central nervous system and pass the BRB. This has been demonstrated with liposomes conjugated with polyethylene glycol chains, that carry a glutathione (GSH) molecule [129]. In this case, a suitable drug delivery system will be crucial for developing a successful treatment.

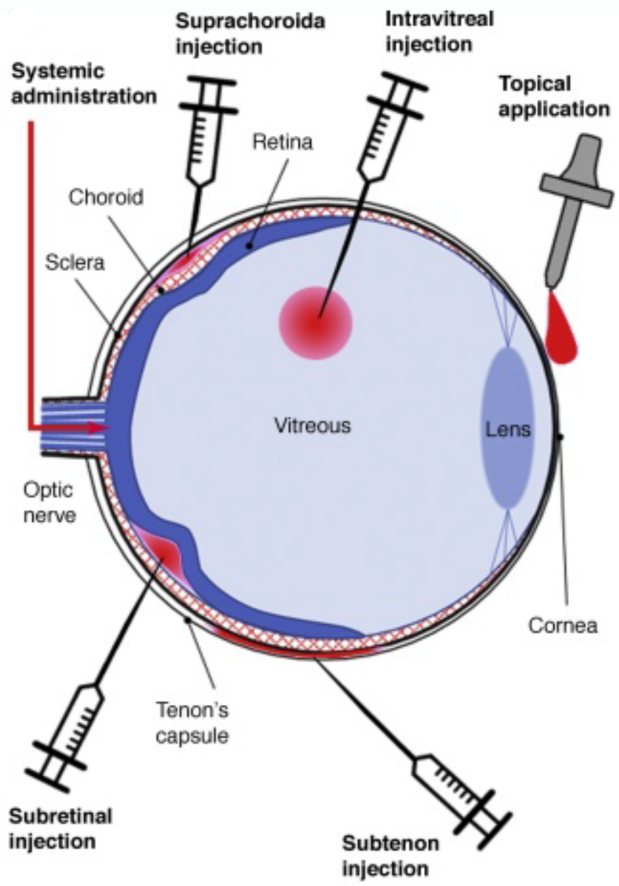

Figure 1.7 Different routes for drug administration to the retina. Image adapted from [176].

1.12 Drug delivery system (DDS)

A drug delivery system (DDS) is defined as a formulation or a device that can favour the introduction of a therapeutic substance into the body with an improvement in the efficacy and safety by controlling the drug release time, rate and location [177]. With the administration, the DDS liberates the substances that are subsequently transported across biological barriers to reach the targeted sites or the DDS is formulated to cross the biological barriers, including the plasma membrane, and to release the therapeutic substance inside the cell. Indeed, it is necessary to develop a suitable DDS to assist the drugs to achieve their desired applications in patients. A number of DDSs have emerged with different formulations, which provide therapeutic agents or compounds the ability to reach the targeted location for treating the diseases.

1.12.1 Nanoparticle (NP)

Recently nano-based formulations have catalyzed interests for those developing advanced systems of drug delivery for the retina. Nanoparticles (NPs) used as drug delivery vehicles are a class of materials with a size generally < 100 nm in at least one dimension [178]. The materials used in NPs are from various biodegradable sources, they can be, for instance, natural, lipids, metal or synthetic polymers. According to their size, morphology, physical and chemical properties, NPs can be classified into various categories. For instance, carbon-based NPs, metal NPs, ceramics NPs, polymeric NPs and lipid-based NPs are common types of NPs based on the physical and chemical properties [179].

Generally, compared to large micromolecules, NPs are uptaken more easily by cells, thus they can be served as an effective delivery system for compounds that need to reach the cytoplasm. The NPs are not simple molecules, they are typically composed of three layers: the surface layer, the shell layer and the core [180]. For therapeutic purposes, the drugs can be attached to the surface of the particles or integrated inside the particles [179]. In this case, the core formulation is an essential central part of the NP.

NPs can be regarded as an ideal DDS irrespective of their types and materials. Firstly, they can protect the cargo from degrading enzymes present in the blood or in the extracellular environment and also regulate a sustained release of the drug. Secondly, they can improve the drug localization and, consequently, efficacy. Due to the fact that some drugs or molecules can be negatively affected by environmental conditions, such as DNA and RNA for the gene therapy, thus, selection of suitable NPs is crucial [181].

Selection of NPs for achieving optimal therapeutic efficiency is based on the properties of NPs and physicochemical features of drugs. Biodegradable NPs are highly considered effective drug delivery systems because they can be effectively delivered to the targeted location and minimize side effects. Liposomes, because of their unique advantages in protecting the drugs from degradation, in site targeting and in reducing side effects, have been considered a potential drug carrier. However, the restriction in developing liposome DDS lies in some intrinsic issues: low encapsulation efficiency, undesired leakage, stability and initial rapid drug release [182]. A more rigid shell of the capsule like solid lipid or polymeric nanoparticle promises some critical advantages over liposomes to better retain the therapeutic molecules [183].

Some conventional solid lipid nanoparticles (SLNs), on the other hand, will suffer from leakage of small hydrophilic molecules during the preparation process, and they also have relatively limited space for drug encapsulation due to their compact lipid matrix networks [184]. More advanced SLNs with a larger aqueous core may be needed to incorporate additional excipient,

to preserve molecules and achieve better encapsulation properties. The application of thermo-responsive gel core or micelles was shown to improve encapsulation of hydrophilic cargo such as protein [185].

1.12.2 Nanoparticle (NP)-based technology application in retina degeneration

Varieties of NPs have been designed to improve the efficiency of drug delivery to the retina, including to the photoreceptors [176, 186, 187], as they harbor specific properties and characteristics to allow them to overcome the retina barriers by delivering with different routes, thus NPs can be applied into various treatments such as gene delivery, cell delivery, drug delivery and retina prosthesis, targeting a wide range of retina diseases.

Gene therapy holds great promise in treating IRDs. The two major gene delivery methods are viral and non-viral, the former one includes AAV, while the latter is based on NPs. Compared to AAV-based therapy, the NP-based therapy offers several unique advantages. For instance, the NPs are easy to synthesize and their structures are convenient to manipulate; Besides, the production cost of NP system is generally lower; More importantly, AAV-based delivery has the size limitation (< 5 kbp) for the genetic cargo, while this is not the case for NPs as they can easily accommodate large vector size up to 20 kbp [188]. NPs with different formulations and effectiveness have been designed and tested in various cells, and many of them have been tested in retina. For example, lipid nanoparticles with PEGylated liposome-protamine-hyaluronic acid showed an enhanced efficiency in siRNA delivery to RPE cells and to a rat model for the treatment of choroidal neovascularization [189]. Compacted DNA nanoparticles containing a plasmid with vitelliform macular dystrophy 2 promoter and a scaffold matrix attachment region promoted the persistent RPE gene expression in RPE65-associated LCA [190].

Nano-based technology also offers a great platform for drug delivery into the retina. Due to the easy manipulation of nanoparticles with different size and other properties to carry different drugs, it is highly possible to use NPs as the carriers to improve the solubility of poorly water-soluble drugs and enhance the cellular uptake of the drug, targeting the retina with different administration routes [191]. One group analyzed the effect of nanoparticles encapsulated with hydrophilic carboplatin for treating murine retinoblastoma, and found it was more effective than the carboplatin in aqueous solution in reducing tumor burden [192]. Another study explored the ability of poly lactic-co-glycolic acid (PLGA) nanoparticles in adjusting the drug release rate in a sustained fashion, which helped to batter the short half-life issue of

Bevacizumab in treating wet AMD [193]. Gold nanoparticles are functioned as a useful tool in ophthalmic diagnosis and therapy due to their antiangiogenic, anti-inflammatory properties and low cytotoxicity features. The loading of gold nanoparticles with human Wharton's Jelly derived mesenchymal stem cells that aimed to develop a cell-based therapy for retinal degeneration was tested, following the transplantation of the cells into subretinal space, a delayed retinal degeneration was observed [194]. In addition, gold nanoparticles with intravenous administration exhibited the capability of crossing blood retina barrier without evoking any cytotoxicity in mice [195].

Overall, to better achieve the protective effect of cGMP analogues against IRDs, a DDS based on the nanoparticles might be imperative. An ideal formulation of NPs should be designed taking into consideration of the delivery route (e.g. intravitreal injection) and the physicochemical features of cGMP analogues.

1.12.3 Solid lipid nanoparticle (SLN)

Solid lipid nanoparticles (SLNs) are a recently-developed nanocarrier that was first introduced in 1991 as an alternative carrier system to traditional colloidal carriers, such as emulsions, liposomes and polymeric nanoparticles [196]. SLNs are mainly constituted by solid lipid (high melting fat matrix) or modified lipid with a 10–1000 nm diameter size range. They combine the advantages of the traditional nanocarriers like polymeric nanoparticles and liposomes but are eliminated with the existing major disadvantages, i.e., polymer and phospholipid degradation, cytotoxicity, inferior stability, sterilization problems and drug leakage and fusion. SLNs are derived from oil-in-water emulsions by replacing liquid lipids with a lipid matrix that is solid at room temperature, so they contain a monolayer coated with biocompatible surfactants and phospholipids, and a hydrophobic solid core, in which both hydrophilic and hydrophobic drugs can be dispersed or dissolved (Figure 1.8) [197]. Due to the solid lipid composition, SLNs can guard the active-drug-counteracting biochemical degradation, thus compared to polymeric nanoparticles and liposomes, they are better substitutes [198]. SLNs also display a sustained release feature in advantage of the solid lipids, modified drugs and the ingredients that keep particles with a long diffusion pathway. The drug release from SLNs is dependent on the drug location in the formulation and solid lipid type. The fabrication from biodegradable and biocompatible ingredients which are able to incorporate both hydrophilic and lipophilic bioactives, makes SLNs an ideal DDS with a controlled and targeted feature.

SLNs have been widely used in the encapsulation of hydrophobic and hydrophilic drugs for avoiding degradation in the body and maintaining a sustainable release.

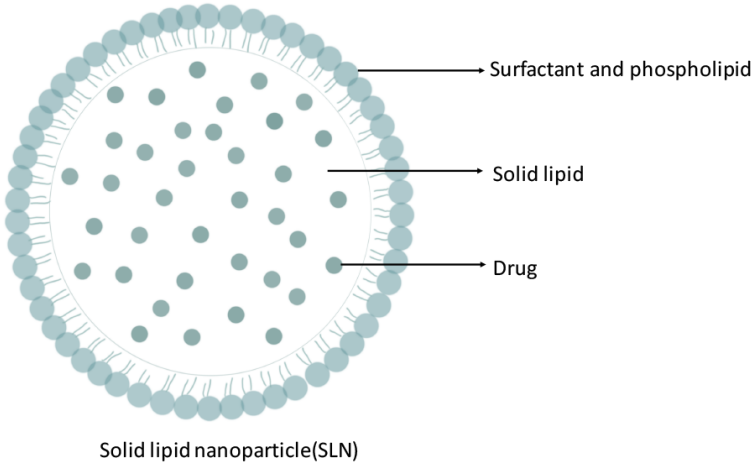

Figure 1.8 General structure of solid lipid nanoparticle (SLN) loaded with drug.

Though SLNs bear excellent features compared to traditional colloidal carriers, they exhibit several disadvantages. SLNs are usually compactly packed with lipid matrix networks, thus the available space for drug encapsulation is limited, leading to a poor drug loading capacity. The loading or encapsulation of drugs in SLNs are affected by many factors: the drug dissolution or dispersal in the lipid matrix and the interaction of lipid melt and drug. Moreover, the possibility of drug expulsion during storage and a water content (70–90%) in the dispersions are hard to ignore [199]. Thus the modification of SLNs with different formulations would be necessary to minimize or diminish these drawbacks. For instance, the surface modification with N-carboxymethyl chitosan coated curcumin-loaded SLN was found to improve the bioavailability of curcumin delivery through enhanced cellular and lymphatic uptake [200]. The modification of surface charge, such as the positively charged SLNs are rising materials for gene delivery, due to the importance of the interaction between NPs and cell membranes to open the entry way into cells. Surfactants and cationic lipids are often used to modulate positive charge of the SLNs surface to enhance cellular uptake and drug bioavailability.

Majorities of SLNs have been used to delivery drugs to the ocular surface such as cornea, the low bio-toxicity of SLNs caused by physiological lipids preparation is especially feasible for ocular drug delivery as they can improve the absorption of drugs as well as the bioavailability of both hydrophilic and lipophilic drugs [201, 202]. Nevertheless, due to their long-term stability, biodegradability, limited toxicity and economic production features, SLNs are considered promising candidates for gene and drug delivery to retina. SLN-based nonviral vectors with a subretinal or intravitreal administration successfully transferred genes to the

RPE and photoreceptors in a mouse model of X-linked juvenile retinoschisis [203]. Another study showed that compritol SLN formulation could enhance the protective effect of betulinic acid derivatives in Müller cells with oxidative injury [204]. SLNs have also been investigated in retinal gene therapy, with the study of transfection and intracellular trafficking in RPE cells [205].

To sum up, SLNs serve as an ideal drug delivery system with various distinct characteristic features such as low toxicity, maximum drug bioavailability, specific tissue targeting, large surface area, controlled drug release, minimal immune response, superior cellular uptake, sufficient drug loading capacity, and cost effectiveness, all these features make SLNs a unique DDS in comparison to polymeric NPs and other formulated NPs. The addition of SLN modifications such as the surface modification, surfactant modification or positive charge modification render the improvement practicable. More advanced nano-system based on SLNs will be further developed and will give new insights in drug delivery applications.

2. AIM OF THE THESIS

RP is one type of IRDs characterized by a primary degeneration of rod photoreceptors followed by the loss of cone photoreceptors. The dysregulation of cGMP and Ca^{2+} has already been linked to photoreceptor cell death. Abnormal accumulation of cGMP in photoreceptors is a common molecular event in several types of hereditary retinal degeneration. It is hypothesized that high levels of cGMP lead to over-activation of PKG and/or CNG channel with excessive Ca^{2+} influx, which bring on photoreceptor cell death, therefore, the PKG and Ca^{2+} are important targets for molecular intervention and for therapeutic approaches. Nevertheless, the downstream processes after PKG and Ca^{2+} influx still remain largely unknown. Several challenges hinder the study of molecular mechanism and the development of therapeutic approaches for RP, one of them is the lack of an appropriate *in vitro* model for drug screening. Due to the fact that photoreceptor cells are postmitotic neurons and cannot regenerate themselves, photoreceptor cell line cannot be generated from adult photoreceptor cells. Secondly, the development of a rod photoreceptor-like cell line would be useful for testing drug candidates that target IRDs. Previous studies have shown the successful protective effect of cGMP analogue, CN03 with a PKG inhibitor activity, in different retina degeneration models. Since then, more and more formulations of novel cGMP inhibitory analogues have been generated for treating IRDs. Nevertheless, the hydrophilic feature of these compounds hampers them from achieving complete entrance into the cells, affecting the compound efficiency. Thus, a DDS would be critical for improving the efficiency of delivering hydrophilic compounds to the retina.

The aim of this project was: i) To develop a new *in vitro* photoreceptor degeneration model based on 661W cells for molecular studies of RP, including the downstream of cGMP pathway: PKG and the Ca^{2+}; ii) Drug screening with cGMP inhibitory analogues and other neuroprotective compounds in the new *in vitro* RP model; iii) To generate a drug delivery system based on nanoparticles and to test the nanoparticles in retinal cells for the purpose of delivering hydrophilic compound such as cGMP analogues to the retina.

3. MATERIALS AND METHODS

3.1 Cell culture and treatment

3.1.1 Cell culture

661W cells were cultured in low glucose Dulbecco's Modified Eagle Medium (DMEM, 22320022, Gibco, Glucose 1 mg/mL) supplemented with 10% fetal bovine serum (FBS, 26140079, Gibco), 2 mM glutamine, 100 U/mL penicillin, and 100 µg/mL streptomycin (Thermo Fisher Scientific, Rodano, Italy) in an incubator at 5% CO_2 and 37°C. ARPE-19 cells were cultured in Dulbecco's modified Eagle's medium and Ham's F12 nutrient mixture (DMEM/F12; 11320033, Gibco) supplemented with 10% FBS, 100 U/mL penicillin, and 100 µg/mL streptomycin in an incubator at 5% CO_2 and 37°C. Cells were passaged and sub-cultured every three days.

3.1.2 Genetic modification of 661W cells

NRL transduction in 661W cells: 661W cells were transduced with a replication-incompetent retrovirus expressing NRL. The retrovirus was generated by cloning murine *Nrl* cDNA (accession number: L14935) between the *Eco*RI and *Xho*I restriction sites of the pLXSN vector. The plasmid was transfected in Phoenix-ECO packaging cells for the production of a retrovirus, which also expressed the neomycin resistance gene.

Isolation of single-cell clones: Transduced cells were selected by treatment with G418 and clones were generated by limiting dilution. Each individual cell was isolated by plating them at low density (i.e. $\leqslant$1 cell per well) in 96-well plates, single colonies were expanded and an aliquot from each colony was stored in liquid nitrogen.

3.1.3 Cell treatment with compounds

Cells were seeded on glass coverslips coated with 3 µg/mL laminin (L2020, Sigma) in a 24-well plate at a density of 20,000 cells per well or in 96-well plates at a density of 6,000 cells per well. Treatments with corresponding compounds started 24 h later.

For zaprinast (Z0878, Sigma) treatment, cells were treated with different concentrations, or with an equal volume of DMSO (vehicle) as control, for 24 h.

For PA5 and PA6 treatments, cells were treated with different concentrations, or with an equal volume of H_2O (vehicle) as control, for 24 h.

For cGMP analogues (Biolog, Bremen, Germany) treatment, following the day of seeding, cells were treated for 2 h with medium containing various concentrations of CN03 or CN238, and

then cells were exposed to 400 μM zaprinast in the presence of CN03 or CN238 for 24 h, control samples were treated with an equal volume of DMSO or H_2O.

For cyclosporine A (B1922, Apexbio) treatment, following the day of seeding, cells were treated with different concentrations of cyclosporine A for 24 h, or cells were treated with 20 μg/mL cyclosporine A together with 400 μM zaprinast for 24 h. Control samples were treated with an equal volume of DMSO (vehicle).

For the other compounds treatment, following the day of seeding, cells were treated for 2 h with medium containing either 10 nM PEDF (a kind gift from S.P. Becerra) or 20 μM calpastatin peptide (208902, Calbiochem) or 50 μM D-*cis*-Diltiazem (D2521, Sigma, Milan, Italy), and then were stressed with 400 μM zaprinast together with the compounds for 24 h, an equal volume of DMSO or H_2O were added to the cells as a control.

3.2 Murine lines

Three animal models for retinitis pigmentosa were used for the experiments: 1) $Rho^{P23H/+}$ mice in a C57BL6J background are knock-in mice bearing the P23H mutation in the murine *Rhodopsin* gene (a kind gift from K. Palczewski); 2) *rd1* mice in a C3H background bearing a *Pde6b* gene mutation (retinas provided by F. Paquet-Durand); 3) *rd10* mice in a C57BL6J background bearing a point mutation in the *Pde6b* gene (retinas provided by F. Paquet-Durand). As control, age-matched wild type (WT) C3H and C57BL6J animals were used. Retinas were collected from two $Rho^{P23H/+}$ animals and two controls at PN19 (postnatal day 19), from three *rd1* mice and three controls at PN11, from three *rd10* mice and three controls at PN18. All animal procedures were carried out according to protocols approved by the European Community Council 2010/63/EU and Italian legislation (Legislative decree 26/2014).

3.3 RT-PCR

3.3.1 RNA extraction

Total RNA was extracted from cells using RNeasy Mini Kit (74104, Qiagen, Milan, Italy) according to the manufacturer's instructions. 700 μL QIAzol lysis reagent were added to the cell sample, disrupting and homogenizing by pipetting and vertexing, then the homogenate was incubated at room temperature for 5 min. 140 μL chloroform were added to the homogenate followed by shaking vigorously for 15 s, and was incubated at room temperature for 2-3 min. Then the sample was centrifuged for 15 min at 12000 x g at 4°C. The upper aqueous phase was transferred to a new collection tube and 1.5 volumes of 100% ethanol was added inside, and

mixed it thoroughly by pipetting. The sample then was pipetted into the mini column in a 2 mL collection tube, followed by the centrifugation at ⩾ 8000 x g for 15 s at room temperature and the flow-through was discarded. 700 µL buffer RWT were added to the mini column, centrifuged for 15 s at ⩾ 8000 x g and the flow-through was discarded. 500 µL buffer RPE were added to the mini column, centrifuged for 15 s at ⩾ 8000 x g and the flow-through was discarded. 500 µL buffer RPE were added to the mini column, centrifuged for 2 min at ⩾ 8000 x g and the flow-through was discarded. The mini column then was transferred to a new 1.5 mL collection tube and 30-50 µL RNase-free water were directly added to the column membrane, centrifuged for 1 min at ⩾ 8000 x g. The RNA concentration was quantified by Nanophotometer (NP80, IMPLEN).

3.3.2 cDNA synthesis

cDNA was synthesized from 1 µg of RNA using Transcriptor High Fidelity cDNA Synthesis Kit (04379012001, Roche). 1 µg RNA was mixed with 1 µL anchored-oligo (dT)18 primer and water to reach 11.4 µL total volume. The mixture was heated at 65°C for 10 min and then chilled on ice. The RT mix (1X Transcriptor High Fidelity Reverse Transcriptase Reaction Buffer, 20U Protector RNase Inhibitor, 1mM Deoxynucleotide, 5 mM DTT, 10U Transcriptor High Fidelity Reverse Transcriptase) was added to the mixture to the final volume of 20 µL. The reaction was incubated for 30 min at 55°C and 5 min at 85°C. The reaction was stopped by placing the tube on ice, the cDNA was used for amplification.

3.3.3 PCR

PCR was performed by Platinum Taq DNA Polymerase (15966055, Invitrogen) with 1 µL cDNA using specific primers (Table 1). Each reaction sample contained:

10x Buffer	2.5 µL
$MgCl_2$ (50µM)	0.75 µL
dNTPs (2.5mM)	2.5 µL
Forward Primer (10 µM)	0.5 µL
Reverse Primer (10 µM)	0.5 µL
Taq Polymerase	0.1 µL
cDNA	1 µL
H_2O	17.15 µL

The reaction was incubated at the following conditions: 30'' at 94°C and 30'' at 60°C and 30'' at 72°C for 35 cycles. Amplified products were analyzed by electrophoresis in a 1% agarose (9012-36-3, Sigma) gel and visualized by Ethidium Bromide (1239-45-8, Sigma) staining.

3.4 Real-time qPCR

Real-time qPCR was carried out with the Universal SYBR Green supermix (1725120, Bio-Rad, Segrate, Italy) using 1 µL cDNA on the CFX96 Real-time PCR Detection system (Bio-Rad). Each reaction sample contained:

SYBR Green supermix	10 µL
Forward Primer (3µM)	1 µL
Reverse Primer (3µM)	1 µL
cDNA	1 µL
Water	7 µL

The following conditions were applied: 30'' at 95°C and 39 cycles of 5''at 95°C, 30'' at 60°C, the relative gene expression level was calculated using the ribosomal protein gene *Rps26* as a reference. The primers used for quantitative PCR are listed in Table 1.

Table 1 Primers used for RT-PCR and real-time qPCR

	Forward primer	Reverse primer
Rps26	AAGTTTGTCATTCGAACATT	GATCGATTCCTAACAACCTTG
Rho	AATCTCGAGGGCTTCTTTGC	CCACGTAGCGCTCAATGGC
Nrl	GCTACTATTCAGGGAGCCC	GCAGCTGCCGGTTCA
Gnat1	GAGCCTCAGAATACCAGCTC	GGCACATATCCTGGAGTCAC
Cngb1	TCTGGCTCCTCATGGATTAC	TGATGTCCCCGCCTTTGAC
Cnga1	CAACTGGACGATGATTATTGC	TCACTAGCAGCCCTT
Pde6b	CGGAATTCCTGAGCCAAGGAAGACCA	GGGTTCGAAGGTGTTCCTGCTGCTGTG
Nr2e3	TCCCACAGAGTTTGCCTGC	CTCCACGTGCTCAGGATCCT
*Nr2e3**	GAAACACGAGGCCTGAAGGA	GGGAGCAGGAGCAATTT
Guca	TGCATAGACAGGGACGAGC	GCACTCATGGATGAGTCGC
Pde6g	ATCCCTGGAATGGAAGGCC	TAAATGATGCCATACTGGGC
Crx	TAAGATCAATCTGCCTGAGTC	GCTGTTGCTGTTTCTGCTGC
Pde6c	GTGGAGTCCCGGAGAAGC	GTCCTGATGGTGTACAGTGC
Pde6h	CAGTTCAAGAGCAAGCCTCC	TTCCCAGGGACAGATGACC
Cnga3	GCTGGTTCGAGCCCGGAC	CCAGCTTGAAGTGCAAGGTC
Cngb3	TGGAAGCCAGCTCTCAGAC	CTCTGGGGTTTGAAACAAAAC
Prkg1a	GCGTTCCGGAAGTTCATCAA	GCCACAATCTCCTGGATCTG
Prkg1b	CTTCTACCCCAAGAGCCCAC	ACAATCTCCTGGATCTGTGACAG
Prkg2	CCTGACATTTCATCCGGAGG	TTCCGTCACCTTTACGGAGAG
Nfatc1	GCCTCGAACCCTATCGAGTG	AGTTATGGCCAGACAGCACC
Il18	CCGCCTCAAACCTTCCAAATC	TGTCTGATTCCAGGTCTCCATTT
Il2	AGATGAACTTGGACCTCTGCG	TGTGTTGTCAGAGCCCTTTAG

* Primers used only for real-time qPCR.

3.5 Immunofluorescence

Cells were seeded on glass coverslips in a 24-well plate at a density of 2×10^4 cells/well. After incubation with corresponding treatments, cells were rinsed with phosphate-buffered saline (PBS), fixed with 2% paraformaldehyde (PFA, 158127, Sigma) for 10 min. Cells were then blocked and permeabilized with 3% bovine serum albumin (BSA, A7906, sigma) and 0.1% TritonX-100 (T8787, Sigma) in PBS for 1 h at room temperature followed by incubation with primary antibodies in PBS overnight at 4°C. The following day cells were washed five times with PBS and incubated with secondary antibodies for 1 h at room temperature. For nuclear

staining, cells were stained with 0.1 µg/mL 4′,6-Diamidino-2-phenylindole dihydrochloride (DAPI, D9542, Sigma). Slides were mounted with Mowiol 4–88 and cells were observed using the Zeiss Axio Imager A2 fluorescence microscope. The antibodies used for immunofluorescence are listed in Table 2.

Table 2. List of primary and secondary antibodies used in IF experiments

Antibody	Provider	Cat.no.	Dilution
Mouse-anti-Rhodopsin (1D4)	Sigma	MAB5356	1:100
Rabbit-anti-PDE6-beta	Abcam	ab5663	1:100
Rabbit-anti-GNAT1	Sigma	SAB4501223	1:300
Sheep-anti-cGMP	Jan de Vente & Harry Steinbusch, Maastricht University, the Netherlands,	///	1:500
Mouse-anti-NAFTc1	Santa Cruz Biotechnology	sc-7294	1:100
Alexa Fluor™ 488 goat anti-mouse	Invitrogen	A1101	1:1000
Alexa Fluor™ 568 goat anti-rabbit	Invitrogen	A11011	1:1000
Alexa Fluor 568 donkey anti-sheep	Life technologies	A21099	1:1000
Alexa Fluor™ 568 goat anti-mouse	Invitrogen	A1104	1:1000

3.6 Flow cytometry analysis of cGMP

Cells were detached, collected by centrifugation at 300 xg for 5 min and fixed with cold 2% PFA at room temperature for 20 min. After washing with PBS and centrifugation, cells were resuspended in permeabilization buffer (0.1%TritonX-100 in PBS) and incubated for 20 min at room temperature. After centrifugation, cells were incubated with blocking buffer (3%BSA in PBS) for 30 min. Cells were, then, incubated with sheep-anti-cGMP primary antibody (Jan de Vente & Harry Steinbusch, Maastricht University, the Netherlands, 1:500) for 30 min at room temperature. After rinsing the cells three times with PBS, cells were resuspended in the secondary antibody (Alexa Fluor™ 488 donkey anti-sheep, A11015, Invitrogen, 1:1000) and incubated for 30 min at room temperature. Cells were washed three times with PBS, resuspended in 500 µL PBS and were immediately analyzed using the Attune® NxT Acoustic Focusing Cytometer. Fluorescence was measured at an excitation wavelength of 488 nm, mean fluorescence intensity and fluorescence positive cells were calculated. Throughout the whole analysis, channel gain and voltage were maintained the same.

3.7 Flow cytometry analysis of calcium

For the analysis of intracellular calcium levels, cells were incubated with 1 μM Fluo-4 AM (F14201, ThermoFisher) at 37°C for 30 min in Hank's balanced salt solution (HBSS, 14170112, Thermofisher) in the dark. After incubation, cells were washed twice with HBSS and once with PBS. Cells were then detached by treatment with Accutase^{TM} (SCR005, Millipore, Milano, Italy), collected by centrifugation at 300 xg for 5 min at room temperature and resuspended in 500 μL of PBS. Cells were immediately analyzed using the Attune® NxT Acoustic Focusing Cytometer. Fluorescence was measured at an excitation wavelength of 488 nm. Mean fluorescence intensity and fluorescence positive cells were calculated. Throughout the whole analysis, channel gain and voltage were maintained unvaried.

3.8 TUNEL assay

3.8.1 TUNEL assay in cells

Cells were seeded on glass coverslips in a 24-well plate at a density of 2×10^4 cells/well. After incubation with corresponding treatments, cells were rinsed with PBS, fixed with 2% PFA for 10 min, followed by permeabilization with 1.0 M Na^+ Citrate and 0.1% TritonX-100 on ice for 2 min. After washing with PBS, cells were incubated with TUNEL solution (In situ Cell Death Detection Kit, 12156792910, TMR red, Roche) for 30 min at 37°C. Cell nuclei were stained with 0.1 μg/mL DAPI. Slides were mounted with Mowiol 4-88 and cells were observed using the Zeiss Axio Imager A2 fluorescence microscope. The dead cells quantification was performed by counting all TUNEL labeled cells in each field and dividing by the total number of cells, based on nuclear DAPI staining, in each counted field. The average cell death percentage from at least 3 independent biological replicates was plotted using GraphPad Prism.

3.8.2 TUNEL and Immunofluorescence double-labeling assay in retina section

Eyes were taken from mice at the day of sacrifice (PN19), and were fixed with Davidson's Fix Solution (8% formaldehyde, 32% ethanol, 11% acetic acid). Eyes were then dehydrated with increasing graded ethanol (70% - 95% - 100%), washed with xylene and included in paraffin (Paraplast, P3558, Sigma). Retinas were sectioned at 14 μm with a microtome (Leica, RM2125RT), and sections containing the optic nerve were rehydrated with decreasing graded ethanol (100% - 95% - 70% - 50%). Then the sections were fixed with 2% PFA for 30 mins. After washing with PBS, retina sections were permeabilized with 0.1 M Na^+ Citrate buffer boiling for 5 min. After PBS wash, sections were incubated with TUNEL solution (In situ Cell

Death detection Kit, TMR red, Roche) for 60 min at 37°C. Then the sections underwent a blocking and permeabilization process with 3% BSA and 0.1% TritonX-100 in PBS for 1 h at room temperature followed by incubation with primary antibody (Mouse-anti-NFATc1, 1:100) in PBS overnight at 4°C. The second day sections were incubated with secondary antibody (Alexa Fluor^{TM} 488 goat anti-mouse, 1:1000) and 0.1 μg/mL DAPI for 40 min. The sections were mounted with Mowiol 4-88 and were observed using the Zeiss Axio Imager A2 fluorescence microscope.

3.9 Ethidium homodimer assay

Cells were seeded on glass coverslips in a 24-well plate at a density of 2×10^4 cells/well. At the end-point of each treatment the medium was removed and cells were fixed in 2% PFA in PBS for 10 min at room temperature. After washing with PBS for three times, slides were incubated in the dark with 1 μM Ethidium Homodimer (46043, Sigma) for 2 min and followed by PBS washes. Nuclei were stained with 0.1 μg/mL DAPI and slides were mounted with Mowiol 4-88. Cells were then photographed using a Zeiss Axio 40 fluorescence microscope. The dead cells quantification was performed by counting all ethidium homodimer labeled cells in each field and dividing by the total number of cells, based on nuclear DAPI staining, in each counted field. The average percentages of dying cells were obtained from at least three independent biological replicates and plotted using GraphPad Prism.

3.10 Calpain activity assay

Cells were seeded on glass coverslips in a 24-well plate at a density of 2×10^4 cells/well, after treatment, cells were washed with PBS and incubated in calpain reaction buffer (CRB: 25 mM HEPES-KOH pH 7.3, 65 mM KCl, 2 mM $MgCl_2$, 1,5 mM $CaCl_2$, 2 mM DTT) for 15 min. Then cells were incubated with fresh CRB containing 2 μM fluorescent calpain substrate 7-amino-4-chloromethylcoumarin (t-BOC-Leu-Met, Molecular Probes) for 1 h at 37°C. After washing with CRB, cells were mounted with Mowiol 4-88 and photographed using a Zeiss Axio 40 fluorescence microscope.

3.11 Total protein extraction

Cells were cultured in a 100 mm petri dish and harvested by detachment with trypsin treatment, the pellet was collected and washed with PBS on ice. After centrifuging, the pellet was lysed in 200 μL lysis buffer (50 mM Tris-HCl pH 7.8, 1% NP-40, 0.25% Na-deoxycholate, 150 mM

NaCl,1 mM EDTA, 1% protease inhibitor, 1% phosphatase inhibitor), agitated on ice for 30 min. The lysis mixture was centrifuged at 10000 xg for 20 min, 4°C, the supernatant was collected in a new tube. The protein was stored at -80°C for future use.

3.12 Protein concentration quantification

The concentration of protein was detected by Bio-Rad protein assay, which is based on the Bradford dye-binding method [206]. After preparing the dye reagent by dilution of 1 part of concentrated dye reagent with 4 parts of double-distilled water, a protein standard was prepared by six dilutions of BSA from 0.1 mg/mL to 2 mg/mL. Protein solutions were assayed in triplicate. 10 μL of each standard or sample protein were pipetted to the microplate in separate wells. 200 μL dye reagent was added and mixed thoroughly. The microplate was incubated at room temperature for at least 5 min and absorbance was measured at 595 nm by a microplate reader (Labsystems Multiskan MCC/340). The relative concentration of sample protein was compared to the standard curve built by the BSA protein standard values.

3.13 Western blot

3.13.1 Buffer and solution preparation

Running buffer:

25 mM Tris base

190 mM glycine

0.1% SDS

Check pH and adjust to 8.3

Transfer buffer:

25 mM Tris base

190 mM glycine

20% methanol

Check pH and adjust to 8.3

TBST buffer:

20 mM Tris base

150 mM NaCl

0.1% Tween-20

Check pH and adjust to 7.6

Blocking buffer:
5% milk or BSA (bovine serum albumin) in TBST buffer

3.13.2 Sample preparation

Protein samples were denatured by adding 4X Laemmli sample buffer (50 mM Tris-HCl pH 6.8, 2% SDS, 10% glycerol, 5% β-Mercaptoethanol, 0.1% Bromphenol Blue) and were boiled at 99°C for 5 min. Samples then were aliquoted and stored at -20°C for future use.

3.13.3 SDS-PAGE gel preparation

The SDS-PAGE gel was composed of the stacking gel and different percentages of separating gel (8%, 10% or 12%). The compositions of the gel were as follows:

Stacking gel	Volume
H_2O	1.4 mL
Acrylamide/Bis solution (30% 29:1; Bio-Rad)	330 µL
Tris-HCl (0.5 M, pH 6.8)	250 µL
10% SDS	20 µL
10% Ammonium persulfate (APS)	20 µL
N,N,N′,N′-tetramethylethylene-diamine	2 µL
Total	2 mL

Separating gel	8%	10%	12%
H_2O	2.3 mL	2 mL	1.7 mL
Acrylamide/Bis solution (30% 29:1; Bio-Rad)	1.3 mL	1.7 mL	2 mL
Tris-HCl (1.5 M, pH 8.8)	1.3 mL	1.3mL	1.3 mL
10% SDS	50 µL	50 µL	50 µL
10% Ammonium persulfate (APS)	50 µL	50 µL	50 µL
N,N,N′,N′-tetramethylethylene-diamine	3 µL	2 µL	2 µL
Total volume	5 mL	5 mL	5 mL

3.13.4 SDS-PAGE gel electrophoresis, protein transfer, immunoblotting and chemiluminescence detection

20 µg of total proteins were loaded into each well of SDS-PAGE gel, along with 5 µL molecular weight marker. The gel was run for 1-2 h at 90-120 V for protein seperation. The P 0.45 PVDF blotting membrane (10600023, Amersham) was activated with dipping in 100% methanol for 1 min and followed by rinsing with transfer buffer. Proteins from the gel were transferred to the PVDF membrane on a blotting support covered with papers and sponges under the condition of a constant voltage (90V) for 90 min at 4°C. The membrane was then blocked at room temperature with blocking buffer for 1 h, followed by incubation with primary antibody at appropriate dilutions overnight at 4°C. The following day the membrane was washed three times with TBST buffer and incubated with HRP-conjugated secondary antibody in blocking buffer at room temperature for 2 h. After washing with TBST buffer, the membrane was incubated in the chemiluminescent substrate (Clarity Max Western ECL Substrate, 170-5062, Bio-Rad) for 5 min according to the manufacturer's instructions. Then the membrane was imaged with a chemiluminescent imaging system (ChemiDoc touch imaging system, Bio-Rad, Segrate, Italy). The antibodies used for western blot are listed in Table 3:

Table 3. List of primary and secondary antibodies used in western blot experiments

Antibody	Provider	Cat.no.	Dilution
Mouse-anti-Rhodopsin (1D4)	Sigma	MAB5356	1:1000
Rabbit-anti-PDE6-beta	Abcam	ab5663	1:500
Rabbit-anti-GNAT1	Sigma	SAB4501223	1:1000
anti-αII-spectrin	Enzo Life	AA6, BML-FG6090	1:2000
Mouse-anti-pVASP (ser239)	NanoTools	S239, 0047-100/VASP-16C2	1:2000
Rabbit-anti-pRhoA (ser188)	Abcam	ab32046	1:1000
Mouse-anti-α-vinculin	Sigma	V4139	1:10,000
Rabbit-anti-α-tubulin	Sigma	T6199	1:2000
Donkey-anti-Rabbit IgG-HRP	Amersham	NA934V	1:1000
Donkey-anti-Mouse IgG-HRP	Amersham	NA931V	1:1000

3.14 Proteomic analysis

3.13.1 Protein extraction

Cells were cultured in a 100 mm petri dish and harvested by detaching with trypsin treatment, the pellet was collected and washed with PBS on ice. After centrifuging, the pellet was lysed in 200 μL lysis buffer (50mM Tris-HCl pH 7.8, 50mM NaCl, 1mM EDTA, 5mM NaH_2PO_4, 1mM DTT, 1% protease inhibitor, 1% phosphatase inhibitor), agitated on ice for 30 min. The lysis mixture was centrifuged at 10000 xg for 20 min, 4°C. The supernatant was collected in a new tube. The protein was stored at -80°C for future detection.

3.14.2 Phosphopeptide Enrichment and LC-MS/MS

The phosphopeptide enrichment and LC-MS/MS analysis were performed at Lund University by our collaborators.

3.15 Cell viability by MTT assay

Cells were cultured on a 96-well plate at a density of 6000 cells/well. After treatments, the medium was aspirated from the 96-well plate and cells in each well were incubated with 50 μL of 1 mg/mL 3-(4,5-dimethylthiazol-2-yl)-2,5-diphenyl tetrazolium bromide (MTT, M5655, Sigma) in culture medium solution for 90 minutes at 37°C. After supernatant removal, the purple formazan crystals were dissolved in 100 μL isopropanol. The plate was shaken for 10 min and optical density (OD) was measured at 570 nm using a microplate reader (Labsystems Multiskan MCC/340, Fisher Scientific, Rodano, Italy). The average absorbance from at least 3 biological replicates was plotted using GraphPad Prism.

3.16 Synthesis and characterization of nanoparticles

The synthesis and physicochemical characterization of nanoparticles were performed by Inocure. The procedure of solid lipid nanoparticle (SLN) formulation is illustrated in Figure 2.1.

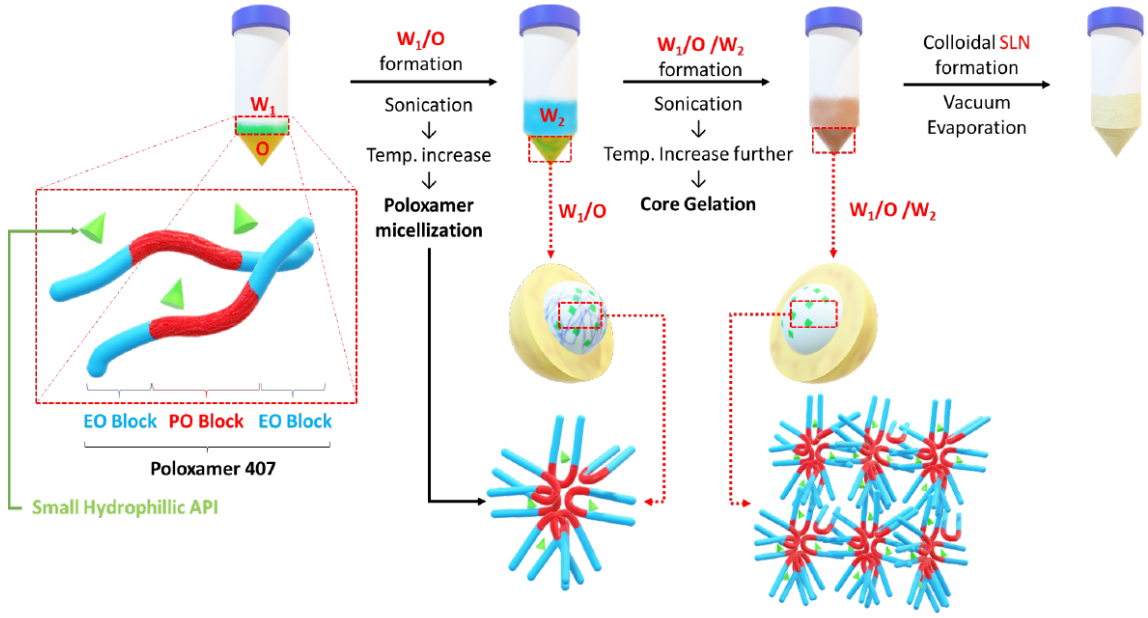

Figure 2.1 Procedure of Solid Lipid Nanoparticle (SLN) formulation. Core gelation procedure of thermo-responsive poloxamer 407 and procedure for SLN generation with a size range of 200-250 nm.

3.17 Fluorescence microscopic analysis for nanoparticle visualization

661W cells were seeded on glass coverslips in a 24-well plate at a density of 4×10^4 cells/well. After 24 h, cells were exposed to different concentrations of RhoB loaded SLN (RhoB-SLN) for 5 h. Cells were then rinsed with PBS for 3 times, fixed with 2% PFA for 10 min and nuclei were stained with 0.1 µg/mL DAPI for 40 min. Slides were mounted with Mowiol 4-88 and cells were observed using the Zeiss Axio Imager A2 fluorescence microscope. Mean fluorescence intensity (MFI) of single cell was quantified by ImageJ software ($n_{cells} \geqslant 10$).

For compound release assays, 24 h after seeding, ARPE-19 cells were treated with medium containing 200 µg/mL blank SLN (blank); freely dissolved tracer (ANTS); free tracer together with quencher (free ANTS/DPX), or 200 µg/mL SLN loaded with ANTS/DPX (ANTS/DPX-SLN). After 5 h, the medium was replaced with fresh medium without any particles or fluorophores and the incubation was continued for 24 h, 48 h, or 72 h.

3.18 Immunofluorescence for nanoparticle visualization

ARPE-19 cells were seeded on glass coverslips in a 24-well plate at a density of 6×10^4 cells/well. After 24 h, cells were exposed to 200 µg/mL RhoB-SLN for 5 h. As control, cells were treated with free RhoB solution at the same concentration (20 µM) of RhoB present in

the nanoparticle solution. A blank was prepared by incubating the cells with nanoparticles containing no fluorophores. After incubation, cells were rinsed with PBS for 3 times, fixed with 2% PFA for 10 min. Following the PBS washing, cells were blocked with 3%BSA for 1 h. Cells were then incubated with Rabbit-anti-ZO-1 (Invitrogen, 33-9100, 1:100) primary antibody overnight at 4°C. After washing three times with PBS, cells were incubated with the Alexa Fluor® 488 goat-anti-rabbit secondary antibody (Life technologies, 1:1000) and 0.1 μg/mL DAPI for 40 min at room temperature. Slides were mounted with Mowiol 4-88 and cells were observed using the Zeiss Axio Imager A2 fluorescence microscope.

3.19 Flow cytometry analysis of nanoparticles uptake in cells

ARPE-19 and 661W cells were seeded on 12-well plates at a density of 1×10^5 cells/well. After treatment with control (20 μM RhoB) or 200 μg/mL RhoB-SLN, cells were washed with PBS and detached with 500 μL Accutase and collected by centrifugation at 300 x g for 5 min at room temperature. The cells were washed three times with 500 μL PBS and collected by centrifugation at 300 x g for 5 min at room temperature. The cell pellet was resuspended with 500 μL of PBS and RhoB fluorescence was immediately analyzed at the Attune® NxT Acoustic Focusing Cytometer. The channel voltage and gain were maintained constant throughout the whole analysis.

3.20 Statistical analysis

Data are presented as the means ± SEM. Unpaired Student's t-test was applied to compare two groups. Analysis of variance (ANOVA) was used for comparisons of data with greater than two groups. Post hoc comparisons were performed with Bonferroni test. Significance was set at * $P < 0.05$, ** $P < 0.01$, *** $P < 0.001$, a value of $P < 0.05$ was considered significant. All statistical analyses were performed using GraphPad Prism version 7 (GraphPad software, San Diego, CA, USA) or SPSS (Statistics 21; IBM Inc., Bentoville, AR, USA). Data for each statistic were obtained from at least three biological replicates or three independent experiments.

4. RESULTS AND DISCUSSION

4.1 Generating a new *in vitro* model for studying retinitis pigmentosa

As a genetic disease, RP bears a great heterogeneity that hinders the study of cell death mechanism and the development of therapeutic approaches. In order to address this limitation, a better understanding of cell biology and molecular mechanism underlying photoreceptor degeneration is required. One of the main hurdles is the lack of an appropriate *in vitro* photoreceptor degeneration model, due to the fact the photoreceptors are postmitotic neurons and are not able to regenerate themselves. Besides, rod photoreceptors are usually the first type of cells that are affected when the disease progresses, thus a new cell line with higher expression of rod specific genes would be necessary for studying RP.

Here, the development of a new *in vitro* model from 661W cells for the study of RP based on zaprinast treatment of rod-like cells is described. To induce the expression of rod-specific genes, 661W cells were genetically modified to stably express the NRL transcription factor. The molecular characterization of this new cell line and the validation of these cells as a new model for the study of retinal degeneration by mimicking the disease upon treatment with a phosphodiesterase 6 (PDE6) inhibitor, which raises intracellular cGMP, were presented. The validity of the cell line for high-throughput screening was confirmed by the effects of previously published neuroprotective drugs.

4.1.1 The generation of rod-like cells

Based on the prominent role of transcription factor NRL in rod development, murine *Nrl* cDNA was cloned in the pLXSN vector. A replication-incompetent retrovirus was produced and used in the transduction of 661W cells. The transduced 661W cells then underwent a selection process with G418 based on neomycin resistance, followed by a PCR analysis for detecting the expression of *Nrl* and Rhodopsin (*Rho*) genes (Figure 4.1 A). Figure 4.1 B shows *Nrl* and *Rho* gene expressions increased in transduced cell bulk (661W *Nrl*+), while the expressions were barely detected in original 661W cells.

In order to obtain the suitable cell clone, a selection of single-cell clones was performed by limiting dilution. Selected clones were assessed by extracting the RNA and analysing the *Nrl* expression with RT-PCR (Figure 4.1 A). Among these selected clones, at least one known NRL target was upregulated, and five out of eleven were chosen (A5, A10, A11, B4 and B10). These selected clones were analyzed for the expression of the NRL targets and other rod specific genes, such as rhodopsin (*Rho*), G protein subunit alpha transducin 1 (*Gnat1*), Cyclic nucleotide gated channel subunit beta 1 (*Cngb1*), Cyclic nucleotide gated channel subunit alpha

1 (*Cnga1*), *Pde6b* and *Nr2e3* (Figure 4.1 C). Five clones showed differential expressions on these rod genes and, among them, A5, A11 and B10 appeared to be more promising as they expressed all the target genes. However, not all of them could be efficiently propagated *in vitro*. Based on this parameter, A11 clone was chosen, and from now on it will be called 661W-A11.

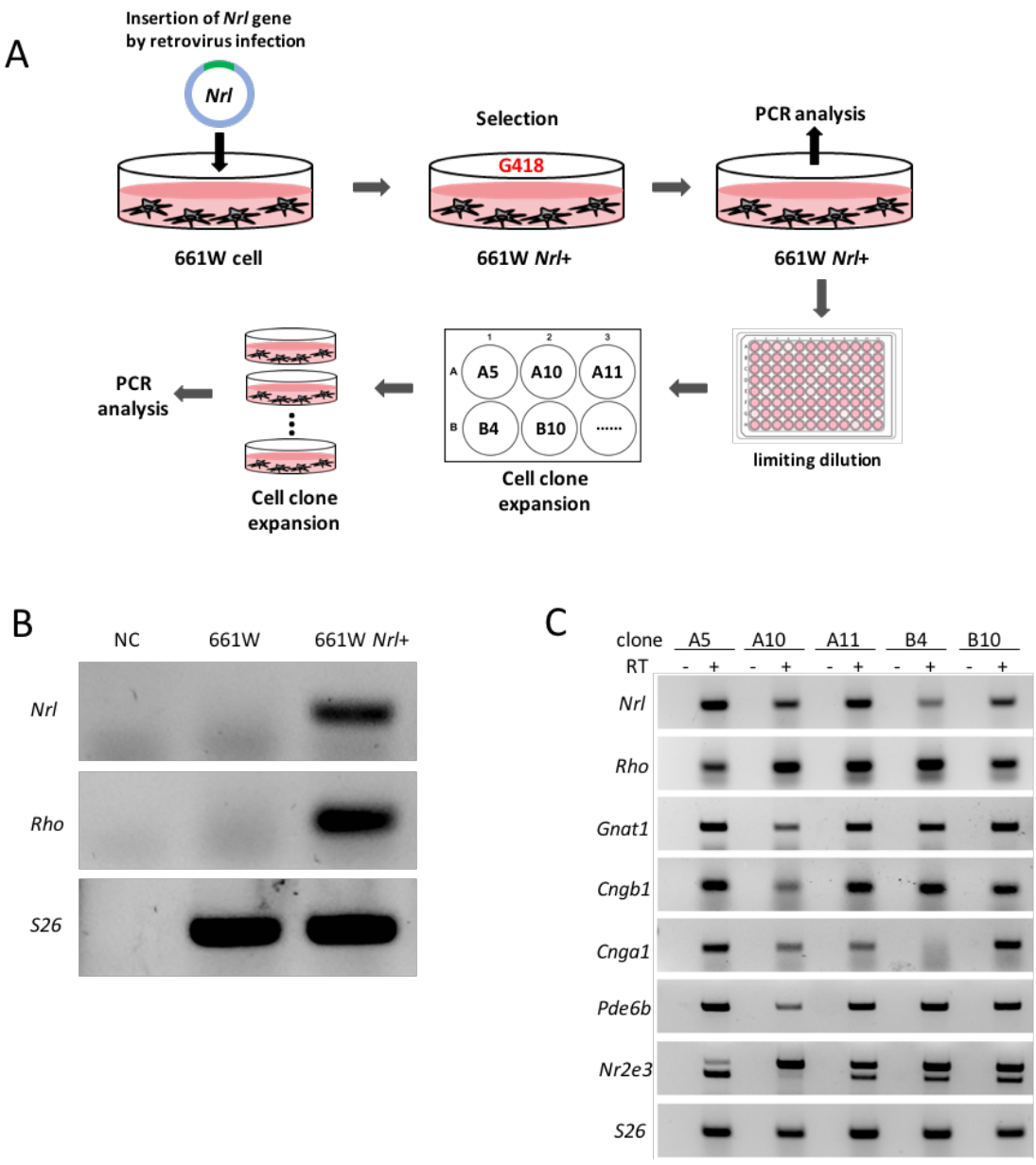

Figure 4.1 Generation and selection of *Nrl* expressing 661W cells. (A) The illustration of general procedure for genetic modification of 661W cells and selection of single cell clones. (B) RT-PCR analysis of *Nrl* and *Rho* mRNAs on 661W and 661W *Nrl*+ cells (bulk of retroviral transduced cells). *Rps26* (*S26*) was analyzed as reference gene. Expression of *Nrl* and *Rho* was confirmed in 661W transduced cells but not 661W cells. NC: negative control without cDNA. (C) Five clones showed differential expression of rod-specific genes when analyzed by RT-PCR. *Rps26* (*S26*) was analyzed as

reference gene. The primers for *Nr2e3* amplified also a transcript variant with an intron inclusion reported in IMAGE:5357172. For *Nr2e3* we evaluated only the lower molecular weight band corresponding to the spliced mRNA.

4.1.2 Characterization of 661W-A11 cells

4.1.2.1 NRL enhanced 661W-A11 rod gene expression

The characterization of 661W-A11 clone was first achieved by the comparison between the clone and the original 661W cells. The expression levels of several rod specific genes and that of cone specific genes were compared by real-time qPCR in the 661W-A11 and 661W cell. We observed that, when compared to 661W, 661W-A11 had a significant up-regulation in rod specific genes expression: *Rho*, *Nrl*, *Guca1a*, *Gnat1*, *Cngb1*, *Cnga1*, *Pde6b*, *Pde6g*, *Crx* and *Nr2e3* (Figure 4.2 A), but similar expression in cone-specific genes: *Pde6c*, *Pde6h*, *Cnga3* and *Cngb3* (Figure 4.2 B).

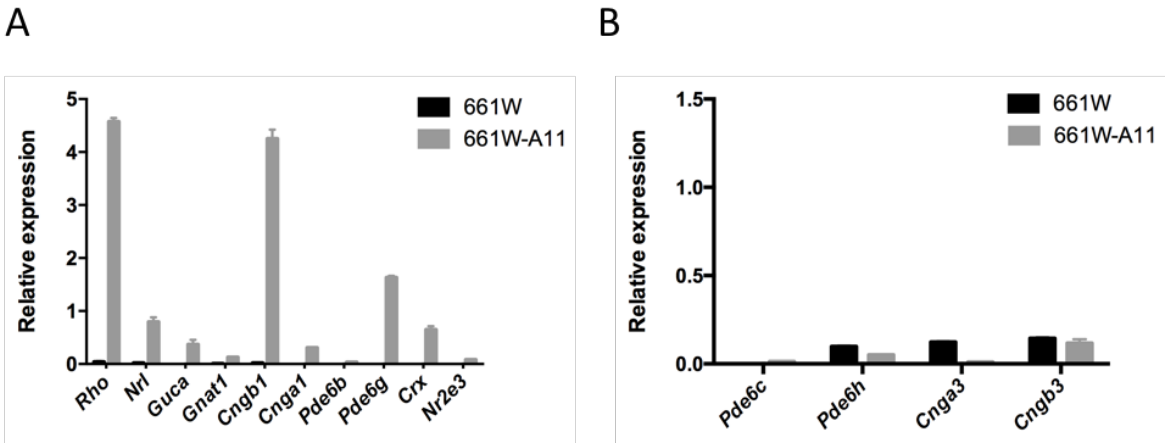

Figure 4.2 661W-A11 cells express rod-specific genes. (A) Rod specific mRNAs and (B) cone specific mRNAs were analyzed by real-time qPCR. *S26* was used as reference gene.

4.1.2.2 NRL enhanced 661W-A11 rod protein expression

Aside from the gene level, immunofluorescence and immunoblotting analyses showed that the proteins Rhodopsin, PDE6B and GNAT1 in 661W-A11 were increased compared to 661W cells (Figure 4.3). Interestingly, we observed that 661W-A11 also changed the phenotype and acquired a longer shape compared to the 661W (Figure 4.3 A).

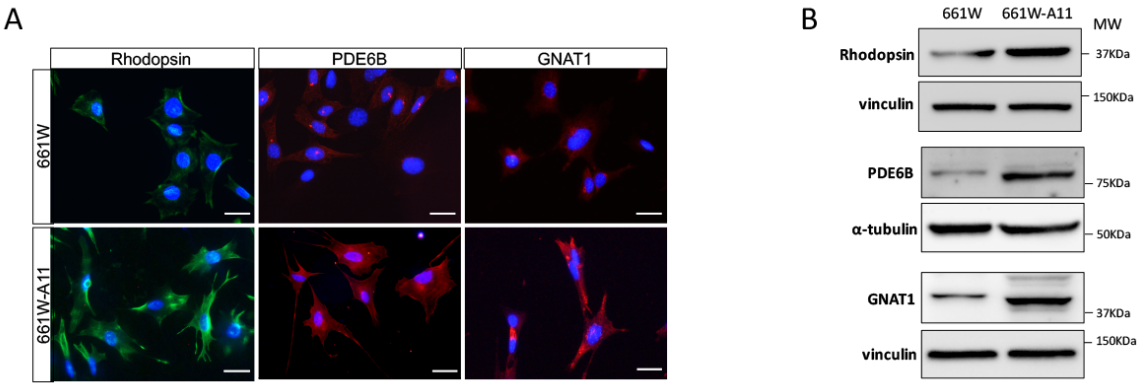

Figure 4.3 661W-A11 cells express rod-specific proteins. (A) Immunofluorescence analysis of Rhodopsin (green) protein, PDE6B (red) and GNAT1 (red) on 661W and 661W-A11 cells. Nuclei were stained with DAPI (blue). Scale bar: 10 μm. (B) Immunoblotting of Rhodopsin, PDE6B and GNAT1 on 661W and 661W-A11 cells.

During retinal development, the rod and cone photoreceptors are generated from a common pool of retinal progenitors under the control of transcription factors and regulatory signaling pathways [207]. NRL is the critical transcription factor determining rod photoreceptor cell fate, in $Nrl^{-/-}$ mice, post-mitotic cells failed to generate rods and resulted in cone-only photoreceptor layer [31]. When NRL-deficient human embryonic stem cells were introduced into retinal organoids, they did not acquire any rod photoreceptor markers, instead S-cone-like photoreceptors were enriched [208]. Conversely, the expression of NRL in developing cones leads to partial suppression on cone-specific gene expression and induction of rod-like characteristics [209]. The orphan nuclear receptor NR2E3, is a key downstream transcriptional target of NRL to repress cone genes development and establish rod identity [210].

Data presented here indicated that, based on the prominent expression of these rod specific genes and rod specific proteins, expression of *Nrl* in 661W promoted the rod development, without evoking the cone gene expression. Given those findings, we confirmed that clone 661W-A11 acquired rod photoreceptor features rather than cone photoreceptor features.

4.1.3 Mimicking photoreceptor degeneration *in vitro*

PDE6 loss of function caused by mutations in *PDE6A* or *PDE6B* causes rod photoreceptor degeneration. Based on this, we developed a protocol with zaprinast treatment on 661W-A11 cells to mimic rod photoreceptor degeneration.

4.1.3.1 Zaprinast treatment induced cell death

With the target to mimic photoreceptor degeneration in 661W-A11 cells, a protocol based on treatment with zaprinast to inhibit PDE6 activity was developed. Zaprinast is a well-known moderate cyclic guanosine monophosphate-specific phosphodiesterase (cGMP-PDEs) inhibitor, acting especially on PDE6 and PDE5 [211]. Scaling concentrations starting from 100 μM to 500 μM of zaprinast were applied to 661W and to 661W-A11 cells. A dose response with a gradual decreasing cell viability was observed in both cells, around 25% viability reduction was observed on 661W and 30% on 661W-A11, respectively, when a concentration of either 400 μM or 500 μM was used (Figure 4.4 A). To evaluate if the reduced viability was related to decreased proliferation or to cell death, TUNEL assay was performed and defined that exposure to 400 μM zaprinast for 24 h induced 9% cell death on 661W and 14% cell death on 661W-A11, respectively (Figure 4.4 B).

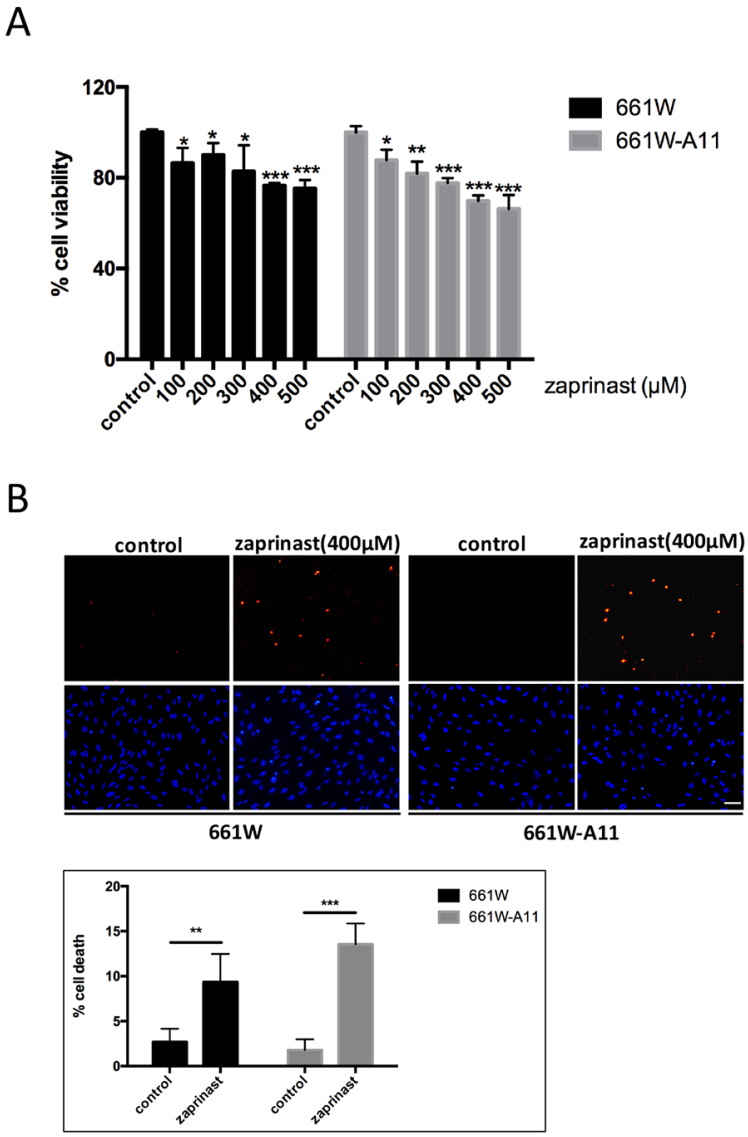

Figure 4.4 Zaprinast treatment induced cell death. (A) Cell viability assay, based on MTT, after treatment with scaling concentrations of zaprinast on 661W and 661W-A11 cells. Values of cells treated with the vehicle (0 μM, control) were set as 100% cell viability. (B) TUNEL assay detected dying cells (upper panels, red) in zaprinast-treated 661W and 661W-A11 cells; nuclei were stained with DAPI (lower panels, blue). Control shows cells treated with the vehicle (DMSO). Scale bar: 40 μm. Below the micrograph panels, quantifications of the $TUNEL^{+}$ cells are reported. Statistical comparison: Student's unpaired two-tailed t-test; * $p < 0.05$, ** $p < 0.01$, *** $p < 0.001$.

4.1.3.2 Zaprinast treatment on 661W-A11 increased cGMP level

To demonstrate that zaprinast treatment could mimic the PDE6 loss of function in 661W-A11, as found in retinal degeneration, the analysis of cGMP was selected due to its prominent role in the degeneration process. We evaluated the change in cGMP level by visualization with

immunofluorescence, where we observed the zaprinast treatment increased cGMP signal intensity (Figure 4.5 A). To further quantify the changed level, flow cytometry using an antibody specifically binding cGMP was applied, which revealed a statistically significant increase of cGMP in 661W-A11 treated with 400 µM zaprinast (Figure 4.5 B).

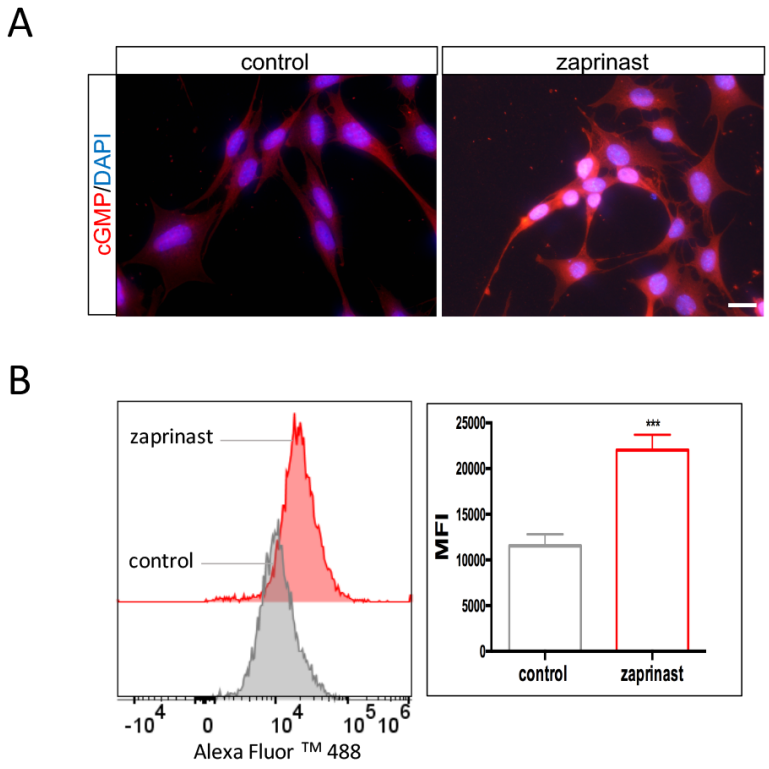

Figure 4.5 Zaprinast treatment elevated cGMP level in 661W-A11. (A) Immunofluorescence analysis of cGMP (red) on zaprinast treated versus not treated 661W-A11 cells. Nuclei were stained with DAPI (blue). Scale bar: 10 µm. (B) Increased cGMP level was detected by flow cytometry in zaprinast treated versus not treated 661W-A11 cells, *** $p < 0.001$. Control: cells were treated with vehicle (DMSO); Zaprinast: cells were treated with 400 µM zaprinast for 24 h.

4.1.3.3 Zaprinast treatment on 661W-A11 activated PKG

As downstream target of cGMP, activation of PKG was investigated in this model. We first analyzed gene expressions of different PKG isoforms, higher mRNA levels of *Prkg1a*, *Prkg1b* and *Prkg2* genes, encoding for the isoforms PKG1α, PKG1β and PKG2, respectively, were found in 661W-A11 compared to 661W cells (Figure 4.6 A).

Due to the higher gene expression of PKGs in 661W-A11, PKG activation was then evaluated indirectly by analyzing the phosphorylation status of two different PKG targets: phosphorylation of the vasodilator-stimulated phosphoprotein (VASP) at serine 239 and

phosphorylation of the Ras homolog family member A (RhoA) at serine 188. VASP is a protein associated to the cytoskeleton and is a major substrate of PKG and PKA with phosphorylation at three sites: serine 157, serine 239, threonine 278, in which serine 239 is the preferred phosphorylation site of PKG especially *in vitro*, whereas *in vivo,* PKG exhibits similar kinetics in phosphorylating at both sites of serine 157 and serine 239. On the other hand, serine 157 phosphorylation is prioritized by PKA no matter *in vitro* or *in vivo*. Thus, the serine 239 is considered to be a specific phosphorylation site of PKG [212, 213]. RhoA is a small GTPase known for regulating diverse cellular processes ranging from cell differentiation to gene expression and cell survival [214]. Serine 188 in RhoA can be phosphorylated by PKG [215]. Here we investigated the expressions of p-VASP (ser239) and p-RhoA (ser188) in zaprinast treated 661W-A11 cells compared to untreated cells, Immunoblotting showed that both p-VASP (ser239) and p-RhoA (ser188) were readily detectable in the zaprinast treated 661W-A11 cells, indicating activation of PKG (Figure 4.6 B and C).

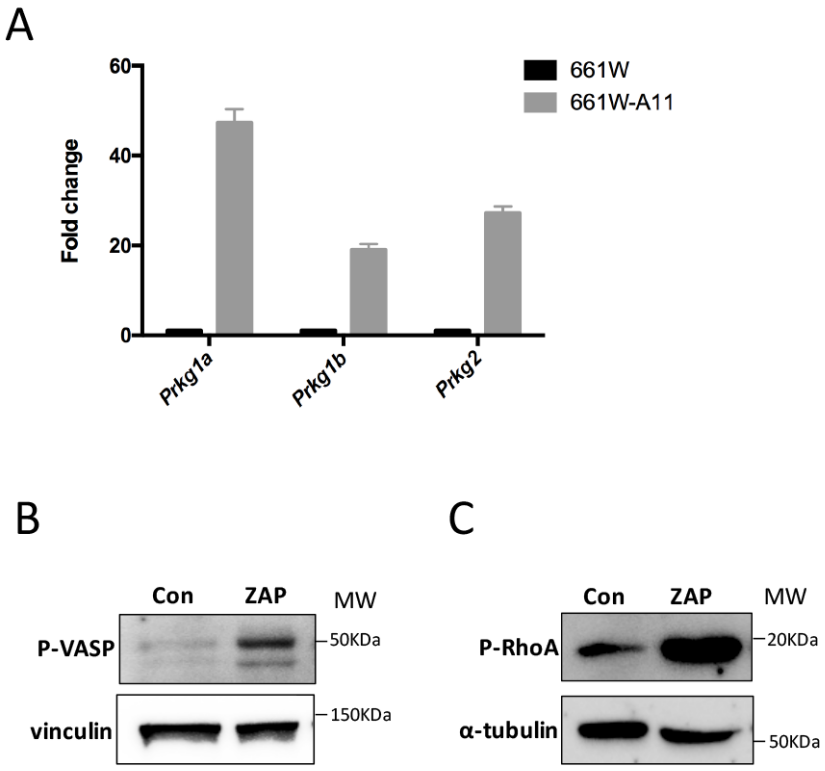

Figure 4.6 Activation of PKG in zaprinast stressed 661W-A11. (A) Real-time qPCR analysis of *Prkg1a*, *Prkg1b* and *Prkg2* mRNAs in 661W-A11 cells and 661W cells. (B-C) Immunoblotting of phosphorylated VASP (P-VASP) at ser239 and phosphorylated RhoA (P-RhoA) at ser188 on control (Con: vehicle treated) and 400 μM zaprinast treated (ZAP) groups.

Though these results implied that increased cGMP could activate PKG, in order to define if zaprinast treatment on 661W-A11 cells can be a valuable model for retinal degeneration, we assessed the correlation of PKG activation and cell death, similarly to what found in the degenerating retina. To this aim, we treated 661W-A11 and 661W cells with increasing concentrations of PA5 and PA6, two cGMP analogues that we previously published as PKG activators. These PKG analogues present different activation constants for the different PKG isoforms, i.e. PA5 targets mostly PKG2 and less PKG1 and PA6 highly activates PKG1 and less PKG2 [163]. We found that PA5 and PA6 showed little effect on 661W cells, while 661W-A11 cells were sensitive to both activators in decreasing the cell viability (Figure 4.7 A and B). These data confirmed that compared to 661W, triggering PKG activity is a toxic event for 661W-A11. Furthermore, cell death detection with ethidium homodimer assay on 661W-A11 cells showed that 50 µM PA5 or PA6 could induce up to 16% cell death (Figure 4.7 C).

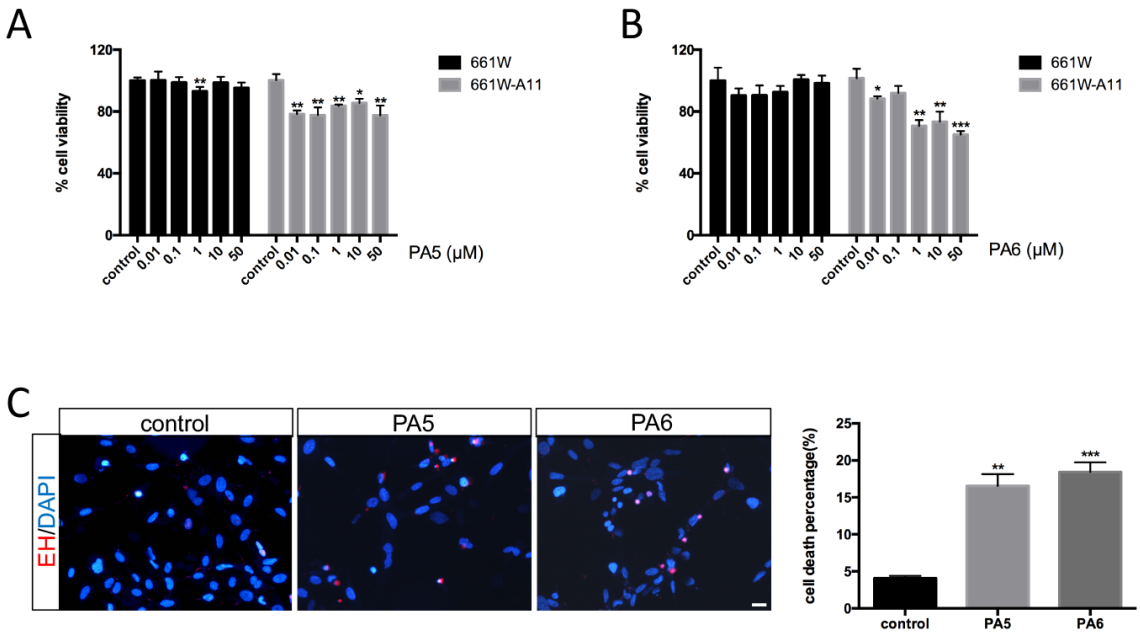

Figure 4.7 PKG activation was toxic to 661W-A11 cells. Cell viability assay, based on MTT, after treatment with increasing doses of PA5 (A) and PA6 (B). Values of cells treated with vehicle (H_2O) were set as 100% cell viability. (C) Ethidium homodimer (EH) staining (red) detected dying cells with 50 µM PA5 or PA6 treatment on 661W-A11 cells; nuclei were stained with DAPI (blue); Scale bar: 10 µm. Histogram with quantitative data is shown on the right-hand side. Statistical comparison: Student's t-test unpaired two tailed; *P<0.05, **P<0.01, ***P<0.001.

4.1.3.4 Zaprinast treatment on 661W-A11 induced calcium influx

The toxic effect of increased Ca^{2+} level has long been associated with photoreceptor degeneration, we thus quantified intracellular Ca^{2+} level by flow cytometry through Fluo-4AM staining in this model. Interestingly, more intracellular Ca^{2+} was found in 661W-A11 after zaprinast treatment (Figure 4.8 A). With the aim of defining the mechanism underlying Ca^{2+} influx, we exposed zaprinast treated 661W-A11 to a blocker of L-type voltage gated Ca^{2+} channels, D-*cis* diltiazem [216]. We defined that D-*cis* diltiazem could interfere with the zaprinast induced Ca^{2+} influx, in which, D-*cis* diltiazem treatment significantly decreased intracellular Ca^{2+} level that resulted by zaprinast (Figure 4.8 B).

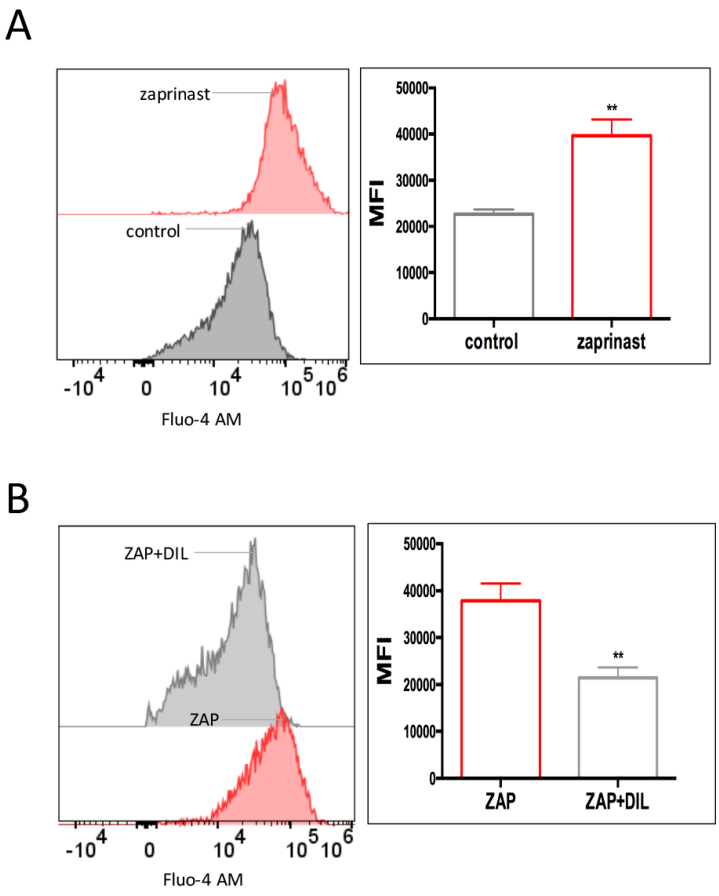

Figure 4.8 Zaprinast treatment enhanced calcium influx in 661W-A11. (A) Increased Ca^{2+} level was detected by flow cytometry in zaprinast treated versus not treated 661W-A11 cells. control: cells treated with vehicle (DMSO), zaprinast: cells treated with 400µM zaprinast for 24 h. (B) Decreased Ca^{2+} level was detected by flow cytometry in zaprinast + D-*cis* diltiazem treated versus zaprinast treated 661W-A11 cells. ZAP: cells treated with 400 µM zaprinast for 24 h. ZAP+DIL: cells were pretreated with 50 µM D-*cis* diltiazem for 2 h, and then were treated with 400 µM zaprinast in the presence of 50 µM D-*cis* diltiazem for 24 h. MFI: mean fluorescence intensity. Statistical comparison: Student's t-test unpaired two tailed, **P<0.01.

4.1.3.5 Zaprinast treatment on 661W-A11 induced calpain activation

Previous studies correlated increased intracellular Ca^{2+} with triggering of calpain proteases. Calpains are Ca^{2+}-dependent cysteine proteases that can cleave various substrates, and one of the sensitive substrates is αII-spectrin. Spectrin is a major component of cytoskeletal network related to cell plasma membrane, the heterotetramer of αII and βII is the most common form of this protein [217]. The activation of calpain proteases was, thus, evaluated by assessing the cleavage of αII-spectrin. An increased amount of the 145–150 kDa fragment of αII-spectrin derived from calpain cleavage was observed in 661W-A11 cells after zaprinast treatment (Figure 4.9 A). We also observed a 120 kDa fragment characteristic of caspase activation (Figure 4.9 A). The calpain activity assay, based on the fluorescent calpain substrate 7-amino-4-chloromethylcoumarin staining, also confirmed the activation of calpains after zaprinast treatment (Figure 4.9 B).

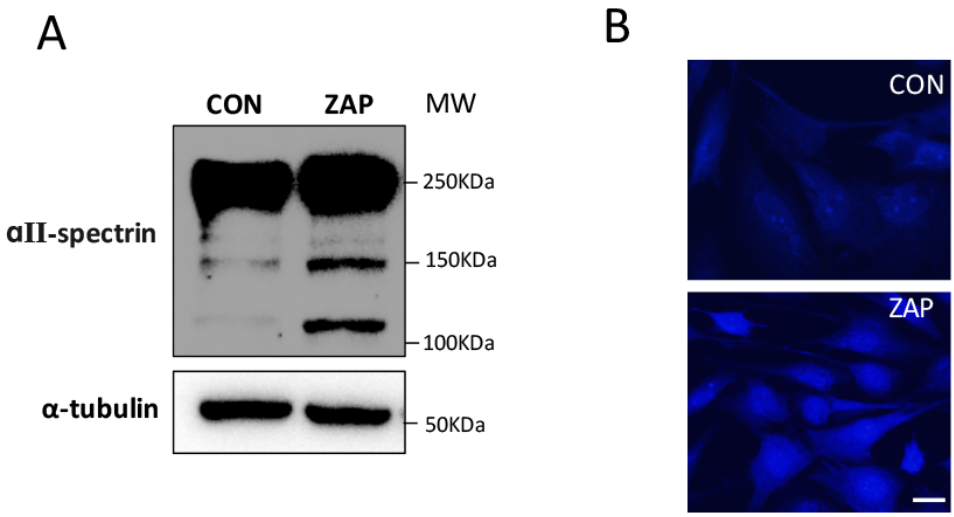

Figure 4.9 Calpain activity in zaprianst treated 661W-A11. (A) Western blot analysis of αII-spectrin on control and zaprinast treated groups showed increase of the 145-150 kDa fragment resulting from calpain cleavage and of the 120 kDa fragment resulting from caspase cleavage. (B) Calpain activity assay showed the activation of calpains upon zaprinast treatment in 661W-A11 cells. CON: cells treated with vehicle (DMSO); ZAP: cells treated with 400 μM zaprinast for 24 h. Scale bar: 10 μm.

The dysregulation of cGMP, typically its high levels, may trigger downstream processes that are toxic to photoreceptor. This abnormal accumulation of cGMP can be found in photoreceptor degeneration caused by different mutations, including the genes encoding rhodopsin, PDE6, CNG channel, GC and Aryl Hydrocarbon Receptor Interacting Protein Like

1 (AIPL1) [113, 114]. The increased intracellular cGMP in our model upon PDE6 inhibition confirmed the effect previously reported in the retina with PDE6 loss of function, suggesting that our model can mimic, at least some aspects of the rod photoreceptor cell death in RP and other IRDs linked to increased intracellular cGMP.

Studies have demonstrated that cGMP-dependent overactivation of PKGs acts as an important cell death mechanism in photoreceptor degeneration [65]. As the target of cGMP, PKGs activity awaken great interest in the study of photoreceptor cell death. The correlation with retinal degeneration was shown in a CNG channel loss-of-function mouse model in which the knock-out of *Prkg1* led to sustained rod cell survival [218]. PKG expression has been demonstrated in the retina and PKG activity was characterized in 661W cells [133, 219, 220]. In 661W-A11, we demonstrated increased expression of *Prkg1* and *Prkg2* genes. The key role of PKG in the cell death mechanism was confirmed by PKG stimulation with specific cGMP analogues, which demonstrated to be detrimental to the cells, and by PKG activation upon intracellular cGMP increase. Interestingly, 661W-A11 cells exhibited low tolerance to PA5, which preferentially activates PKG2. PA6, which acts preferentially on PKG1, was less effective. Several studies have shown that specific activation of PKG2 interferes with proliferation and triggers pro-apoptotic effects in cancer cell lines [127, 164, 221, 222]. Until now, not much is known about the role of different PKG isoforms in photoreceptors, thus the identification of PKG substrates and their downstream pathways would significantly accelerate the identification of new targets in IRD drug development.

The reduction in intracellular calcium upon D-*cis* diltiazem exposure suggests that the calcium enters in 661W-A11 cells mainly through the L-type channel. However, D-*cis* diltiazem has also a moderate effect on CNG channel [223], so we cannot exclude the possibility of calcium influx through CNG channel, as we showed the expression of mRNA encoding the CNGC subunits in the cells. We favor the first hypothesis because transport and diffusion of Ca^{2+} between outer segment, harboring the CNGC, and the inner segment, containing the photoreceptor cytoplasm, appears to be limited in the retina. L-type calcium channels are, in fact, the main pathway of Ca^{2+} entrance from the extracellular space in photoreceptor cells [68] .

One aspect of this new *in vitro* model that needs to be discussed here is that we noticed the application of zaprinast was active on both 661W-A11 and 661W cell lines, in the form of decreasing cell viability and increasing cell death (Figure 4.4). The fact that zaprinast is exerting an effect on original 661W cells, could be attributed to that 661W cell is a cone like

cell line, which also expresses PDE6 but with different subunits, while zaprinast targets all the PDE6 proteins. Thus it is not a surprise that 661W cells are also sensitive to zaprinast.

Another aspect is that we used pharmaceutical approach to mimic the degeneration, however, with this new cell line, a high possibility of mimicking PDE6B mutation by genetic manipulation instead of pharmaceutical inhibition can be achieved, which would more approach the genetic cause of PDE6 loss of function in RP.

The increased cGMP and Ca^{2+} levels, the activation of PKGs and calpains, altogether suggested that our cell model harbored several cell death mechanisms featuring what were found in RP, and this model might be used for the study of cell death mechanism for RP or other IRDs linked to cGMP, and for drug screening.

4.2 Validation of the *in vitro* model for drug screening

Various drugs have been reported to have a neuroprotective effect in retinal degeneration models. For instance, the cGMP analogue CN03 functions as PKG inhibitor and could reduce the activities of PKG and CNGC, protecting photoreceptors from degeneration. Recombinant human pigmented epithelium derived factor (PEDF) protein was also shown to be able to decrease intracellular calcium and photoreceptor cell death in mouse models of retinal degeneration [224, 225]. Similarly, calpastatin peptide, an endogenous calpain inhibitor, was reported to protect photoreceptors from cell death when administered *in vivo* [149]. To validate our *in vitro* model, the neuroprotective effects of the above-mentioned drugs were tested in 661W-A11 cells and percentage of cell death or cell viability was analyzed after zaprinast treatment with or without the neuroprotective drugs.

4.2.1 The effect of cGMP analogues on the new *in vitro* system

The activation of PKG linked to photoreceptor cell death has highlighted the PKG is a target for treating photoreceptor degeneration diseases. Several cGMP analogues designed to inhibit PKG activity have been synthetized in order to develop new treatments for retina degeneration. Those analogues harbor an Rp-configured phosphorothioate that could bind to the cGMP binding sites in the regulatory domain and antagonize the activation of PKG [226].

The treatment with cGMP analogue CN03 was previously shown to successfully rescue photoreceptor from cell death in different animal models [129]. Since then, new cGMP analogues have been developed but need to be tested and confirmed as neuroprotective molecules for RP.

In addition to CN03, a novel but very similar cGMP analogue called CN238 (Figure 4.10 A) was also tested in our *in vitro* system. We investigated the effects of these two analogues in the zaprinast stressed 661W-A11 cells, and compared their effects on cell viability, cell death and Ca^{2+} influx.

4.2.1.1 Dose response of zaprinast stressed 661W-A11 cells to cGMP analogues

We propose that our model can be a rapid *in vitro* compound screening system. Zaprinast stressed 661W-A11 cells were exposed to various concentrations of CN03 and CN238, and the effects were evaluated with the cell viability MTT assay. The dose-response curves of CN03 and CN238 (Figure 4.10 B) showed that both analogues exerted a protective effect. CN03 started to show the effect at 1 μM and with the application of higher concentration, it reached

up to 70% cell viability. Interestingly, the stressed cells seemed to be more sensitive to CN238, which started to exhibit the protective at a low dose (1 nM), and cell viability reached more than 80% until it came to a plateau (Figure 4.10 B).

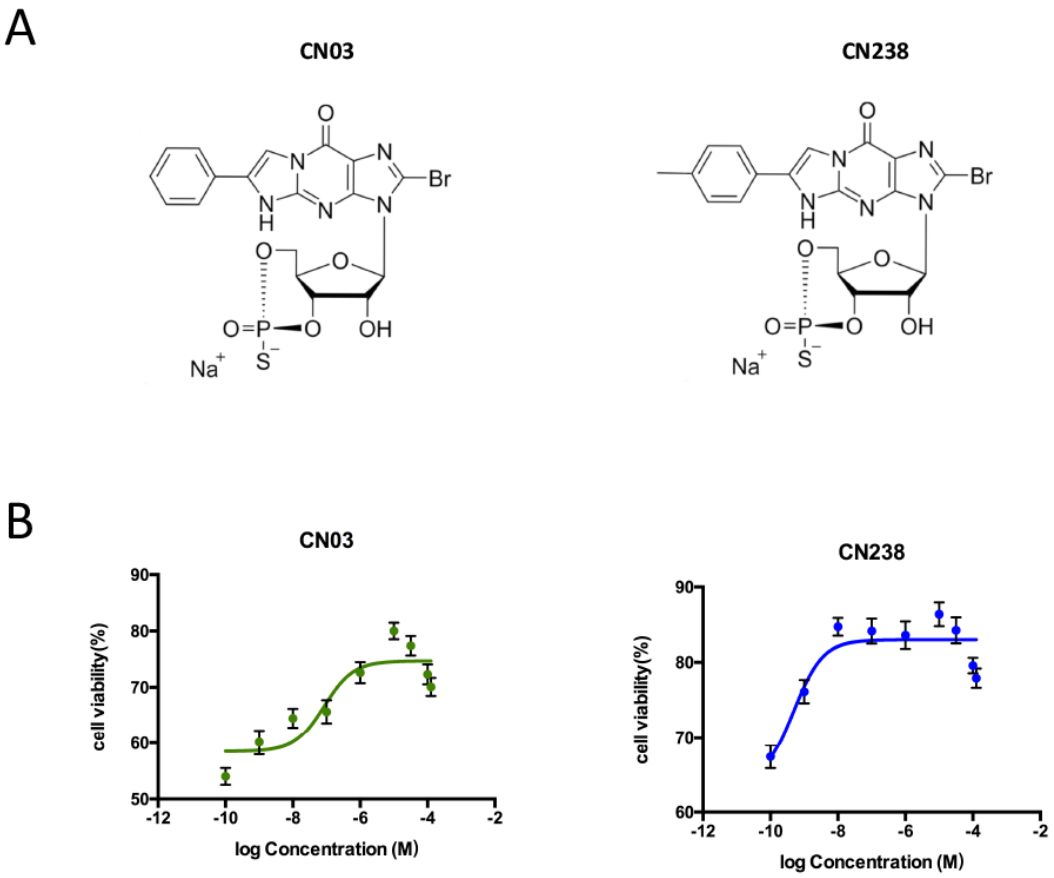

Figure 4.10 Zaprinast stressed 661W-A11 cells were rescued by cGMP analogues. (A) Structure of cGMP analogues CN03 and CN238. (B) Dose-response curves of CN03 and CN238 on zaprinast stressed 661W-A11 cells. Cells were pretreated with different concentrations of CN03 or CN238 for 2 h, then were stressed with 200 μM zaprinast in the presence of CN03 or CN238 for 48 h.

4.2.1.2 cGMP analogues reduced zaprinast-induced 661W-A11 cell death

We further investigated the effect of cGMP analogues on cell death based on the TUNEL assay, and found that, 50 μM CN03 confirmed its previously reported protective effect, with a 45% reduction in detected cell death. With 50 μM CN238, a better rescue effect was observed, the cell death percentage decreased about 67% (Figure 4.11 A and B).

We then investigated the effect of those PKG inhibitors on the Ca^{2+} level. Interestingly, CN03 and CN238 could also reduce the Ca^{2+} influx resulted by zaprianst treatment (Figure 4.11 C).

Figure 4.11 D shows the significant decrease of mean fluorescence intensity (MFI) of Ca^{2+} after CN03 and CN238 treatment.

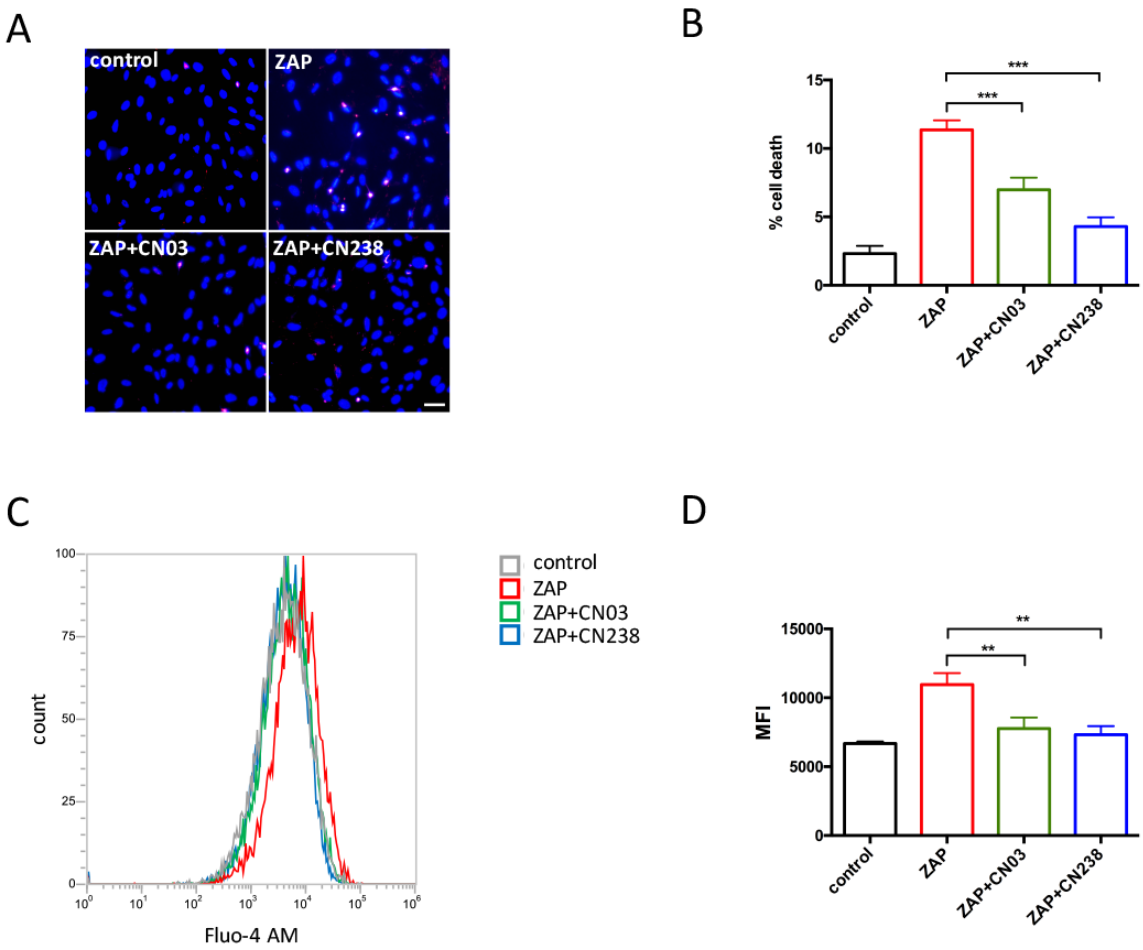

Figure 4.11 cGMP analogues effects on cell death and Ca^{2+} influx. (A) TUNEL assay detected dying cells in 661W-A11 treated with vehicle (DMSO) or zaprinast or zaprinast with CN03 or zaprinast with CN238. Scale bar: 20 µm. (B) Percentage of cell death was calculated by counting TUNEL labeled cells in different experimental groups. (C) Inhibitory cGMP analogues reduced zaprinast induced Ca^{2+} influx. Decreased Ca^{2+} levels were detected by flow cytometry in CN03 or CN238 + ZAP treated versus ZAP treated 661W-A11 cells. (D) Mean fluorescence intensity calculation in the Ca^{2+} level. Control: cells treated with corresponding volume of DMSO was used as a vehicle control; ZAP: cells treated with 400 µM zaprinast for 24h. ZAP+ CN03: cells were pre-treated with 50 µM DF003 for 2 h, and treated with 400 µM zaprinast together with 50 µM DF003 for 24 h; ZAP+ CN238: cells were pre-treated with 50 µM DF238 for 2 h, and then were treated with 400 µM zaprinast together with 50 µM DF238 for 24 h. MFI: Mean fluorescence intensity. Statistical comparison: Student's t-test unpaired two tailed; *P<0.05, **P<0.01, ***P<0.001.

4.2.2 The validation of other neuroprotective drugs

Apart from PKG inhibitors, we also tested other neuroprotective drugs in this new system. The treatment with calpastatin and PEDF significantly increased the cell viability (Figure 4.12), thus we can also confirm their neuroprotective effects on the newly developed photoreceptor cell model.

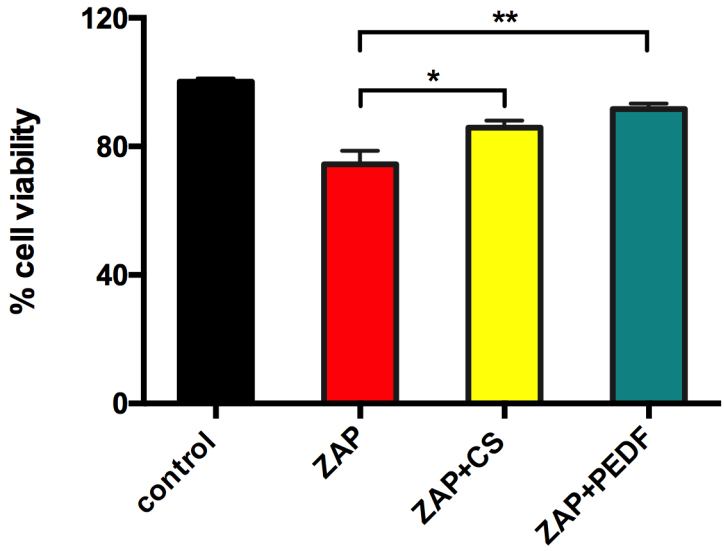

Figure 4.12 Effect of neuroprotective drugs in zaprinast stressed 661W-A11. Cell viability, assessed by MTT assay, in cells treated with vehicle (DMSO) was set as 100% cell viability. Control: cells treated with DMSO; ZAP: cells treated with 400 μM zaprinast. ZAP+ CS or ZAP+PEDF: cells were pretreated with 20 μM calpastatin peptide (CS) or 10 nM PEDF for 2 h then were stressed with 400 μM zaprinast in the presence of 20 μM CS or 10 nM PEDF. Statistical comparison: Student's t-test unpaired two tailed; *P<0.05, **P<0.01, ***P<0.001.

With the validation of these compounds, we proposed that this *in vitro* model could be used as a rapid drug screening model for potential target candidates.

4.3 Characterization of PKG phosphorylated substrates

Though the PKG activity has already been linked to photoreceptor cell death, the cGMP-PKG downstream pathway still remains largely unknown. PKG is a protein kinase that phosphorylates various substrates, previous studies observed the changes of several PKG targets such as VASP and cAMP response element-binding protein (CREB) in dying photoreceptors [135, 227], but the vast majority of substrates are still poorly characterized. The identification of downstream targets of PKG and the phosphorylated substrates will accelerate the study of cell death mechanism in photoreceptor degeneration as well as the development of new neuroprotective strategies.

In collaboration with Lund University, a phosphoproteomic study was performed based on phosphorylated peptides enrichment and LS/MS to identify phosphorylation events dependent on PKG activity. In this study we compared cells exposed to zaprinast in combination or not to the PKG inhibitor (CN03) by mass spectrometry-based phosphoproteomics to identify candidate substrates and kinases regulated by cGMP-PKG in 661W-A11 cells.

4.3.1 Protein samples were normally distributed and well clustered

The sample information and general process are illustrated in Figure 4.13 A. We analysed cells stressed with zaprinast, which activates PKGs, cells exposed to CN03 during the zaprinast stress and control cells treated only with vehicles. We chose to expose the cells for only 2 hours to CN03 with the aim to identify direct PKG targets. All the samples were normally distributed after log2 transformation, besides, the principal component analysis (PCA) analysis showed that the three groups were well clustered and separated (Figure 4.13 B and C).

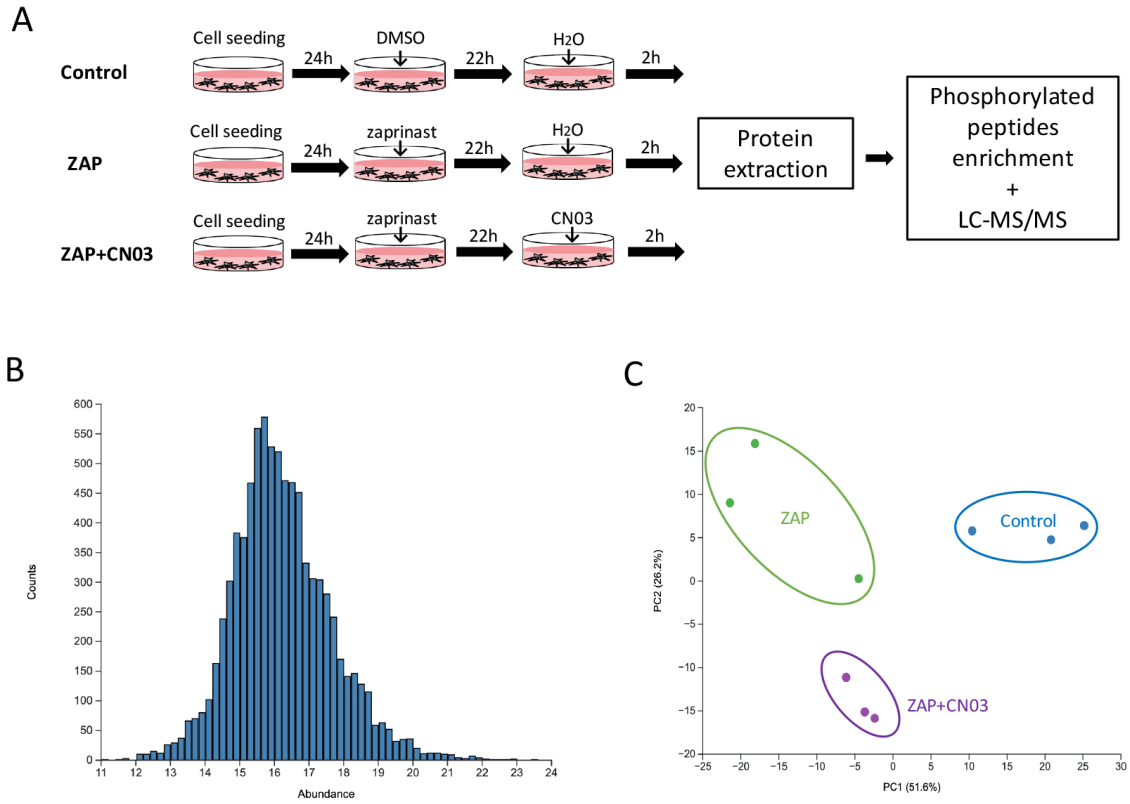

Figure 4.13 The protein samples were normally distributed and well clustered. (A) Schematic of experimental design for proteomic analysis. (B) After log2 transformation, the samples were all in normal distribution. (C) Principal component analysis (PCA) analysis showed that the three groups of protein samples (control, ZAP, ZAP+ CN03) clustered separately. Control: 661W-A11 cells treated with vehicle (DMSO and H_2O as the equal volume of zaprinast and CN03, respectively); ZAP: 661W-A11 cells treated with 400 µM zaprinast for 24 h; ZAP+ CN03: 661W-A11 cells treated with 400 µM zaprinast for 24 h, 2 h prior to the end point of zaprinast treatment, cells were exposed to 50 µM CN03 for 2 h.

4.3.2 Phosphoproteomic profiling of 661W-A11 cells treated with zaprinast

In order to analyze the changes in phosphorylated substrates in photoreceptor degeneration, the phosphorylated sites between untreated 661W-A11 and zaprinast treated 661W-A11 were compared. We were able to identify 945 phosphorylated sites, in which 302 of them were found to have a significant change ($P<0.05$) in zaprinast treated 661W-A11 compared to untreated 661W-A11. Of these statistically significant sites, 177 sites were upregulated and 125 were downregulated in response to zaprinast treatment (Figure 4.14 A).

To investigate the differences in the differentially expressed phosphorylated peptides between untreated 661W-A11 group and zaprinast treated 661W-A11 group, Gene Ontology (GO) analysis was performed. Among the significantly downregulated phosphorylated peptides, the most enriched GO term in the molecular function (MF) category was RNA binding (GO:0003723), and in the biological process (BP) category, the main enriched GO terms were regulation of cellular amide metabolic process (GO:0034248), cellular component biogenesis (GO:0044085), cytoskeleton organization (GO:0007010) and regulation of translation (GO:0007417), while in the cellular compartment (CC) category, the most enriched term was intracellular non-membrane-bounded organelle (GO:0043232) (Figure 4.14 B). Among the significantly upregulated phosphorylated peptides, the main enriched GO terms were viral process (GO:0016032), establishment of cell polarity (GO:0030010), establishment or maintenance of cell polarity (GO:0007136) and macromolecule localization (GO:0033036) in the biological process category; RNA binding (GO:0003723) and cadherin binding (GO:0045296) in molecular function category; and anchoring junction (GO:0070161), cell junction (GO:0030054), nuclear lumen (GO:0031981) and nucleus (GO:0005634) in the cellular compartment category (Figure 4.14 C).

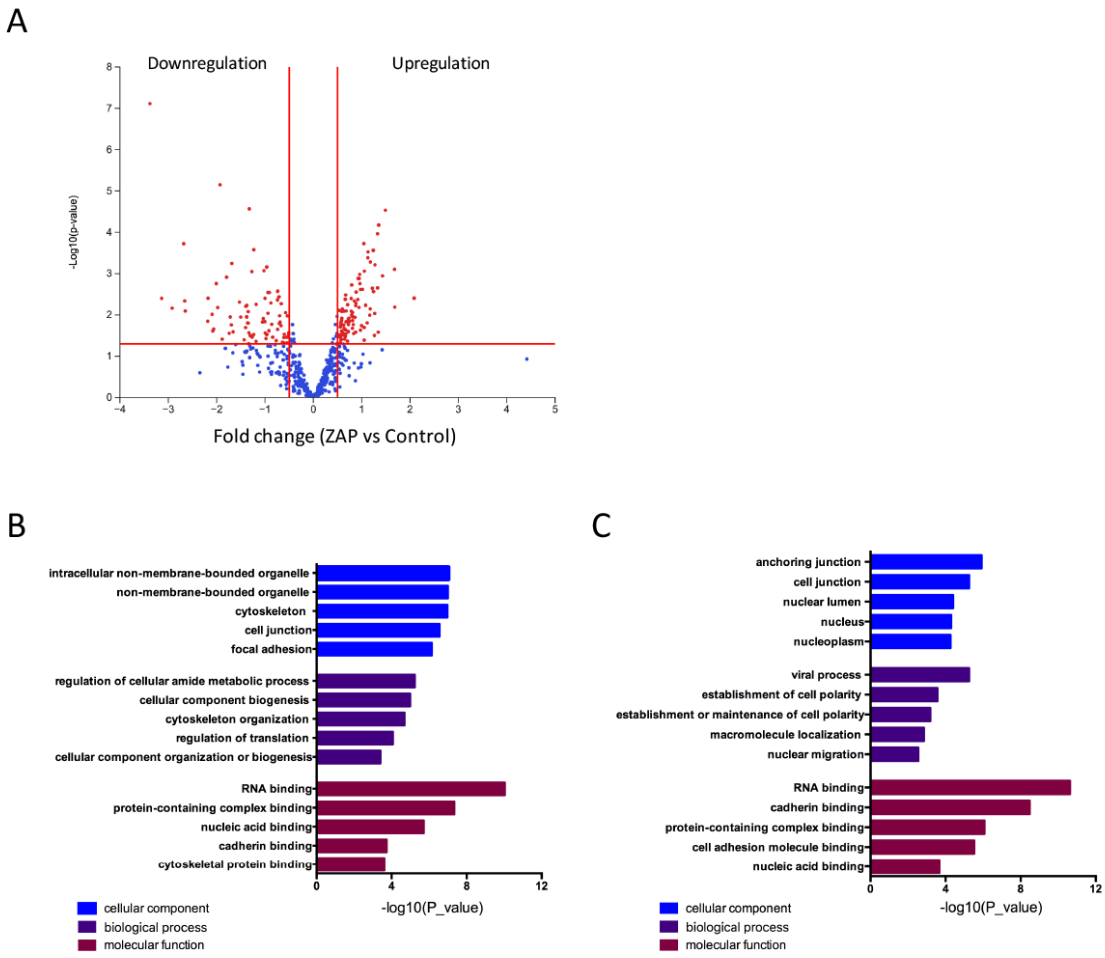

Figure 4.14 Phosphorylated substrates in zaprinast treated 661W-A11 and untreated 661W-A11. (A) Volcano plot representing log fold change and -log10 p-value for phosphorylated substrates between zaprinast treated 661W-A11 and untreated 661W-A11 (ZAP vs Control). Red dots indicate significantly changed phosphorylation sites (p-value < 0.05), blue dots represent sites with no significant alteration in phosphorylation. (B) GO analysis of downregulated phosphorylated peptides in the zaprinast treated 661W-A11 compared with untreated 661W-A11. (C) GO analysis of upregulated phosphorylated peptides in the zaprinast treated 661W-A11 compared with untreated 661W-A11.

4.3.3 Phosphoproteomic profiling of zaprinast stressed 661W-A11 cells interfered with PKG inhibitor CN03

As we found the differentially expressed phosphorylated peptides after zaprinast treatment, we sought to investigate the effect of the PKG inhibitor CN03 on the phosphorylation profile. Upon CN03 treatment, a total of 150 phosphorylation sites significantly changed when

compared to only zaprinast treatment; Of these, 105 were upregulated and 45 were downregulated (Figure 4.15 A).

To select the substrates that were possibly regulated by PKG, we then overlapped the 302 significant altered phosphorylated substrates in the cells after zaprinast treatment with the 150 altered phosphorylated substrates in zaprinast stressed cells that were interfered with CN03 treatment, and 39 substrates were identified (Figure 4.15 B). Substrates such as myristoylated alanine-rich C kinase substrate-like 1 (MARCKSL1), synaptosome associated protein 23 (SNAP23) and nuclear factor kappa b subunit 2 (NFKB2) were estimated to be positively regulated by PKG, because these phosphorylated substrates were decreased upon inhibition of PKG by CN03 treatment. Otherwise, phosphorylation of substrates such as G3BP stress granule assembly factor 1 (G3BP1), eukaryotic translation initiation factor 5B (EIF5B) and RAD23 homolog A, nucleotide excision repair protein (RAD23A) were negatively regulated by PKG. The phosphorylated substrates positively and negatively regulated by PKG are listed in Table 4 and Table 5, respectively.

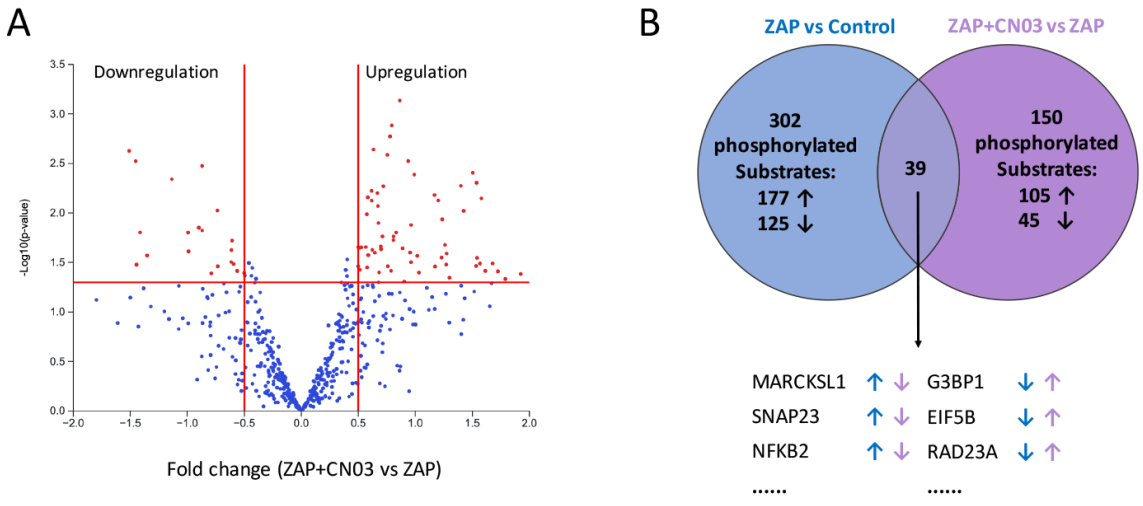

Figure 4.15 Altered phosphorylated substrates upon CN03 treatment in zaprinast stressed 661W-A11. (A) Volcano plot representing log fold change and -log10 p-value for phosphorylated substrates between PKG inhibitor CN03 plus zaprinast treated 661W-A11 and zaprinast treated 661W-A11 (ZAP + CN03 vs ZAP). (B) The overlap between phosphorylated substrates changes in ZAP vs Control (blue) and ZAP + CN03 vs ZAP (purple). Increased or reduced phosphorylation of a substrate is indicated by arrows pointing upwards or downwards, respectively.

Table 4 List of phosphorylated substrates candidates positively regulated by PKG

UPID	Substrates	Phosphorylated substrates activity	
		ZAP vs Control	ZAP+CN03 vs ZAP
P49006	MARCKSL1	↑	↓
O00161	SNAP23	↑	↓
Q9H1E3	NUCKS1	↑	↓
Q9NY27	PPP4R2	↑	↓
Q9C0C2	TNKS1BP1	↑	↓
Q8WX93-6	PALLD-6	↑	↓
Q9UQ35	SRRM2	↑	↓
Q9NZN3	EHD3	↑	↓
Q12888	TP53BP1	↑	↓
Q5VSL9	STRIP1	↑	↓
Q13188	STK3	↑	↓
P49792	RANBP2	↑	↓
O00429-3	DNM1L	↑	↓
Q00653	NFKB2	↑	↓
O43148	RNMT	↑	↓
Q9Y608	LRRFIP2	↑	↓
P35221	CTNNA1	↑	↓
Q9Y4F1	FARP1	↑	↓
Q6WCQ1	MPRIP	↑	↓
Q14498	RBM39	↑	↓
O00567	NOP56	↑	↓
Q9Y2X7	GIT1	↑	↓
O75648	TRMU	↑	↓
P11717	IGF2R	↑	↓
P48681	NES	↑	↓
Q8ND56	LSM14A	↑	↓
Q8ND56	RTN4	↑	↓
Q13409	DYNC1I2	↑	↓

Table 5 List of phosphorylated substrates candidates negatively regulated by PKG

UPID	Substrates	Phosphorylated substrates activity	
		ZAP vs Control	ZAP+CN03 vs ZAP
Q13283	G3BP1	↓	↑
P54725	RAD23A	↓	↑
O60841	EIF5B	↓	↑
Q9H6Z4	RANBP3	↓	↑
Q6PKG0	LARP1	↓	↑
P55196	AFDN	↓	↑
Q15149-3	PLEC	↓	↑
P23588	EIF4B	↓	↑
Q13501	SQSTM1	↓	↑
Q6P1N0	CC2D1A	↓	↑
Q8N1G4	LRRC47	↓	↑

4.3.4 Protein kinases activity in zaprinast stressed 661W-A11

We then analyzed the upstream kinases that were most likely responsible for the differential phosphorylation between zaprinast treated 661W-A11 group and the untreated 661W-A11 group. A total 117 protein kinases were predicted to regulate the differentially expressed phosphorylation peptides, and 53 of them were significantly changed. 31 kinases that were highly active after zaprinast treatment, and 22 kinases were downregulated. The protein–protein interaction (PPI) networks of these identified kinases are visualized by STRING (http://string-db.org/cgi/input.pl) in Figure 4.16 A, in which PPI of 31 upregulated kinases after zaprinast treatment are shown. The most enriched highly connected kinases were as follows: mitogen-activated protein kinase 12 (MAPK12), which interacted with 13 predicted kinases; protein kinase CAMP-activated catalytic subunit beta (PRKACB), which interacted with 11 predicted kinases, and raf-1 proto-oncogene serine/threonine kinase (RAF1), which interacted with 11 predicted kinases. Notably, PKG activation (i.e. Prkg1) was confirmed by this analysis (Figure 4.16 A, red circle). Figure 4.16 B shows the PPI of the 22 downregulated kinases, in which aurora kinase A (AURKA) and polo like kinase 1 (PLK1) were the most enriched highly connected kinases, each interacted with other 9 kinases.

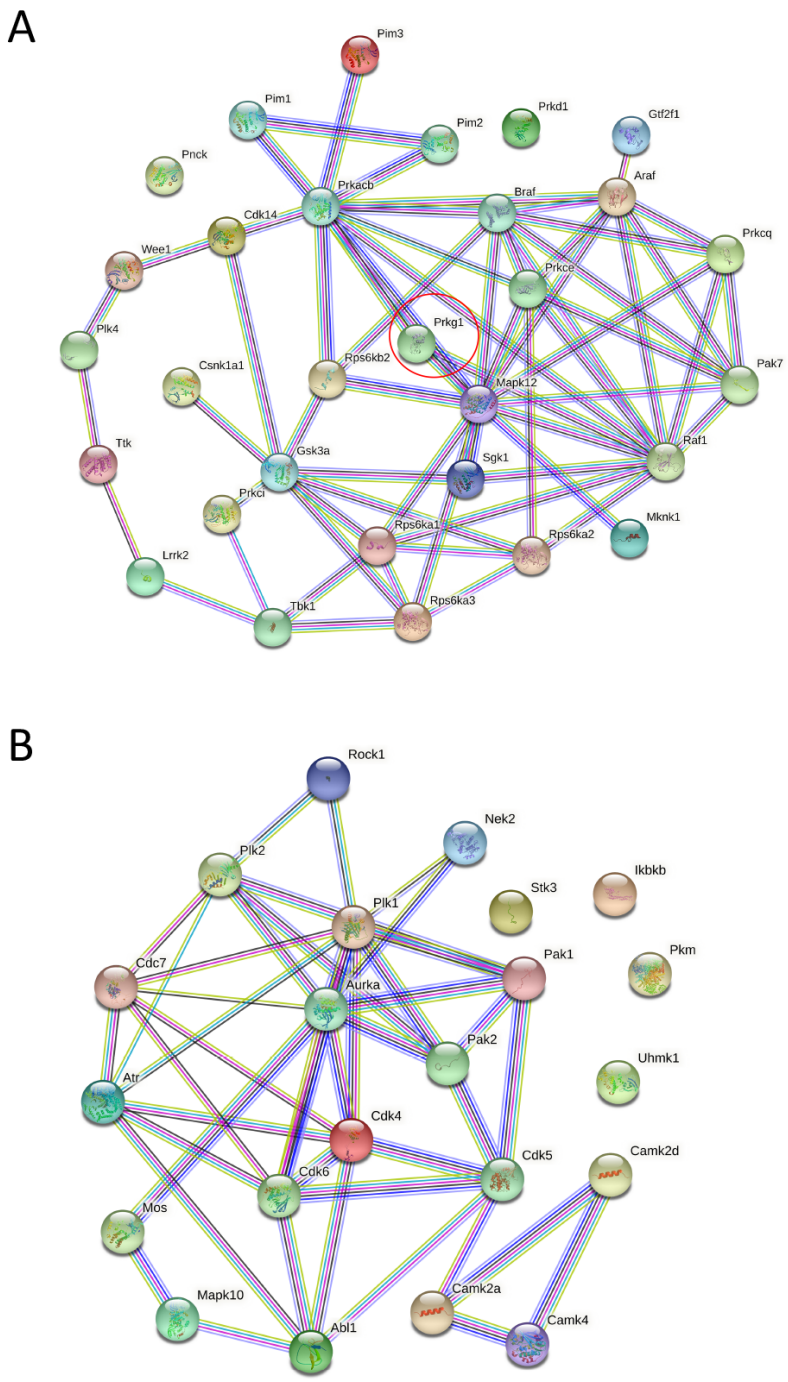

Figure 4.16 The protein–protein interaction (PPI) networks of identified kinases in 661W-A11 cells after zaprinast treatment. (A) PPI of 31 upregulated kinases in zaprinast treated 661W-A11 compared to untreated 661W-A11. (B) PPI of 22 downregulated kinases in zaprinast treated 661W-A11 compared to untreated 661W-A11.

4.3.5 Protein kinases activity in zaprinast stressed 661W-A11 treated with PKG inhibitor CN03

Upon CN03 treatment, 29 kinases were identified with a significant change compared to zaprinast treated group. Among them, 16 kinases were upregulated and 13 were downregulated. In the upregulated kinases, protein kinase C delta (PRKCD) and protein kinase C zeta (PRKCZ) were with the most abundant connections, each interacted with 6 other predicted kinases in the PPI networks (Figure 4.17 A). While mitogen-activated protein kinase 7 (MAP3K7) and TANK binding kinase 1 (TBK1) were with the most abundant connections in the downregulated kinases, each connected with 4 predicted kinases (Figure 4.17 B).

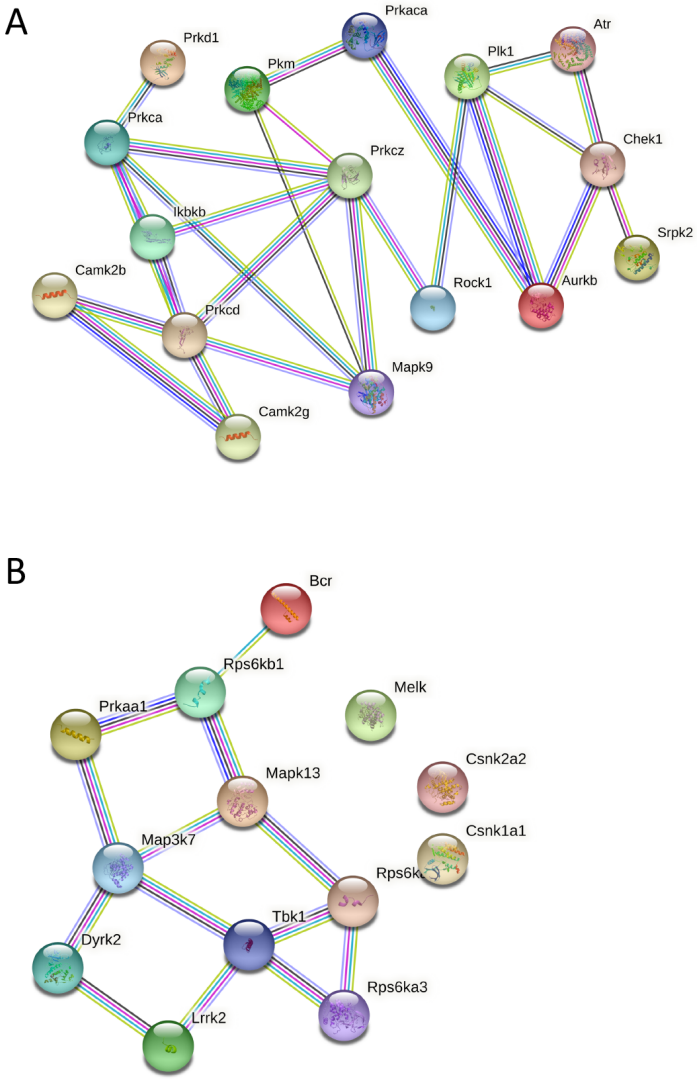

Figure 4.17 The protein–protein interaction (PPI) networks of identified kinases in zaprinast stressed 661W-A11 treated with the cGMP analogue CN03. (A) The PPI of 16 upregulated kinases in CN03 + zaprinast treated 661W-A11 compared to zaprinast treated 661W-A11. (B) The PPI of 13

downregulated kinases in CN03 + zaprinast treated 661W-A11 compared to zaprinast treated 661W-A11.

To select the upstream kinases that were possibly regulated by PKG, we overlapped the changed kinases in ZAP vs control and in ZAP+CN03 vs ZAP, and identified 10 kinase candidates that were possibly regulated by PKG (Figure 4.18). Among them, rho associated coiled-coil containing protein kinase 1 (ROCK1), ataxia-telangiectasia and rad3 (ATR), polo like kinase 1 (PLK1), pyruvate kinase M1/2 (PKM) and inhibitor of nuclear factor kappa B kinase subunit beta (IKBKB) were downregulated after zaprinast treatment, but were upregulated upon CN03 treatment, thus they were possibly negatively regulated by PKG. Conversely, TBK1, leucine rich repeat kinase 2 (LRRK2), ribosomal protein S6 kinase A3 (RPS6KA3), ribosomal protein S6 kinase A1 (RPS6KA1) and casein kinase 1 alpha 1 (CSNK1A1), which were upregulated in the cells treated with zaprinast and downregulated upon CN03 treatment, were positively regulated by PKG. The kinases candidates regulated by PKG were listed in Table 6.

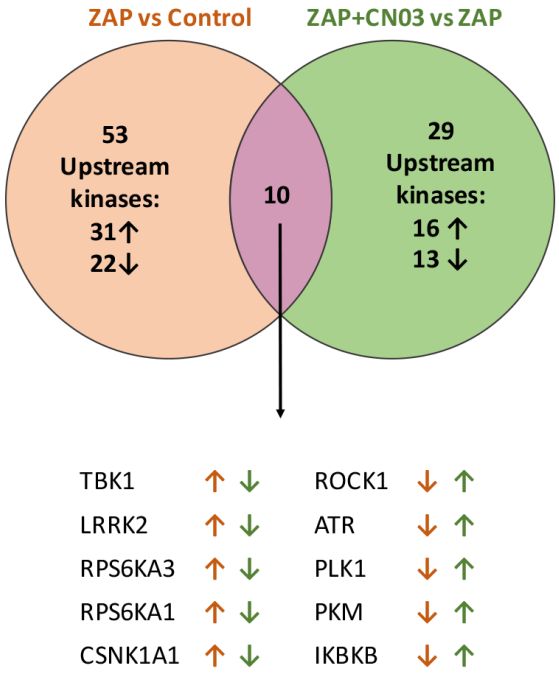

Figure 4.18 The overlap of between kinases changed in ZAP vs Control (orange) and ZAP + CN03 vs ZAP (green). Increased or reduced activity of a kinase is indicated by arrows pointing upwards or downwards, respectively.

Table 6 List of kinase candidates regulated by PKG

Kinase	Full name	Kinase activity	
		ZAP vs Control	ZAP+CN03 vs ZAP
ROCK1	Rho associated coiled-coil containing protein kinase 1	↓	↑
ATR	Ataxia-telangiectasia and Rad3	↓	↑
PLK1	Polo like kinase 1	↓	↑
PKM	Pyruvate kinase M1/2	↓	↑
IKBKB	Inhibitor of nuclear factor kappa B kinase subunit beta	↓	↑
TBK1	TANK binding kinase 1	↑	↓
LRRK2	Leucine rich repeat kinase 2	↑	↓
RPS6KA3	Ribosomal protein S6 kinase A3	↑	↓
RPS6KA1	Ribosomal protein S6 kinase A1	↑	↓
CSNKA1	Casein kinase 1 alpha 1	↑	↓

Till now it is still unknown how PKG exerts its detrimental effects in photoreceptors during retina degeneration and what are the targets of PKG phosphorylation. Here, we applied phosphoproteomic analysis in our cell model and identified several phosphorylated substrates and kinases candidates that were possibly regulated by PKG. These results are a first step towards the identification of new cell death mechanism activated during photoreceptor degeneration based on novel targets of PKG activity.

The significant difference in phosphorylated sites between zaprinast treated cells and CN03 plus zaprinast treated cells indicated PKG inhibition influenced those phosphorylated substrates, thus their upstream kinases could be the candidates for PKG targets and may play a role in photoreceptor cell death mechanism. We identified 10 kinase candidates that were possibly regulated by PKG, and further studies will be necessary on these candidates to explore their potential links to photoreceptor degeneration. For instance, one isoform of PKM, PKM2, was previously found abundantly expressed in rod photoreceptors and was able to regulate the visual function through PDE6B in photoreceptor [228]. PKM2 plays a critical role in photoreceptor survival in different retinal diseases that resulted in photoreceptor cell death, including diabetic retinopathy and retinal detachment [229, 230]. In addition, PKM2 inhibition could reduce the levels of apoptosis and oxidative stress in 661W cells induced by photodamage [231]. More importantly, a recent study showed that the ablation of PKM2 resulted in thicker retinal layers and enhanced retina function and survival in a PDE6B

preclinical model of RP [232]. We also identified ROCK1 as one of the kinase candidates. A previous study linked the increased ROCK1 level to augmented intracellular calcium, in addition, it showed that ROCK1 was a major target of RhoA [233]. ATR was demonstrated to be localized in the connecting cilium and to regulate the ciliary function in photoreceptors possibly through poly (ADP-ribose) polymerase (PARP) [234]. More advanced research is required to elucidate the potential link between these kinases candidates and photoreceptor degeneration.

Among the substrates candidates that were possibly regulated by cGMP/PKG, we did not detect the substrates p-VASP and p-RhoA that were reported as known PKG substrates. A possible reason could be that during protein extraction process, the lack of detergent in lysis buffer may contribute to the loss of some transmembrane or anchored proteins. Another postulation is, if the target proteins such as p-VASP and p-RhoA are buried under a number of other more abundant proteins, which may mask the mass spectrometry detection and the identification of proteins of interest. This also might explain why we didn't see the PKGs among the downregulated kinases in response to CN03, as the detected PKG substrates variances may not be as evident as the substrates variances regulated by other kinases.

The identification of novel downstream PKG targets opens future studies for PKG-mediated photoreceptor degeneration, and for the application in determining novel diagnostic and therapeutic biomarkers for retinal degeneration. A subset of the identified proteins that were differentially modified in response to zaprinast and to CN03 in the 661W-A11 cell line but, more relevantly, in retinas from murine models of IRD, will be validated.

4.4 Targeting the downstream of Ca^{2+} influx

. It is hypothesized that high levels of cGMP lead to Ca^{2+} influx through the CNG channel and the excessive Ca^{2+} triggers photoreceptor cell death. However, the downstream process following Ca^{2+} influx is still a mystery. Intracellular Ca^{2+} concentration regulation is essential for neuronal function and survival and one of the Ca^{2+} functions is to regulate calcineurin, which in turn controls transcription factor NFATc (nuclear factor of activated T cells) through its binding to Ca^{2+} /calcineurin-dependent translocation regulatory domain. The NFATc family (NFATc1, NFATc2, NFATc3, NFATc4 and NFATc5) comprises transcription factors that are sensitive to Ca^{2+} levels in many types of cells. NFATc proteins in their phosphorylated forms reside in the cytoplasm when cells are in resting conditions. Upon stimulation, with the increasing intracellular Ca^{2+} concentration, the phosphatase calcineurin is activated and dephosphorylates NFATc, eventually resulting in NFATc translocation to nucleus [235]. Of the five NFATc members, four isoforms (NFATc1-4) are subject to this dephosphorylation process. Previous studies have directly linked the NFATc4 signaling to cGMP-dependent protein kinase (PKG) activity. In fact, activation of PKG by cGMP in cardiomyocytes could suppress NFATc4 transcriptional activity [236, 237] . NFATc1 is one of the isoforms of the NFATc family, it has been found to play a role in retina neovascularization and other angiogenesis diseases [238].

4.4.1 NFATc1 expression in zaprinast stressed 661W-A11

To determine if the increased Ca^{2+} level resulted from zaprinast treatment could activate calcineurin and NFATc, we first tested and compared the gene expression level of *Nfatc1* between untreated and zaprinast treated 661W-A11 cells. By real-time qPCR, we observed that the *Nfatc1* gene expression level was increased after zaprinast treatment (Figure 4.19 A).

We then wondered if the NFATc1 could be dephosphorylated and translocated to nucleus after zaprinast stimulation. By immunofluorescence we observed that the NFATc1 mainly resided in the cytoplasm around the nuclei in the absence of zaprinast, however, after zaprinast treatment, nuclear staining of NFATc1 could be detected (Figure 4.19 B, white arrows), indicating its translocation to the nuclei. By calculating the number of NFATc1 nuclear positive cells, around 7% cells were estimated to display the NFATc1 nuclear translocation (Figure 4.19 B).

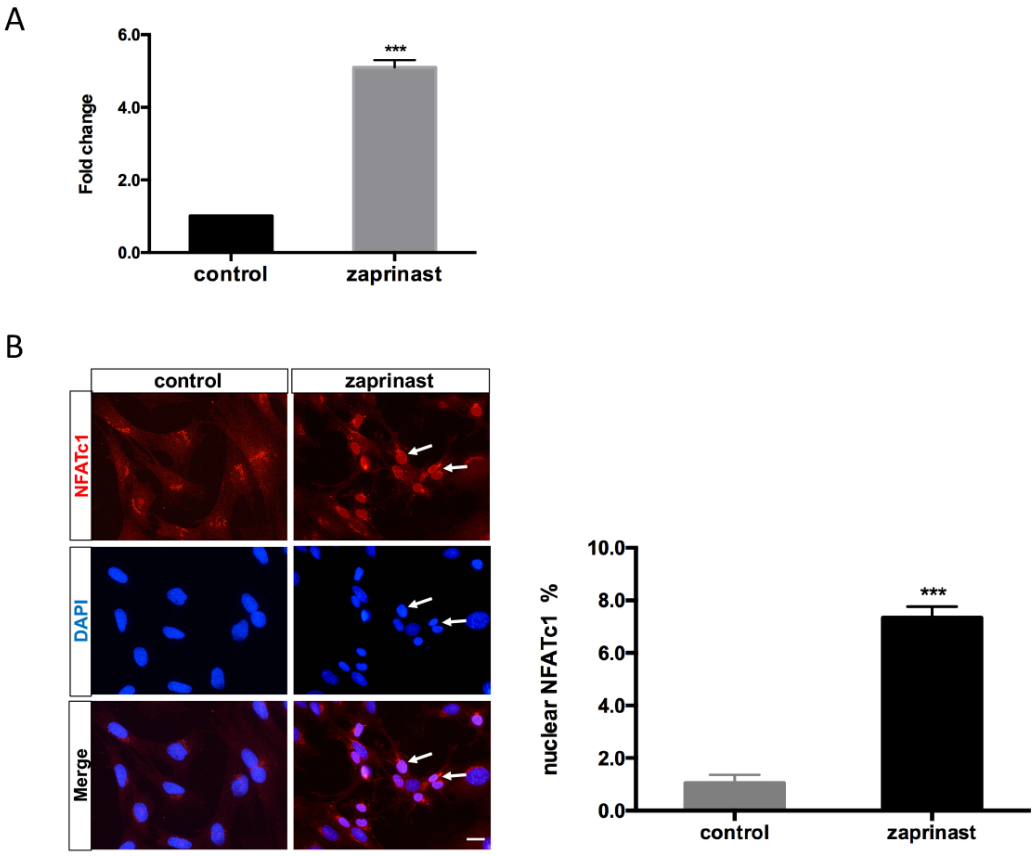

Figure 4.19 NFATc1 expression in 661W-A11 cells. (A) Real-time qPCR analysis revealed an increase in gene expression of *Nfatc1* after zaprinast treatment. control: cells were treated with equivalent DMSO for 24 h as the control; zaprinast: cells treated with 400 μM zaprinast for 24 h. (B) NFATc1 nuclear translocation in zaprinast treated 661W-A11. Immunofluorescence analysis of NFATc1 (red) protein in 661W-A11 cells, white arrows indicate the nuclear translocation of NFATc1 in the cells treated with zaprinast. On the right-hand side, the percentage of NFATc1 nuclear positive cells was calculated. control: cells treated with corresponding volume of DMSO as a vehicle control; ZAP: cells treated with 400 μM zaprinast for 24 h. Nuclei were stained with DAPI (blue). Scale bar: 10 μm.

4.4.2 NFATc1 expression in different IRD models

To define if the observation of NFATc1 found in the cells could also be confirmed in RP animal models, we first tested the *Nfatc1* gene level in three different animal models: *rd1*, *rd10* and $Rho^{P23H/+}$, that were previously reported to be characterized by increased intracellular calcium in degenerating photoreceptors. The former two models bear the mutations in PDE6B, the third is a dominant murine model of RP, with a mutation in Rhodopsin. By real-time PCR, we

compared the gene levels of *Nfatc1* in the three mutant retinas to age-matched wild types, and found that *Nfatc1*gene expressions were increased in all three animal models (Figure 4.20 A). To investigate if NFATc1 was relevant for the progression of photoreceptor degeneration, we analyzed by immunofluorescence the subcellular localization of NFATc1 in the retina of $Rho^{P23H/+}$ mice. The double staining of TUNEL and NFATc1 showed that NFATc1 staining (green) could be detected in around 60% nuclei of dying cells (Figure 4.20 B). These results linked NFATc1 nuclear translocation to photoreceptor degeneration.

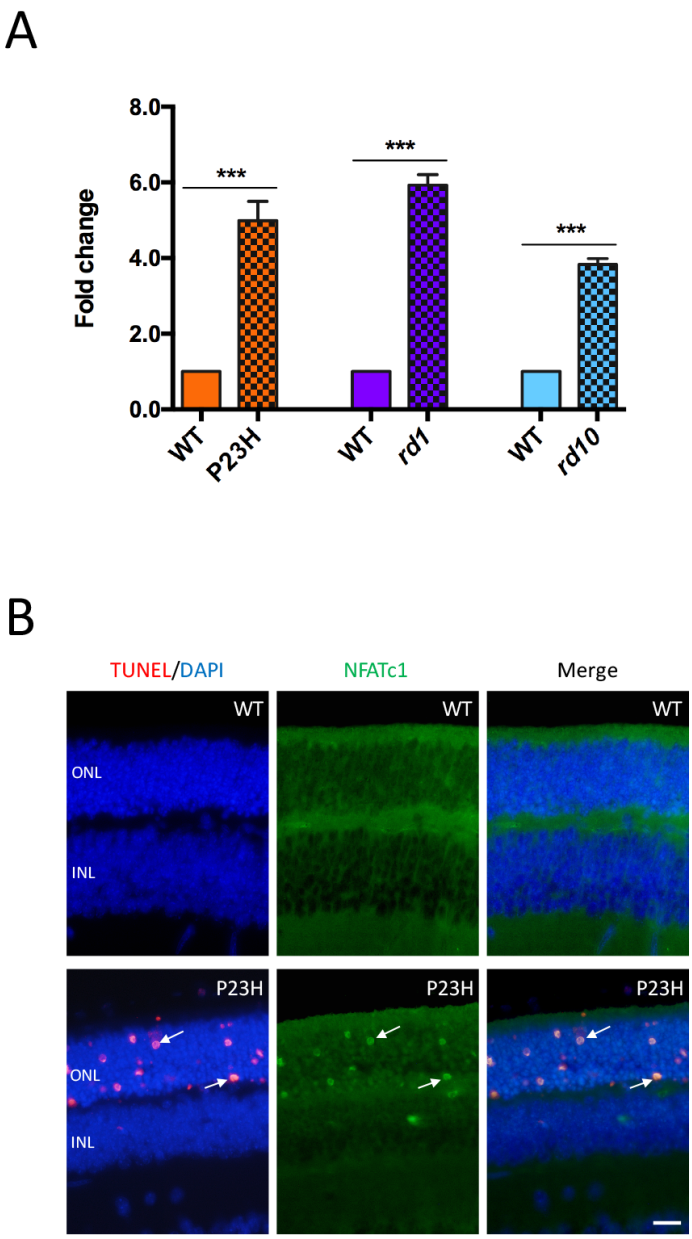

Figure 4.20 NFATc1 expression in IRD animal models. (A) The gene expressions of *Nfatc1* in retinas from $Rho^{P23H/+}$ (P23H), *rd1* and *rd10* animal models compared to wild type (WT) retinas. (B) NFATc1 nuclear translocation in $Rho^{P23H/+}$ mouse model. Double staining of TUNEL assay (red) and of

NFATc1 (green) protein in $Rho^{P23H/+}$ (P23H) and wild type (WT) retinas. White arrows indicate the co-staining of NFATc1 and TUNEL. Nuclei were stained with DAPI (blue). Scale bar: 50 μm.

4.4.3 Calcineurin inhibitor blocked NFATc1 nuclear translocation

In order to investigate if the NFATc1 nuclear translocation observed in zaprinast treatment cells was regulated by calcineurin, an inhibitor targeting calcineurin activity called cyclosporin A (CSA) was applied. Cyclosporin is a cyclic nonribosomal peptide which is widely used as an immunosuppressant drug in post-allogeneic organ transplant.

As first step, the cytotoxicity of CSA was evaluated. Concentrations of CSA ranging from 1 μg/mL to 50 μg/mL were applied to 661W-A11 cells and no significant toxicity was observed (Figure 4.21 A). Next CSA was added to zaprinast stressed cells to assess if the compound could exert a protective effect against zaprianst induced PDE6 inhibition. By cell viability assay, we found a significant protective effect of CSA starting from the concentration of 20 μg/mL (Figure 4.21 B).

Based on the cell viability results, 20 μg/mL CSA was chosen for assessing its effect on NFATc1 nuclear translocation induced by zaprinast treatment. A 75% reduction in the positive nuclear NFATc1 cells was observed, from 7% (before CSA treatment) to less than 2% (after CSA treatment) (Figure 4.21 C and D).

Altogether this evidence indicated that the NFATc1 nuclear translocation was mediated by calcineurin and that blocking the calcineurin activity might have a protective effect in photoreceptor degeneration.

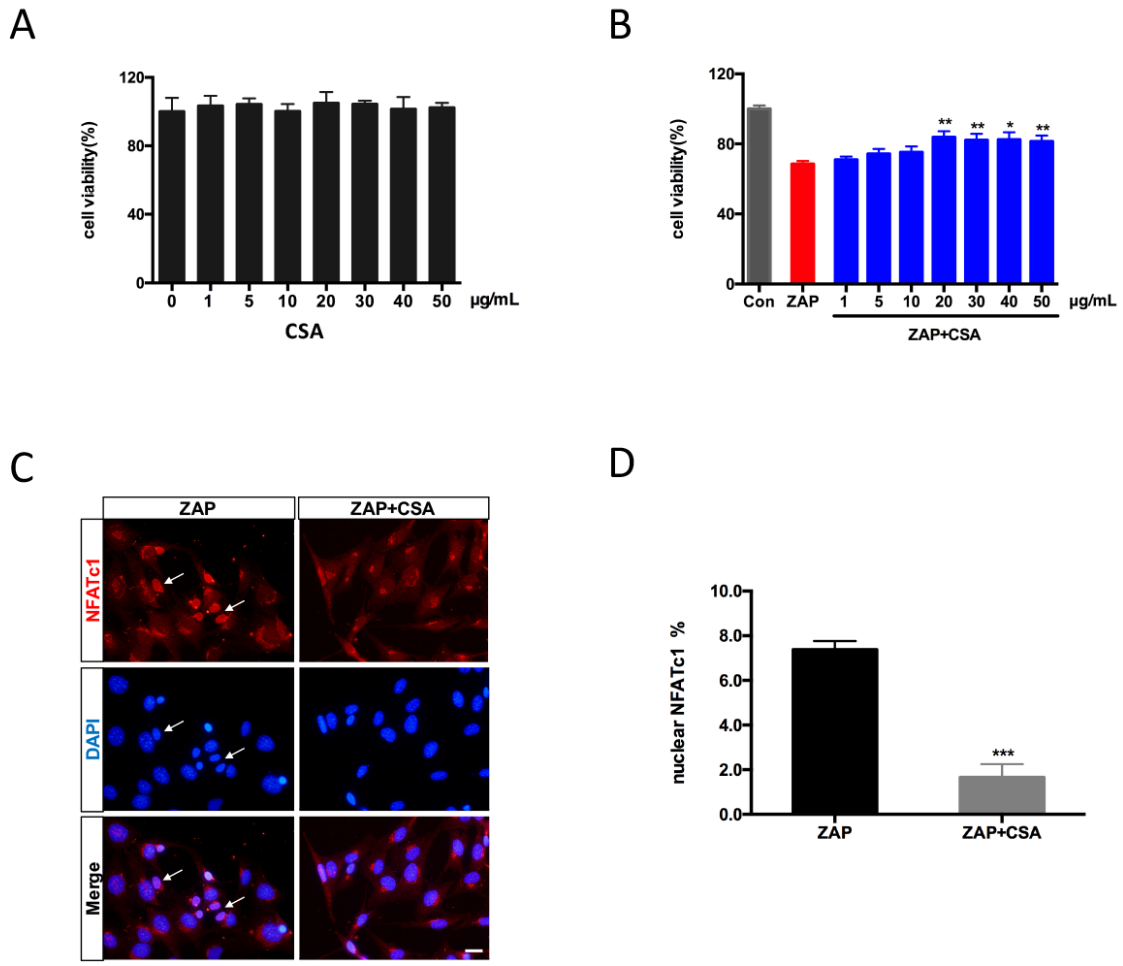

Figure 4.21 The effects of calcineurin inhibitor in zaprinast stressed 661W-A11 cells. (A) Cytotoxicity of cyclosporin A (CSA) on 661W-A11 cells based on MTT assay. (B) The effect of CSA on zaprinast stressed 661W-A11 cells based on MTT assay. (C) Immunofluorescence analysis showed that CSA decreased the NFATc1 nuclear translocation in zaprinast stressed 661W-A11 cells. NFATc1 was stained in red, nuclei were stained with DAPI (blue). Scale bar: 10 μm. (D) Quantification of nuclear NFATc1 positive cells presented in panel C. Con: cells were treated with DMSO as a control; ZAP: cells were treated with 400 μM zaprinast for 24 h; ZAP+CSA: cells were treated with different concentrations of cyclosporin A together with 400 μM zaprinast for 24 h. *P<0.05, **P<0.01, ***P<0.001.

4.4.4 IL2 and IL18 gene expression was upregulated during photoreceptor degeneration

NFATc transcription factors are involved in inflammation and regulate expressions of a variety of interleukins (IL). We thus investigated the gene expression of IL2 and IL18 in our photoreceptor degeneration model.

The gene expressions of IL2 and IL18 were assessed in 661W-A11 cells with or without zaprianst treatment, and we found that zaprinast significantly increased expression of these genes (Figure 4.22 A). The application of CSA in zaprinast stressed 661-A11 cells reduced the gene expressions of IL2 and IL18 (Figure 4.22 B), which suggested the increasing interleukins were regulated by calcineurin. Then we also evaluated the expression of IL2 and IL18 in retinas derived from *Rho*$^{P23H/+}$, *rd1* and *rd10* compared to age-matched wild type retinas, and detected an increased IL2 and IL18 gene level in all three models (Figure 4.22 C and D). The altered gene expression of IL2 and IL18 indicated the possible involvement of inflammation in photoreceptor degeneration, which might be regulated by NFATc transcription factors through a Ca^{2+}/ calcineurin pathway.

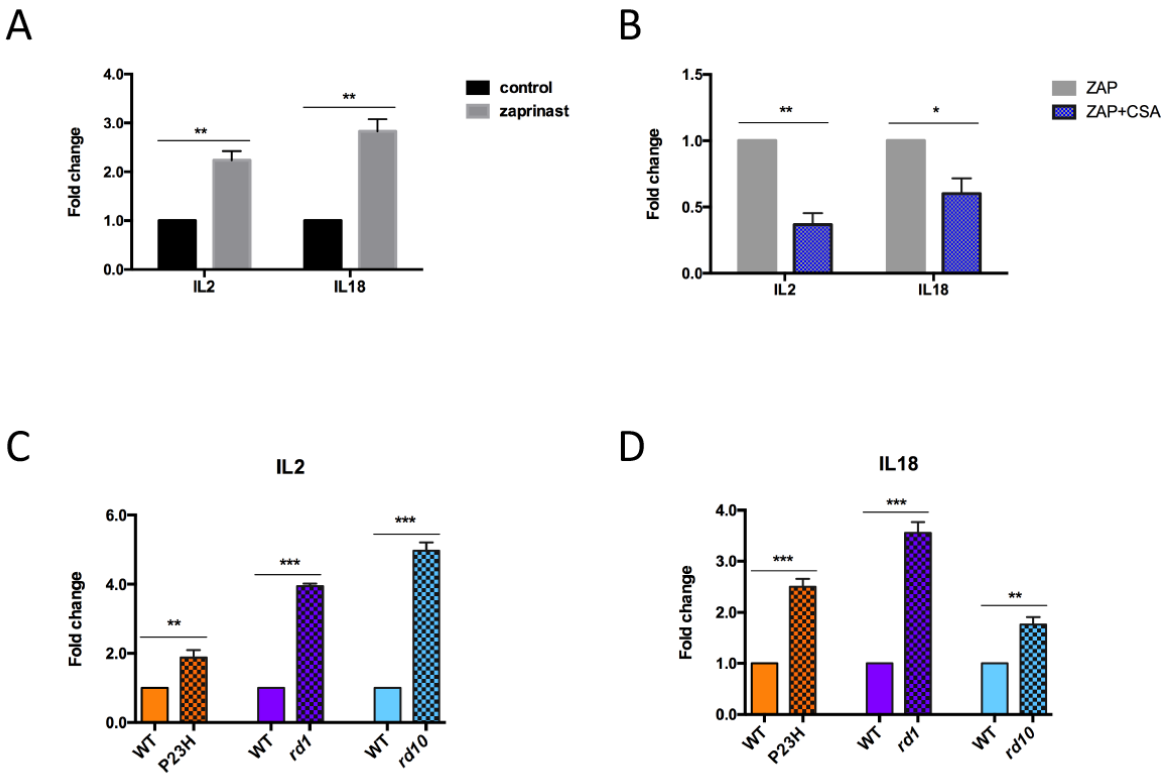

Figure 4.22 Gene expression of IL2 and IL18 in cells and IRD animal models. (A) Increased gene expression of IL2 and IL18 was detected by real-time qPCR in 661W-A11 cells upon zaprinast treatment. (B) Cyclosporine A (CSA) treatment decreased gene expression of IL2 and IL18 in zaprinast stressed 661W-A11 cells. Increased gene expressions of IL2 (C) or IL18 (D) were detected by real-time qPCR in retinas derived from *Rho*$^{P23H/+}$, *rd1* and *rd10* mouse compared to age-matched wild type (WT) retinas. ZAP: cells were treated with 400 µM zaprinast for 24 h; ZAP+CSA: cells were treated with 20 µM cyclosporin A together with 400 µM zaprinast for 24 h. *P<0.05, **P<0.01, ***P<0.001.

The downstream of Ca^{2+} signaling pathway in photoreceptor degeneration remains largely unknown. The elevated intracellular Ca^{2+} activates various signaling pathways and one of them know to date is the calmodulin–calcineurin pathway, with the activation of NFATc and Ca^{2+}-dependent kinase-calmodulin (CAMK). The nuclear translocation of NFATc1 in our cell model and the detection of the link between NFATc1 and dying cells in the IRD animal models revealed that NFATc transcription factors may contribute to the degeneration of photoreceptors. Interestingly, we calculated that around 60% of the dying cells (TUNEL positive cells) showed nuclear staining of NFATc1. Not all the dying cells were observed with NFATc1 nuclear translocation. We cannot exclude that our detection of NFATc1 might fail to detect low amounts of this transcription factor in some dying cells. In fact, NFATc1 is not abundantly expressed in mouse retina [239]. We can also postulate that other isoforms of NFATc transcription factors are activated during photoreceptor degeneration under Ca^{2+}/calcineurin pathway. This is similar with a previous study in our lab showing that in retinas derived from *rd1* mice, 80% of the dying cells were detected with AIF nuclear translocation [108].

The application of calcineurin inhibitor in the cells demonstrated that the nuclear translocation of NFATc1 was regulated by calcineurin in the cell model, and that the calcineurin inhibition even showed a protective effect against PDE6 inhibition. This is not surprising as CSA was reported to have neuroprotective effects in neurological disorders, ischemic stroke and traumatic brain injury [240]. CSA was also demonstrated to be able to protect glutamate-induced damage in different types of neuronal cells [241, 242]. Furthermore, in retina diseases, such as retinal ischemia, CSA promoted the ganglion cell survival by preventing mitochondrial alteration [243].

The increasing gene expression of IL2 and IL18 in the cell model and in animal models may indicate the involvement of inflammatory response in photoreceptor degeneration, this is consistent with the previous findings that in the vitreous humor of patients with RP, the pro-inflammatory interleukins such as IL2, IL4, IL6 and IL8 were elevated [244]. IL18 was also linked to degenerative retinopathies, such as AMD [245].

Those results indicate the activation of NFATc1 by nuclear translocation may trigger inflammatory interleukins that might be linked to photoreceptor degeneration. Overexpression of an activated form of NFATc1 could help address whether this transcription factor directly regulates interleukins expression in photoreceptor cells.

Experiments with CSA on the effect of IL2 and IL18 suggest that activation of NFATc1 transcription factor may correlate with increased interleukins and inflammation in photoreceptor degeneration. However, we will need more evidences that can be produced by

overexpression of a constitutively activated NFATc1 in 661W-A11 cells, and analysis of activated microglia in degenerating retinas upon exposure to CSA *in vivo*.

4.5 Drug delivery system (DDS) based on nanoparticles

The delivery of a drug to the neural retina is challenging due to the different barriers that need to be crossed and the physicochemical environment of the vitreous that may affect the entrance of the drug in the target cells. Molecules such as cGMP and its analogues can be processed into different salts forms to address physicochemical and biological concerns such as solubility, stability and toxicity. A high-water solubility and relatively good membrane permeability are generally desired from the salt form to improve uptake from targeted tissue, but one characteristic is in conflict with the other one. While this is true in most cases, in the ocular vitreous, small active molecule with such properties may suffer from a fast clearance and therefore using a proper drug delivery system could be crucial if the target tissue is the retina.
In this chapter, one-pot synthesis of advanced solid lipid nanoparticle was developed to encapsulate and deliver small hydrophilic molecules such as a cGMP analogue to retinal cells. Some characteristics were defined as optimal for the movement of a drug in the vitreous when an intravitreal delivery is envisioned. A negatively charged surface and size below 500 nm are preferred qualities for DDS because these features may improve particle mobility [246, 247].
Encapsulation efficiency, surface charge, particle size and its polydispersity were the physiochemical responses investigated in the early stage development. For the shell formulation, a comparison between using pure solid lipid and solid lipid/polymer composite was explored. In case of the core formulation, the effect of adding a hydrogel core was investigated. At the later stage of the development, *in vitro* study was performed using ARPE-19 and 661W retinal cell lines to validate the nanoparticle cytotoxicity as well as the cellular uptake properties. Finally, efficacy study was performed by using the hydrophilic cGMP analogue, Rp-8-Br-PET-cGMPS (CN03), in sodium salt form which has been shown to exhibit neuroprotective properties.

4.5.1 The generation and characterization of nanoparticles

The generation and characterization of solid lipid nanoparticle (SLN) were performed by our partner Inocure. Six types of solid lipid nanoparticles (SLN.01-SLN.06) with different formulations were generated. The formulation and components of SLNs are illustrated in Table 7 and Figure 4.23.

Table 7. Formulation code and component mass dissolved in O-phase for each formulation.

Drug Delivery System (DDS)	Tripalmitin (GTP; mg)	Soy-Bean Lecithin (LCT; mg)	Stearic Acid (SA; mg)	Poly-Ɛ-caprolactone (PCL; mg)	50/50 DL-lactide/glycolide (PLGA; mg)	Core
SLN.01	15	15	1	-	-	Aqueous
SLN.02	15	15	1	10	-	Aqueous
SLN.03	15	15	1	-	10	Aqueous
SLN.04	15	15	1	-	-	Gel core
SLN.05	15	15	1	10	-	Gel core
SLN.06	15	15	1	-	10	Gel core

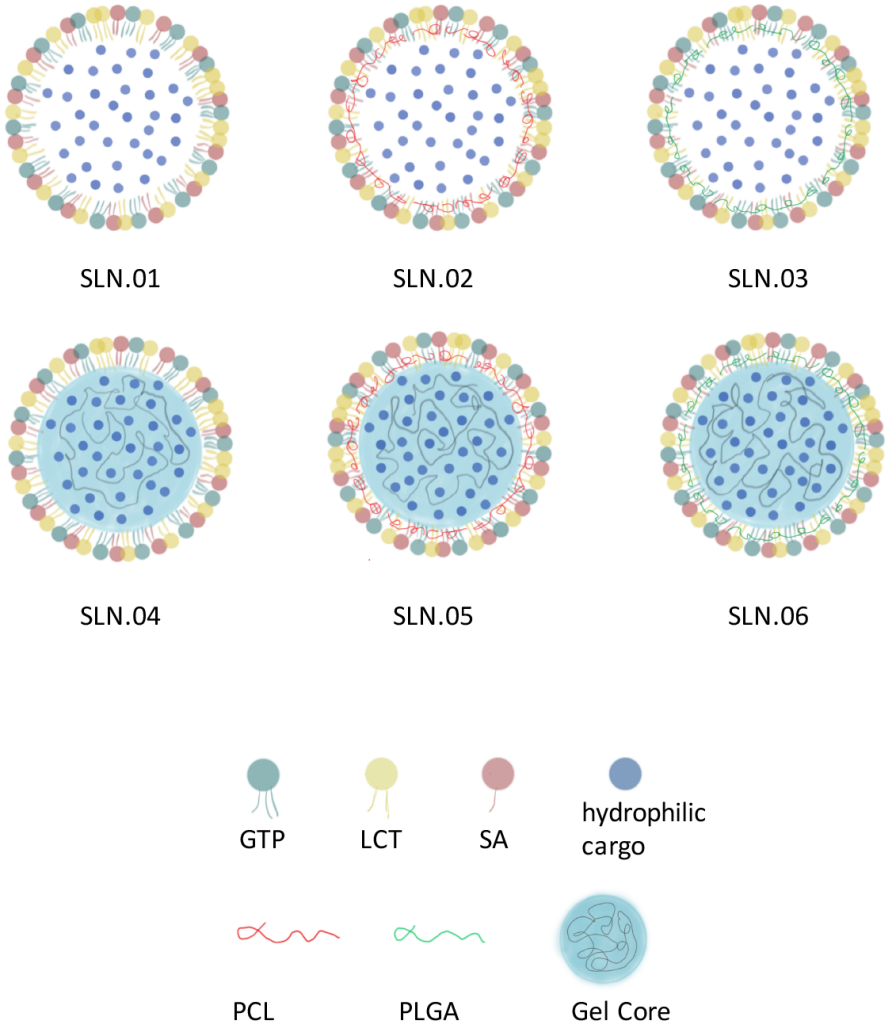

Figure 4.23 Formulation and components of SLNs (SLN.01-SLN.06). GTP: tripalmitin; LCT: soy-bean lecithin; SA: stearic acid; PCL: poly-Ɛ-caprolactone; PLGA: 50/50 DL-lactide/glycolide.

In the study physicochemical characteristics of SLNs performed by Inocure, the particle size did not vary quite much among those six nanoparticles, which were all falling in the range of 200nm to 250nm. Figure 4.24 reports data from Inocure summarizing the characteristics of the different SLNs.

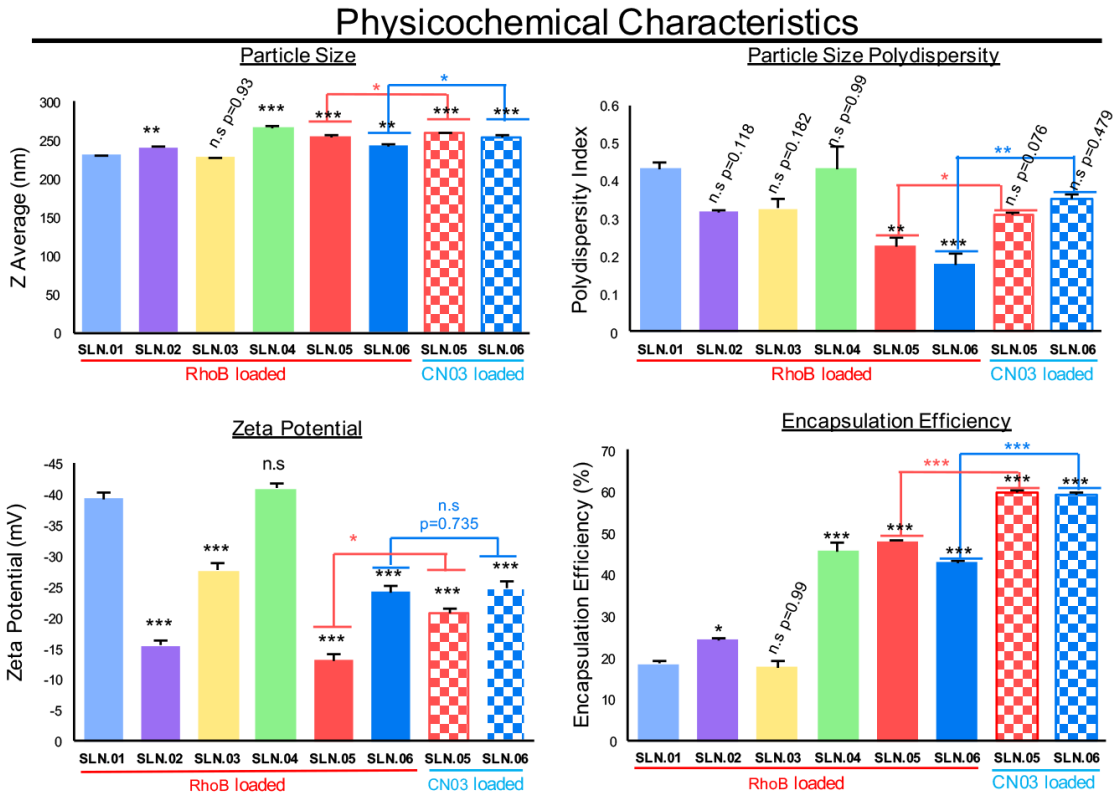

Figure 4.24 Characterization of SLN. Physicochemical characteristics of the generated SLN compared to conventional SLN (SLN.01). Data are presented as mean ± SEM (Standard error of the mean), n = 3 independent experiments. Significance at * P < 0.05, ** P < 0.01, *** P < 0.001, ANOVA followed by Bonferroni's post hoc test. Statistical analysis comparing SLN.05 and SLN.06 loaded with either RhoB or CN.03 were performed using Student's t test.

Based on the analytical analyses of the generated SLN, we chose to focus on SLN.05 and SLN.06 for further studies, since they showed an improvement in PDI, a low negative zeta potential and encapsulation efficiency compared to conventional SLN with pure lipid shell and no gel core (SLN.01). When Inocure assessed the formulation encapsulation capability of SLN.05 and SLN.06 with CN03 they found that both SLNs were able to encapsulate CN03 and

resulted in negatively charged particles of 200-250 nm. Importantly, when the stability test was performed, the particle size was maintained below 300 nm regardless of storage temperature within 1 month of storage in both SLNs (Figure 4.25).

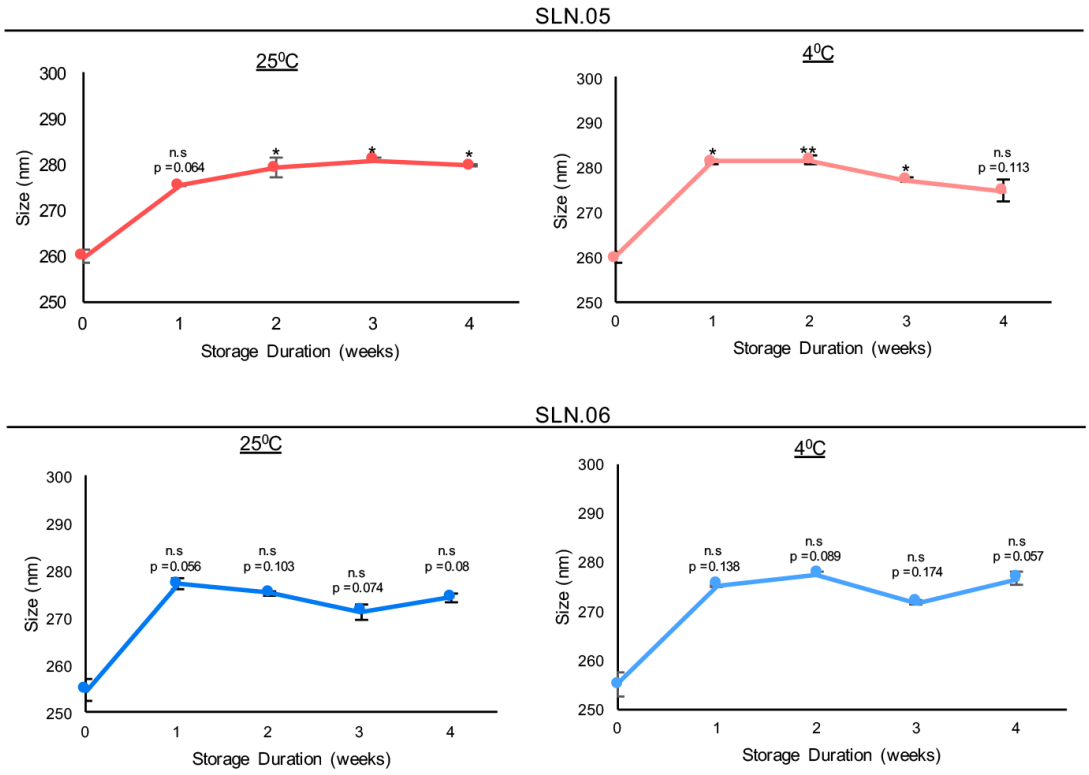

Figure 4.25 Stability study of nanoparticle containing CN03 in 10 mM PBS at different storage temperature. Stability of SLN.05 and SLN.06 stored in PBS at 25 °C and 4 °C was evaluated by analyzing the particle sizes every week up to 4 weeks. Data are presented as mean ± SEM (Standard error of the mean), n = 3 independent experiments. Significance at * $P < 0.05$, ** $P < 0.01$, *** $P < 0.001$, ANOVA followed by Bonferroni's post hoc test.

4.5.2 Evaluation of SLN.05 and SLN.06 toxicity to ARPE-19 and 661W retinal cell lines

We used ARPE-19 cells (human retinal pigment epithelium cell line) and 661W cells (mouse photoreceptor-like cell line) to evaluate the toxicity of SLNs on retinal cells. We exposed ARPE-19 and 661W cells to either SLN.05 or SLN.06 at different concentrations and evaluated toxicity by the MTT cell viability assay at different time points. Both SLN.05 and SLN.06 showed increasing toxicity in dose-dependent manner and time-dependent manner (Figure 4.26).

Overall, SLN.05 showed higher toxicity in both cell types compared to SLN.06. Toxicity of SLN.05 on ARPE-19 cells started to be detected at 200 µg/mL after 5 h of exposure, with a

slight increase at 500 µg/mL and 800 µg/mL. Interestingly, the SLN.05 toxicity of time-dependent manner was not as obvious as expected, with only a negligible decrease at 24 and 48 h. On the other hand, 661W cells showed higher resistance to SLN.05 toxicity at 5 and 24 h, in fact 200 µg/mL of SLN.05 did not significantly reduce the viability even after 24 h of exposure but started to be toxic at 500 µg/mL.

SLN.06 demonstrated to be less toxic to both cell lines. ARPE-19 cells could tolerate up to 500 µg/mL of SLN.06 within 5 h of exposure, while 661W cells could tolerate up to 800 µg/mL of SLN.06 within 24 h exposure. Noticeably, 661W cells showed rather high tolerance within 24 h exposure regardless of concentration, even at 800 µg/mL, no toxicity could be detected. SLN.06 reduced viability of both ARPE-19 and 661W cells after 48 h of exposure.

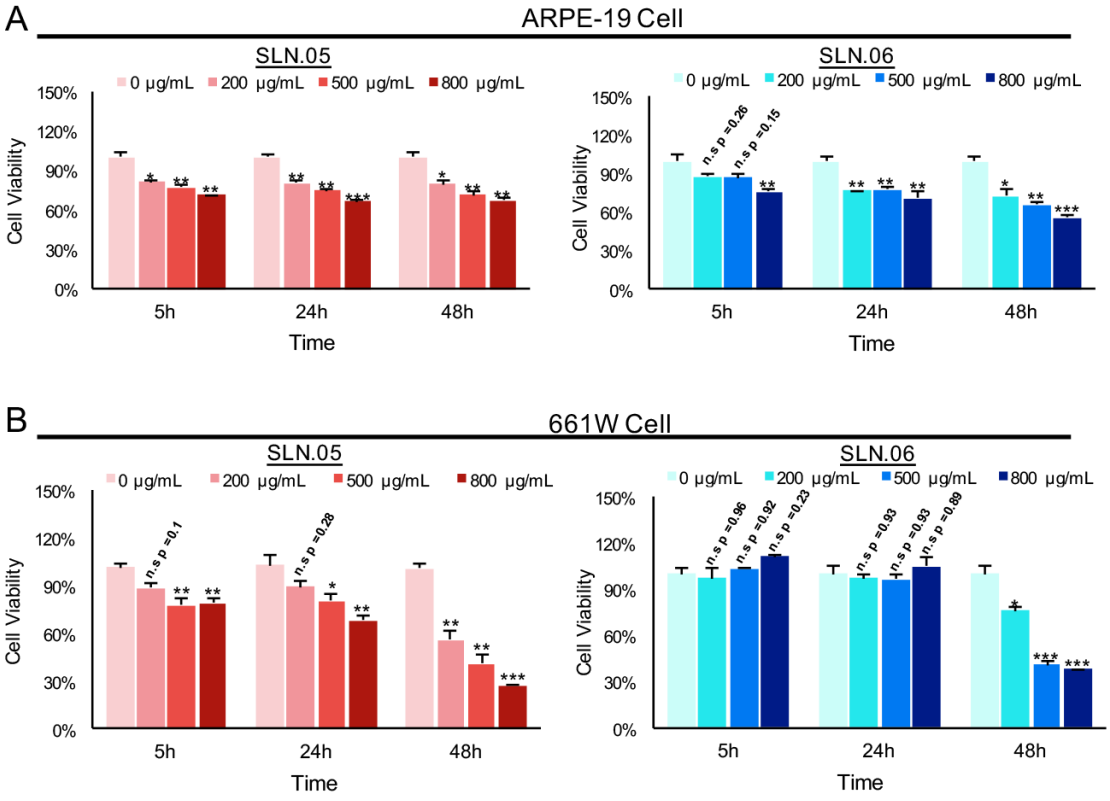

Figure 4.26 Toxicity of SLN to ARPE-19 and 661W retinal cell lines. Toxicity of SLN.05 and SLN.06 to retinal cells lines was assessed by measuring the percentage of cell viability after exposure of SLN at various concentrations and at different time points using MTT assay. Untreated cells (0 µg/mL) were set as 100% cell viability and used as a control. (A) Percentage of ARPE-19 cells viability after exposure of SLN.05 or SLN.06. (B) Percentage of 661W cells viability after exposure of SLN.05 or SLN.06.

Data are presented as mean ± SEM (Standard error of the mean), n = 3 independent experiments. Significance at * P < 0.05, ** P < 0.01, *** P < 0.001, ANOVA followed by Bonferroni's post hoc test.

4.5.3 SLN.05 and SLN.06 internalization by 661W cells

To deliver small hydrophilic molecules to retinal cells, SLNs need to be efficiently internalized by cells. To visualize SLN uptake, Rhodamine B (RhoB; 479.02 g/mol) was used as a small hydrophilic cargo to be encapsulated into SLNs (RhoB-SLN). Different concentrations of RhoB-SLN range from 0 µg/mL to 400 µg/mL were incubated with 661W for 5 h. Figure 4.27 A shows that both RhoB loaded SLNs (RhoB-SLN.05 and RhoB-SLN.06) could be efficiently internalized by 661W cells with the red signal of RhoB detectable in the cell cytoplasm. We also found that the RhoB intensity in the cytosol increased in a concentration dependent manner (Figure 4.27 B).

In consideration of the internalization efficiency and toxicity of the nanoparticles that exerted on the cells, we exposed 661W cells to 200 µg/mL of RhoB-SLN.05 and RhoB-SLN.06, and quantified the fluorescence signal at different time points by flow cytometry, to further study the relationship between internalization efficiency and exposure time. Since free RhoB can also penetrate the cells, we used cells treated with free RhoB suspension for 5 h as control. Only 0.08% of 661W cells were positive for RhoB after treated with free RhoB for 5 h, indicating that RhoB diffusion inside the cells was very low. One hour exposure to RhoB-loaded SLN was sufficient to detect 3.28% of RhoB positive 661W cells after incubation with RhoB-SLN.05 and 3.35% of positive 661W cells after incubation with RhoB-SLN.06. The percentage of RhoB positive cells increased with longer incubation times, within 5 h, it reached 11.87% with RhoB-SLN.05 and 14.65% with RhoB-SLN.06, respectively (Figure 4.27 C).

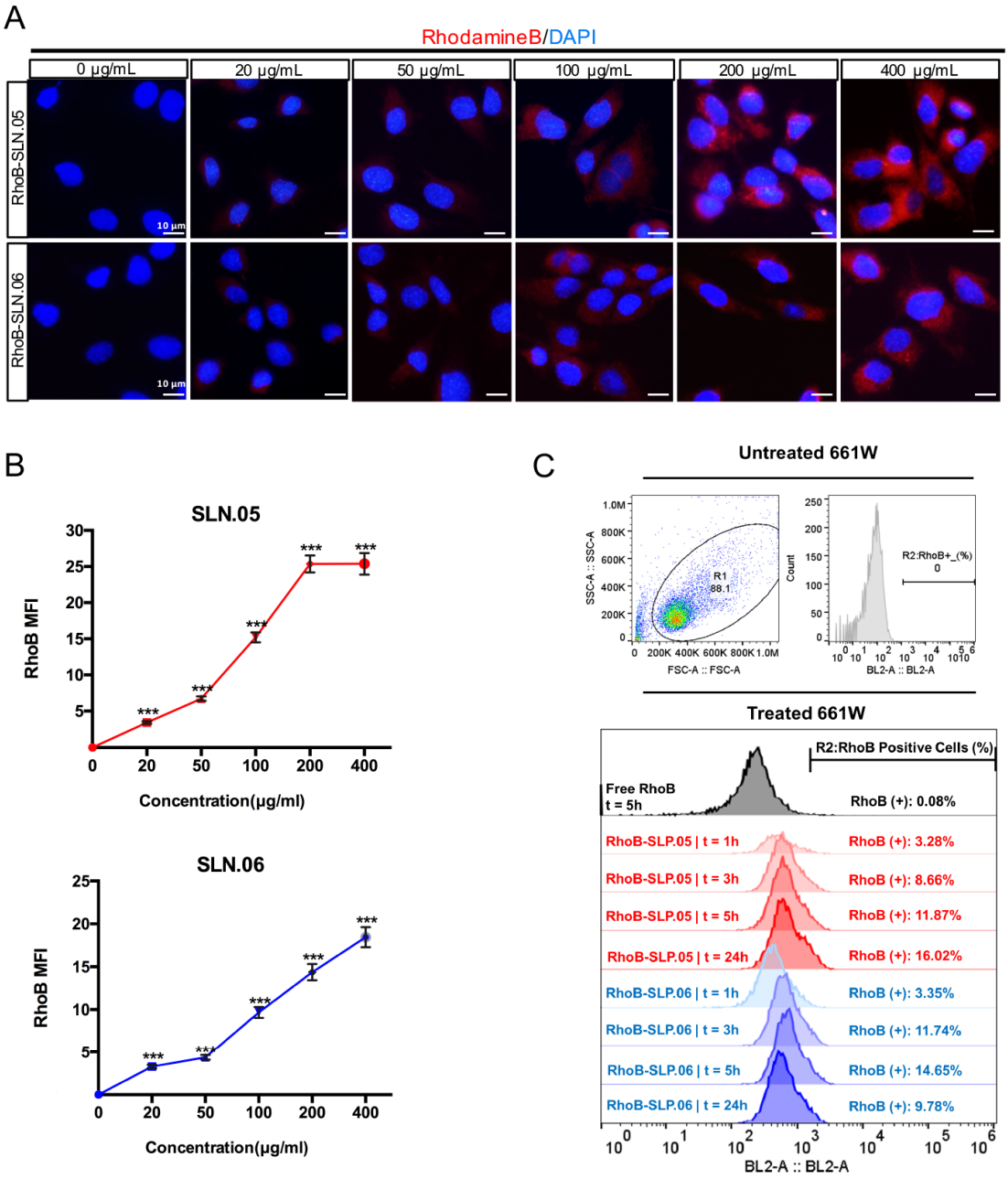

Figure 4.27 Internalization of SLN.05 or SLN.06 by 661W cells. (A) Visualization of internalized SLN by 661W cells using Rhodamine B-loaded SLN (RhoB-SLN). Micrographs of internalized RhoB-SLN.05 or RhoB-SLN.06 (red signal) at various concentrations after 5 h of exposure. Nuclei were stained with DAPI (blue). Scale bar, 10 µm. (B) Mean fluorescence intensity (MFI) of Rhodamine B signal inside the cells was quantified using the Image J software (ncells ≥ 10). (C) Histogram overlay of RhoB relative fluorescence intensity and percentage of RhoB positive cell (RhoB+) assessed by flow cytometry in 661W cells. R1: gating for selecting cells population; R2: gating to select RhoB+ cells based on blue laser (BL2-A) detector; FSC-A: forward scattering channel; SSC-A: side scattering channel.

4.5.4 SLN.05 and SLN.06 internalization by ARPE-19 cells

To further investigate if the nanoparticles could be uptaken by other retinal type of cells, we then added 200 µg/mL of RhoB-SLN.05 and RhoB-SLN.06 to the culture medium of ARPE-19 cells for 5 h. We visually confirmed the intracellular localization of both SLNs after being internalized by the ARPE-19 cells by staining the membrane of the cells with an anti-ZO-1 antibody (specific antibody that recognizes a peripheral membrane protein in epithelial cells), and we observed that RhoB-SLNs were localized inside the cytosol after the internalization process (Figure 4.28 A).

We also investigated the tendency of internalization efficiency with prolonged time exposure to nanoparticles in ARPE-19 cells. Similar trend as found in 661W cells of SLN uptake was observed in ARPE-19 cells (Figure 4.28 B). 0.09% of ARPE-19 cells were positive for RhoB after treatment with free RhoB for 5 h. With 1 h exposure to RhoB-loaded SLN, 7.98% cells were detected as RhoB positive after incubation with RhoB-SLN.05 and 1.58% with RhoB-SLN.06. Surprisingly, within 3 h, nearly 50% cells were positive with RhoB-SLN.05 incubation, while only 5.87% cells were positive with RhoB-SLN.06. After 5 h, the uptake of RhoB-SLN.05 seemed to reach a plateau since at 5 h and 24 h, the percentage of positive cells remained similar. With RhoB-SLN.06, the percentage of positive cells was lower nevertheless it rose steadily until 24 h, with the number reaching 15.54% (Figure 4.28 B).

Taken together, these data indicate that SLN.05 and SLN.06 can be internalized by both photoreceptor and RPE cell types.

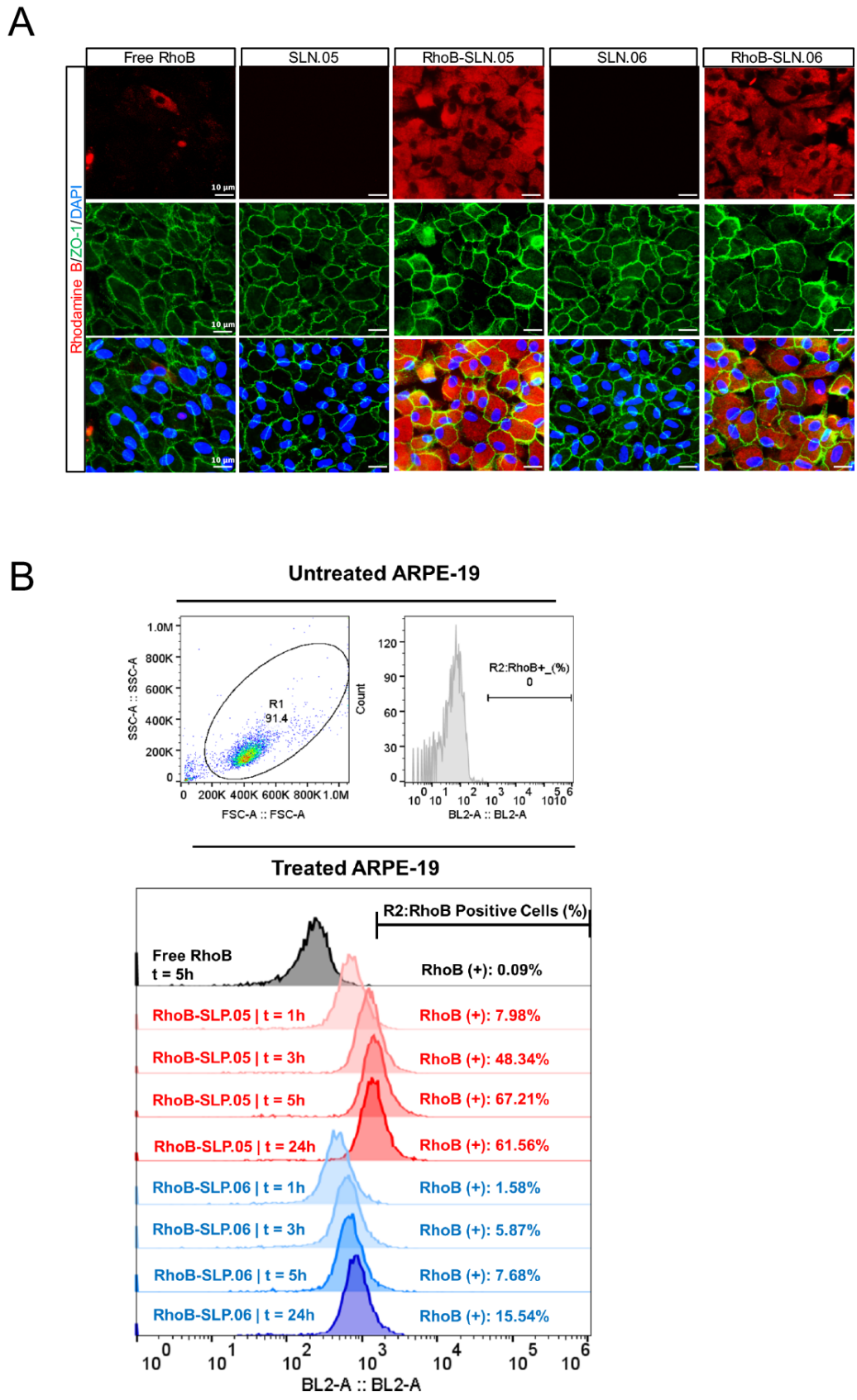

Figure 4.28 Internalization of SLN.05 or SLN.06 by ARPE-19 cells. (A) Micrographs showing intracellular localization of RhoB-SLN.05 or RhoB-SLN.06 (red signal) in ARPE-19 cells. Cell

membranes were stained with anti-ZO-1 antibody (green). Nuclei of cells were stained with DAPI (blue). Scale bar: 10 µm. (B) Histogram overlay of RhoB relative fluorescence intensity and percentage of RhoB positive cell (RhoB+) assessed by flow cytometry in ARPE-19 cells. R1: gating for selecting cells population; R2: gating to select RhoB+ cells based on blue laser (BL2-A) detector; FSC-A: forward scattering channel; SSC-A: side scattering channel.

4.5.5 Energy-dependent uptake of SLN.05 and SLN.06

To elucidate the mechanism of internalization of SLN.05 and SLN.06 by the photoreceptor cells, we exposed 661W cells to 200 µg/mL of RhoB-SLN.05 and RhoB-SLN.06 for 1 h at either 37°C or 4°C. We observed that incubation at 4°C highly limited the uptake of Rho-SLNs, indicating the process is temperature dependent, thus the uptake is an active energy-dependent process rather than passive membrane passage (Figure 4.29). Based on the knowledge that most of nanoparticles are internalized by cells through endocytosis, these data confirmed that SLN.05 and SLN.06 were uptaken via the endocytic process rather than membrane permeation.

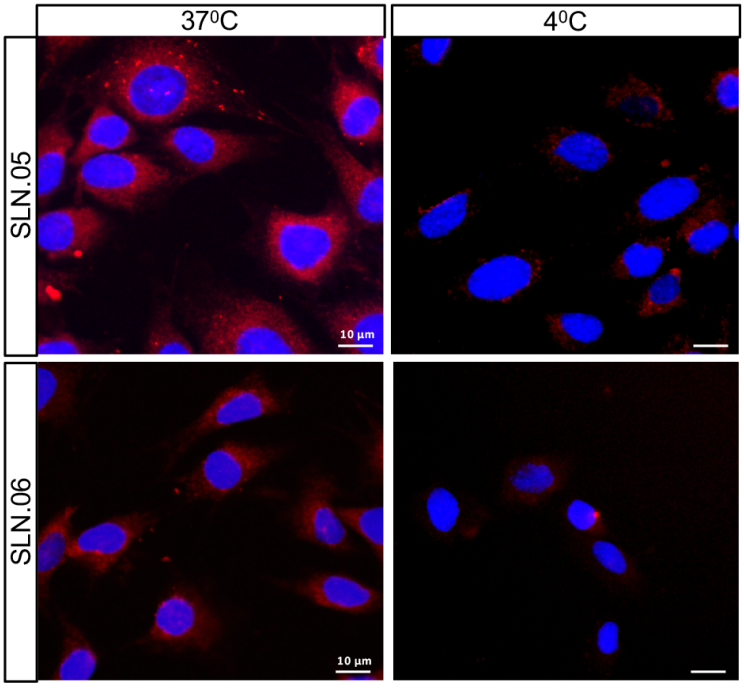

Figure 4.29 Representative images showing temperature-dependent RhoB-SLN.05 or RhoB-SLN.06 (red signal) uptaken by 661W cells at either 37°C or 4°C. Nuclei of cells were stained with DAPI (blue). Scale bar, 10 µm.

4.5.6 Encapsulated cargo release inside the cells

The efficiency of drug effects is based on the cargo release inside the target cell. To evaluate if SLN.05 and SLN.06 could successfully release the cargo after being uptaken by the cells, we performed a fluorescence leakage assay using ANTS/DPX which has been widely used to study vesicle leakage. We encapsulated the ANTS fluorescent dye together with its quencher DPX. When they are together, the ANTS is in a silent state. Once the SLN shell breaks and releases the cargo inside the cells, DPX will not be able to quench ANTS anymore, due to the increase of the molecular distance between ANTS and DPX, allowing free ANTS inside the cells to emit green fluorescence (Figure 4.30 A). In this experiment we exposed cells to either free ANTS or DPX, that are not able to penetrate the cells, as control. Encapsulated ANTS/DPX in SLN or the control were co-cultured with ARPE-19 cells for 5 h. After that, the medium was refreshed without any SLN or dye and continued incubation until 72 h (Figure 4.30 B). Only cells exposed to SLN.05 and SLN.06 loaded with ANTS/DPX resulted fluorescent demonstrating that SLNs could successfully deliver ANTS/DPX inside the cells and release the cargo (Figure 4.30 C). A faint signal could be detected at 24 h, but a full signal was easily detected after 48 h of exposure (Figure 4.30 C). Even at 72 h, the signal was still detectable. Taken together, these data demonstrate that the new formulated SLNs are able to release a hydrophilic molecule inside a retinal cell and can be an efficient drug delivery system for the retina.

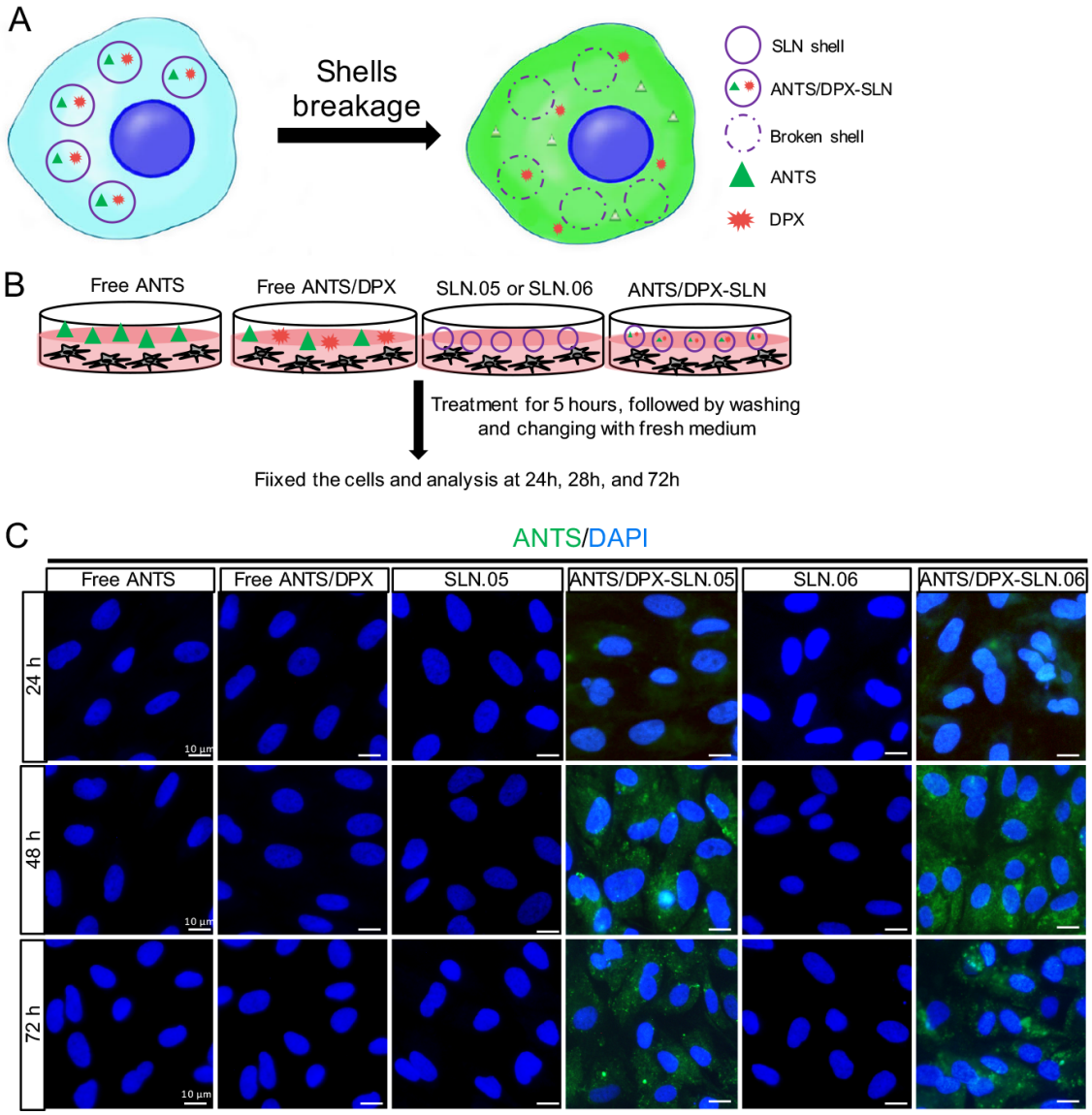

Figure 4.30 SLN.05 or SLN.06 cargo release inside the cells. Fluorescence leakage assay using ANTS/DPX was used to determine cargo delivery and release by the SLN.05 or SLN.06 inside the cells. (A) Schematic summary of fluorescence leakage assay using ANTS/DPX. (B) Schematic of experimental design for fluorescence leakage assay. (C) Micrographs of ARPE-19 cells exposed to ANTS/DPX loaded SLN.05 and SLN.06. Released ANTS (green) was detectable only in cells exposed to ANTS/DPX loaded into SLNs but not in cells exposed to free ANTS and/or DPX. Nuclei of cells were stained with DAPI in blue. Scale bar, 10 µm.

4.5.7 The effect of CN03 loaded SLN on *in vitro* RP model

With the evidence showing that the SLNs could release their cargos inside the cells, we then validated the effect of SLNs in delivering hydrophilic compound to the cells. CN03 was

encapsulated into SLN.05 and SLN.06 and the protective effect of SLN.05-CN03 and SLN.06-CN03 compared to free CN03 was evaluated by TUNEL assay. Preliminary data showed that SLN.05-CN03 and SLN.06-CN03 significantly improved the efficiency of CN03 against zaprinast induced cell death. Treatment with free CN03 decreased cell death percentage by about 40%, while SLN loaded CN03 showed a reduction of more than 65% in cell death (Figure 4.31).

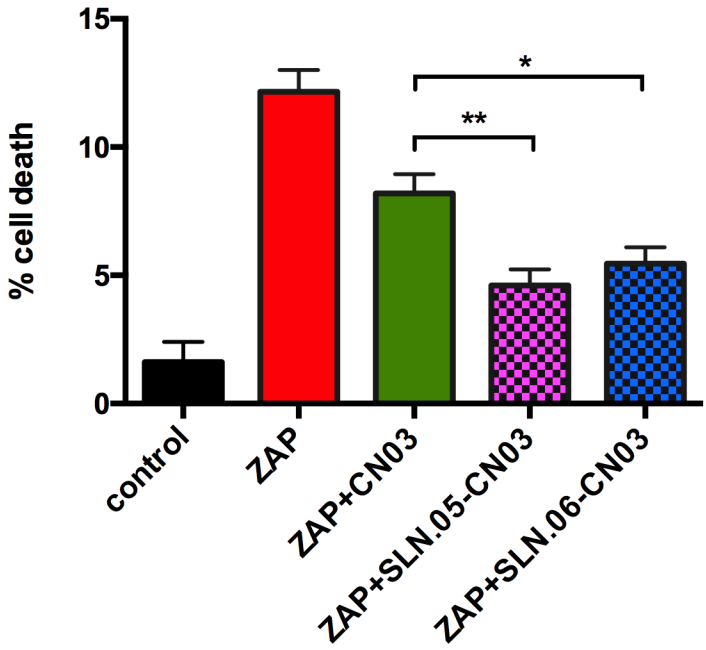

Figure 4.31 Effect of SLN encapsulated CN03 on 661W-A11 cell death induced by zaprinast. Control: cells treated with corresponding volume of vehicle (DMSO) was used as control; ZAP: cells treated with 400 µM zaprinast for 24h. ZAP+ CN03: cells were pre-treated with 50 µM CN03 for 2 h, and treated with 400 µM zaprinast together with 50 µM CN03 for 24 h; ZAP+ SLN.05-CN03: Cells were first exposed to SLN.05-CN03 for 5 h, then were treated with 400 µM zaprinast for 24 h. ZAP+ SLN.06-CN03: Cells were first exposed to SLN.06-CN03 for 5 h, then were treated with 400 µM zaprinast for 24h. * $P < 0.05$, ** $P < 0.01$.

Here we characterized new formulations of nanoparticles could enter retinal cells while having features that may facilitate navigation across the vitreous (e.g., size < 500 nm and anionic). The key findings from the formulation development studies were: (i) the gel core improved the encapsulation efficiency by up to 2-fold; (ii) the addition of hydrophobic polymer to the shell

could be used to tailor the surface charge of the final DDS. Our results on encapsulation efficiencies suggested that the gel core could improve the small hydrophilic cargo retention during formulation. This agrees with previous reports that used large macromolecules as cargo [248]. Particle surface charge should be considered in terms of cellular uptake. Cellular membrane is generally negatively charged and thus, a strongly anionic particle more difficultly will enter the cells compared to a cationic particle [249]. When the particle is cationic however, it will have tendency to aggregate in the vitreous [246]. Thus, there is a need to tailor particle surface charge during DDS development. The addition of polyester to the shell formulation reduced the strong negative charge of the pure lipid SLN shell (SLN.01; -39 mV).

The SLN formulation initially developed with RhoB, as the hydrophilic cargo, was validated with a real drug for retinal degeneration (i.e. CN03). The freshly synthesized CN03-loaded SLN particle size was maintained in the range of 200-250 nm. There was a significant change in surface charge when CN03 salts were used instead of RhoB for SLN.05. Yet, this was not observed in SLN.06. Without CN03 salts, SLN.05 (-13 mV) had a less negative charge compared to SLN.06 (-24 mV). Thus, unencapsulated CN03 salts had a weaker influence or had a less surface absorption on a more negatively charged SLN. Based on this finding, we surmise that this DDS may also work for other hydrophilic cargos with lower solubility in the organic solvent (e.g. DNA) for different pharmaceutical application.

While both SLN.05 and SLN.06 showed a time and dose dependent toxicity towards the cells, the *in vitro* cytotoxicity studies provided the insight that the two retinal cell lines had different sensitivity to these SLNs. This agrees with previous studies reporting that distinctive cell physiology, proliferation rate, metabolic activity, membrane, and phagocytosis characteristics are responsible for the different sensitivity to external factors [249, 250]. Physicochemical elements of nanoparticles can also affect the cytotoxicity of cells [249]. Specifically, distinct shell composition of SLN.05 and SLN.06 may differently affect viability of retinal cells. With regards to cytotoxicity, SLN.06 seemed to perform better than SLN.05 as a DDS.

Internalization studies in the two retinal cell types demonstrated that: (i) the SLN formulation helped internalization of small hydrophilic compounds; (ii) the SLN shell component might be used to tailor the uptake rate in different cell types. We observed that ARPE-19 cells could better uptake SLN containing PCL in the shell (SLN.05). This might be due to the fact that SLN.05 is less negatively charged compared to SLN.06 (Figure 4.24) and the uptake level is directly affected by physicochemical properties of SLN, such as shape, size and surface charge [251]. In 661W cells, the uptake profile of SLN.06 was similar to the one measured in APRE-19 cells and limited to a low percentage of cells that internalized the nanoparticles. For SLN.05,

less uptake was observed in 661W compared to ARPE-19. This difference may be attributed to the fact that uptake rates are also specific to each cell type [252]. It is not surprising that photoreceptor cells have a lower uptake rate compared to ARPE-19 cells, because RPE cells are characterized by a high rate of phagocytosis, which is one of their functions to daily remove the apical part of photoreceptor outer segments [6]. The reduced uptake at 4°C suggested that the SLN mainly enter the cells via endocytosis, as the energy de-pendent endocytosis will be largely inhibited at this temperature [253, 254] . We also demonstrated that SLN could release their cargo after being internalized by the cells. This result highlights that the newly developed DDS can be appropriate for encapsulation of small hydrophilic drugs and for their release into the target cells.

Overall, both SLN.05 and SLN.06 could successfully improve the uptake of small hydrophilic cargos into retinal cell lines *in vitro*. However, SLN.06 seemed to perform better as a DDS when compared to SLN.05 considering its slight advantage in terms of stability and cytotoxicity. Finally, the preliminary test with SLN.05-CN03 and SLN.06-CN03 in zaprinast treated 661W-A11 cells showed that both SLNs enhanced the efficiency of delivering CN03 to the cells.

While the relatively simple cell culture environment yielded interesting data, a full drug/DDS efficacy testing will likely require more complex test systems. More advanced *in vitro* tests using organotypic retinal explant cultures, in which the normal histotypic context of the retina is preserved [255], or in vivo injections will further characterize the suitability of the new SLN for the delivery to the retina. The fate of SLN materials after being broken down inside the cells, and the specific mechanism on how they are metabolized, will be the focus for further research. Nevertheless, based on these developments and initial validation studies, our work may open new perspectives for developing a treatment for retinal diseases based on SLN with small hydrophilic cargos.

5. CONCLUSION

In this project, we developed a cell line, 661W-A11, with rod-specific features and showed that upon PDE6 inhibition, cell death, elevated cGMP and calcium levels, activation of PKG, as well as of calpains were observed. These are all molecular events previously described in rodent models of RP in degenerating photoreceptors. Although we could not rule out the possibility that not all the cell death mechanisms were mirrored in this *in vitro* model, 661W-A11 cell line still could be used as a model for the study of rod photoreceptor cell death in RP and other IRDs linked to increased intracellular cGMP. The validation of cGMP inhibitory analogues and other neuroprotective compounds in this model, in which all the compounds exhibited protective effects against PDE6 inhibition treatment, indicate the potential for using this system as a feasible platform to test therapeutic approaches targeting IRDs. 661W-A11 cells may serve as an alternative cell model for studying the cGMP-dependent pathway in photoreceptor cell death and for high-throughput drug screening.

Based on this *in vitro* model, we sought to explore more extensively the cGMP-dependent cell death mechanism, which mainly focused on the downstream events of PKG activation and excessive Ca^{2+} influx. With phosphoproteomic analysis, we identified several candidates among phosphorylated substrates and kinases that might be regulated by cGMP/PKG. We also found the potential targets of excessive Ca^{2+} influx and had verified them in retina from three murine models of IRD. These evidences emphasized the feasibility of studying cGMP dependent cell death mechanism in photoreceptor degeneration based on this cell model.

With the purpose of delivering hydrophilic compound such as CN03 to the retina, a SLN formulation capable of encapsulating a small hydrophilic cargo and delivering it to retinal cells *in vitro* was pursued. It highlighted that a gel core could significantly increase the encapsulation efficiency of small hydrophilic cargo inside the SLN. We also observed that the type of hydrophobic polymer used in the composite shell may affect the particle surface charge, a key factor for intravitreal drug delivery systems. The physicochemical properties of the DDS developed using RhoB were retained when CN03 was used as a cargo. The *in vitro* study demonstrated that the DDS could be uptaken by model retinal cell lines with different uptake rates based on the particle shell composition and cell type. Equally important, the DDS could release its cargo inside the cells. Finally, *in vitro* test with CN03 loaded SLN showed an improvement in protective effect compared to free CN03. While the current results are promising for an early-stage formulation development study, more complex *in vivo* studies are needed to demonstrate the clinical relevance of the newly developed DDS.

REFERENCES

[1] H.J. Kaplan, Anatomy and function of the eye, Chemical immunology and allergy, 92 (2007) 4-10.
[2] M. Hoon, H. Okawa, L. Della Santina, R.O. Wong, Functional architecture of the retina: development and disease, Prog Retin Eye Res, 42 (2014) 44-84.
[3] R.G. Gregg, M.A. McCall, S.C. Massey, Chapter 15@ Function and Anatomy of the Mammalian Retina, 2013.
[4] M. Boulton, P. Dayhaw-Barker, The role of the retinal pigment epithelium: topographical variation and ageing changes, Eye (London, England), 15 (2001) 384-389.
[5] J.R. Sparrow, D. Hicks, C.P. Hamel, The retinal pigment epithelium in health and disease, Current molecular medicine, 10 (2010) 802-823.
[6] E. Bertolotti, A. Neri, M. Camparini, C. Macaluso, V. Marigo, Stem cells as source for retinal pigment epithelium transplantation, Prog Retin Eye Res, 42 (2014) 130-144.
[7] N. Mahabadi, Y. Al Khalili, Neuroanatomy, Retina, StatPearls, StatPearls Publishing Copyright © 2021, StatPearls Publishing LLC., Treasure Island (FL), 2021.
[8] C. Spencer, S. Abend, K.J. McHugh, M. Saint-Geniez, Identification of a synergistic interaction between endothelial cells and retinal pigment epithelium, Journal of cellular and molecular medicine, 21 (2017) 2542-2552.
[9] W.W. Pan, T.J. Wubben, C.G. Besirli, Photoreceptor metabolic reprogramming: current understanding and therapeutic implications, Communications biology, 4 (2021) 245.
[10] S. Omri, M. Omri B Fau - Savoldelli, L. Savoldelli M Fau - Jonet, B. Jonet L Fau - Thillaye-Goldenberg, G. Thillaye-Goldenberg B Fau - Thuret, P. Thuret G Fau - Gain, J.C. Gain P Fau - Jeanny, P. Jeanny Jc Fau - Crisanti, F. Crisanti P Fau - Behar-Cohen, F. Behar-Cohen, The outer limiting membrane (OLM) revisited: clinical implications.
[11] D. Goldman, Müller glial cell reprogramming and retina regeneration, Nature reviews. Neuroscience, 15 (2014) 431-442.
[12] R.H. Masland, The neuronal organization of the retina, Neuron, 76 (2012) 266-280.
[13] T. Euler, S. Haverkamp, T. Schubert, T. Baden, Retinal bipolar cells: elementary building blocks of vision, Nature reviews. Neuroscience, 15 (2014) 507-519.
[14] K. Ning, B.E. Sendayen, T.J. Kowal, B. Wang, B.W. Jones, Y. Hu, Y. Sun, Primary Cilia in Amacrine Cells in Retinal Development.
[15] K. Peynshaert, J. Devoldere, A.-K. Minnaert, S.C. De Smedt, K. Remaut, Morphology and Composition of the Inner Limiting Membrane: Species-Specific Variations and Relevance toward Drug Delivery Research, Current eye research, 44 (2019) 465-475.
[16] R.S. Molday, O.L. Moritz, Photoreceptors at a glance, Journal of cell science, 128 (2015) 4039-4045.
[17] S.A. Baker, V. Kerov, Photoreceptor inner and outer segments, Current topics in membranes, 72 (2013) 231-265.
[18] A.F. Goldberg, O.L. Moritz, D.S. Williams, Molecular basis for photoreceptor outer segment architecture, Prog Retin Eye Res, 55 (2016) 52-81.
[19] B.D. Perkins, J.M. Fadool, Photoreceptor structure and development analyses using GFP transgenes, Methods in cell biology, 100 (2010) 205-218.
[20] J.B. Jonas, U. Schneider, G.O. Naumann, Count and density of human retinal photoreceptors, Graefe's archive for clinical and experimental ophthalmology = Albrecht von Graefes Archiv fur klinische und experimentelle Ophthalmologie, 230 (1992) 505-510.

[21] E.M. Wells-Gray, S.S. Choi, A. Bries, N. Doble, Variation in rod and cone density from the fovea to the mid-periphery in healthy human retinas using adaptive optics scanning laser ophthalmoscopy, 30 (2016) 1135-1143.
[22] A. Morshedian, G.L. Fain, The evolution of rod photoreceptors, Philosophical transactions of the Royal Society of London. Series B, Biological sciences, 372 (2017).
[23] T.G. Wensel, Z. Zhang, I.A. Anastassov, J.C. Gilliam, F. He, M.F. Schmid, M.A. Robichaux, Structural and molecular bases of rod photoreceptor morphogenesis and disease, Prog Retin Eye Res, 55 (2016) 32-51.
[24] D. Mustafi, A.H. Engel, K. Palczewski, Structure of cone photoreceptors, Prog Retin Eye Res, 28 (2009) 289-302.
[25] F. Zhang, K. Kurokawa, A. Lassoued, J.A. Crowell, D.T. Miller, Cone photoreceptor classification in the living human eye from photostimulation-induced phase dynamics, 116 (2019) 7951.
[26] J.L. Zagozewski, Q. Zhang, D.D. Eisenstat, Genetic regulation of vertebrate eye development, Clinical genetics, 86 (2014) 453-460.
[27] D.V. Telegina, O.S. Kozhevnikova, A.K. Antonenko, N.G. Kolosova, Features of Retinal Neurogenesis as a Key Factor of Age-Related Neurodegeneration: Myth or Reality?, International journal of molecular sciences, 22 (2021).
[28] M.A. Kautzmann, D.S. Kim, M.P. Felder-Schmittbuhl, A. Swaroop, Combinatorial regulation of photoreceptor differentiation factor, neural retina leucine zipper gene NRL, revealed by in vivo promoter analysis, J Biol Chem, 286 (2011) 28247-28255.
[29] M. Xiang, Intrinsic control of mammalian retinogenesis, Cellular and molecular life sciences : CMLS, 70 (2013) 2519-2532.
[30] R. Laranjeiro, D. Whitmore, Transcription factors involved in retinogenesis are co-opted by the circadian clock following photoreceptor differentiation, Development (Cambridge, England), 141 (2014) 2644-2656.
[31] A.J. Mears, M. Kondo, P.K. Swain, Y. Takada, R.A. Bush, T.L. Saunders, P.A. Sieving, A. Swaroop, Nrl is required for rod photoreceptor development, Nature genetics, 29 (2001) 447-452.
[32] L.L. Daniele, C. Lillo, A.L. Lyubarsky, S.S. Nikonov, N. Philp, A.J. Mears, A. Swaroop, D.S. Williams, E.N. Pugh, Jr., Cone-like morphological, molecular, and electrophysiological features of the photoreceptors of the Nrl knockout mouse, Investigative ophthalmology & visual science, 46 (2005) 2156-2167.
[33] D.A. Bessant, A.M. Payne, K.P. Mitton, Q.L. Wang, P.K. Swain, C. Plant, A.C. Bird, D.J. Zack, A. Swaroop, S.S. Bhattacharya, A mutation in NRL is associated with autosomal dominant retinitis pigmentosa, Nature genetics, 21 (1999) 355-356.
[34] K.M. Nishiguchi, J.S. Friedman, M.A. Sandberg, A. Swaroop, E.L. Berson, T.P. Dryja, Recessive NRL mutations in patients with clumped pigmentary retinal degeneration and relative preservation of blue cone function, Proceedings of the National Academy of Sciences of the United States of America, 101 (2004) 17819-17824.
[35] D.G. Luo, T. Xue, K.W. Yau, How vision begins: an odyssey, Proceedings of the National Academy of Sciences of the United States of America, 105 (2008) 9855-9862.
[36] X.E. Zhou, K. Melcher, H.E. Xu, Structure and activation of rhodopsin, Acta pharmacologica Sinica, 33 (2012) 291-299.
[37] A. Tsin, B. Betts-Obregon, J. Grigsby, Visual cycle proteins: Structure, function, and roles in human retinal disease, J Biol Chem, 293 (2018) 13016-13021.
[38] U.B. Kaupp, K.W. Koch, Role of cGMP and Ca2+ in vertebrate photoreceptor excitation and adaptation, Annual review of physiology, 54 (1992) 153-175.

[39] T.M. Lincoln, T.L. Cornwell, Intracellular cyclic GMP receptor proteins, FASEB journal : official publication of the Federation of American Societies for Experimental Biology, 7 (1993) 328-338.
[40] U. Walter, Cyclic-GMP-regulated enzymes and their possible physiological functions, Advances in cyclic nucleotide and protein phosphorylation research, 17 (1984) 249-258.
[41] D.F. Ashman, R. Lipton, M.M. Melicow, T.D. Price, Isolation of adenosine 3', 5'-monophosphate and guanosine 3', 5'-monophosphate from rat urine, Biochem Biophys Res Commun, 11 (1963) 330-334.
[42] R.G. Pannbacker, D.E. Fleischman, D.W. Reed, Cyclic nucleotide phosphodiesterase: high activity in a mammalian photoreceptor, Science (New York, N.Y.), 175 (1972) 757-758.
[43] L. Stryer, Cyclic GMP cascade of vision, Annual review of neuroscience, 9 (1986) 87-119.
[44] X. Zhang, R.H. Cote, cGMP signaling in vertebrate retinal photoreceptor cells, Frontiers in bioscience : a journal and virtual library, 10 (2005) 1191-1204.
[45] M.E. Burns, A. Mendez, J. Chen, D.A. Baylor, Dynamics of cyclic GMP synthesis in retinal rods, Neuron, 36 (2002) 81-91.
[46] K. Palczewski, I. Sokal, W. Baehr, Guanylate cyclase-activating proteins: structure, function, and diversity, Biochem Biophys Res Commun, 322 (2004) 1123-1130.
[47] R.H. Cote, Photoreceptor phosphodiesterase (PDE6): activation and inactivation mechanisms during visual transduction in rods and cones, Pflugers Archiv : European journal of physiology, 473 (2021) 1377-1391.
[48] J.S. Anant, O.C. Ong, H.Y. Xie, S. Clarke, P.J. O'Brien, B.K. Fung, In vivo differential prenylation of retinal cyclic GMP phosphodiesterase catalytic subunits, J Biol Chem, 267 (1992) 687-690.
[49] R.H. Cote, Characteristics of photoreceptor PDE (PDE6): similarities and differences to PDE5, International journal of impotence research, 16 Suppl 1 (2004) S28-33.
[50] T.S. Li, K. Volpp, M.L. Applebury, Bovine cone photoreceptor cGMP phosphodiesterase structure deduced from a cDNA clone, Proceedings of the National Academy of Sciences of the United States of America, 87 (1990) 293-297.
[51] X.J. Zhang, K.B. Cahill, A. Elfenbein, V.Y. Arshavsky, R.H. Cote, Direct allosteric regulation between the GAF domain and catalytic domain of photoreceptor phosphodiesterase PDE6, J Biol Chem, 283 (2008) 29699-29705.
[52] P.G. Gillespie, J.A. Beavo, cGMP is tightly bound to bovine retinal rod phosphodiesterase, Proceedings of the National Academy of Sciences of the United States of America, 86 (1989) 4311-4315.
[53] M. Biel, S. Michalakis, Cyclic nucleotide-gated channels, Handbook of experimental pharmacology, (2009) 111-136.
[54] U.B. Kaupp, T. Niidome, T. Tanabe, S. Terada, W. Bönigk, W. Stühmer, N.J. Cook, K. Kangawa, H. Matsuo, T. Hirose, et al., Primary structure and functional expression from complementary DNA of the rod photoreceptor cyclic GMP-gated channel, Nature, 342 (1989) 762-766.
[55] C. Peng, E.D. Rich, M.D. Varnum, Subunit configuration of heteromeric cone cyclic nucleotide-gated channels, Neuron, 42 (2004) 401-410.
[56] S. Michalakis, E. Becirovic, M. Biel, Retinal Cyclic Nucleotide-Gated Channels: From Pathophysiology to Therapy, International journal of molecular sciences, 19 (2018).
[57] T.P. Dryja, J.T. Finn, Y.W. Peng, T.L. McGee, E.L. Berson, K.W. Yau, Mutations in the gene encoding the alpha subunit of the rod cGMP-gated channel in autosomal recessive retinitis pigmentosa, Proceedings of the National Academy of Sciences of the United States of America, 92 (1995) 10177-10181.

[58] C. Bareil, C.P. Hamel, V. Delague, B. Arnaud, J. Demaille, M. Claustres, Segregation of a mutation in CNGB1 encoding the beta-subunit of the rod cGMP-gated channel in a family with autosomal recessive retinitis pigmentosa, Human genetics, 108 (2001) 328-334.
[59] S. Kohl, T. Marx, I. Giddings, H. Jägle, S.G. Jacobson, E. Apfelstedt-Sylla, E. Zrenner, L.T. Sharpe, B. Wissinger, Total colourblindness is caused by mutations in the gene encoding the alpha-subunit of the cone photoreceptor cGMP-gated cation channel, Nature genetics, 19 (1998) 257-259.
[60] S. Kohl, B. Baumann, M. Broghammer, H. Jägle, P. Sieving, U. Kellner, R. Spegal, M. Anastasi, E. Zrenner, L.T. Sharpe, B. Wissinger, Mutations in the CNGB3 gene encoding the beta-subunit of the cone photoreceptor cGMP-gated channel are responsible for achromatopsia (ACHM3) linked to chromosome 8q21, Human molecular genetics, 9 (2000) 2107-2116.
[61] F. Hofmann, R. Feil, T. Kleppisch, J. Schlossmann, Function of cGMP-dependent protein kinases as revealed by gene deletion, Physiological reviews, 86 (2006) 1-23.
[62] S.H. Francis, J.L. Busch, J.D. Corbin, D. Sibley, cGMP-dependent protein kinases and cGMP phosphodiesterases in nitric oxide and cGMP action, Pharmacological reviews, 62 (2010) 525-563.
[63] F. Hofmann, D. Bernhard, R. Lukowski, P. Weinmeister, cGMP regulated protein kinases (cGK), Handbook of experimental pharmacology, (2009) 137-162.
[64] P.A. Ekström, M. Ueffing, E. Zrenner, F. Paquet-Durand, Novel in situ activity assays for the quantitative molecular analysis of neurodegenerative processes in the retina, Current medicinal chemistry, 21 (2014) 3478-3493.
[65] F. Paquet-Durand, S.M. Hauck, T. van Veen, M. Ueffing, P. Ekström, PKG activity causes photoreceptor cell death in two retinitis pigmentosa models, Journal of neurochemistry, 108 (2009) 796-810.
[66] D.E. Clapham, Calcium signaling, Cell, 131 (2007) 1047-1058.
[67] M.J. Berridge, P. Lipp, M.D. Bootman, The versatility and universality of calcium signalling, Nature reviews. Molecular cell biology, 1 (2000) 11-21.
[68] D. Krizaj, D.R. Copenhagen, Calcium regulation in photoreceptors, Frontiers in bioscience : a journal and virtual library, 7 (2002) d2023-2044.
[69] L. Cervetto, L. Lagnado, R.J. Perry, D.W. Robinson, P.A. McNaughton, Extrusion of calcium from rod outer segments is driven by both sodium and potassium gradients, Nature, 337 (1989) 740-743.
[70] K. Nakatani, K.W. Yau, Calcium and light adaptation in retinal rods and cones, Nature, 334 (1988) 69-71.
[71] A.M. Dizhoor, E.V. Olshevskaya, I.V. Peshenko, Mg2+/Ca2+ cation binding cycle of guanylyl cyclase activating proteins (GCAPs): role in regulation of photoreceptor guanylyl cyclase, Molecular and cellular biochemistry, 334 (2010) 117-124.
[72] V.A. Klenchin, P.D. Calvert, M.D. Bownds, Inhibition of rhodopsin kinase by recoverin. Further evidence for a negative feedback system in phototransduction, J Biol Chem, 270 (1995) 16147-16152.
[73] K. Palczewski, A.S. Polans, W. Baehr, J.B. Ames, Ca(2+)-binding proteins in the retina: structure, function, and the etiology of human visual diseases, BioEssays : news and reviews in molecular, cellular and developmental biology, 22 (2000) 337-350.
[74] D. Weitz, M. Zoche, F. Müller, M. Beyermann, H.G. Körschen, U.B. Kaupp, K.W. Koch, Calmodulin controls the rod photoreceptor CNG channel through an unconventional binding site in the N-terminus of the beta-subunit, The EMBO journal, 17 (1998) 2273-2284.
[75] Y. Koutalos, K. Nakatani, T. Tamura, K.W. Yau, Characterization of guanylate cyclase activity in single retinal rod outer segments, The Journal of general physiology, 106 (1995) 863-890.

[76] A. Koskelainen, K. Donner, G. Kalamkarov, S. Hemilä, Changes in the light-sensitive current of salamander rods upon manipulation of putative pH-regulating mechanisms in the inner and outer segment, Vision research, 34 (1994) 983-994.
[77] T. Szikra, D. Krizaj, Intracellular organelles and calcium homeostasis in rods and cones, Visual neuroscience, 24 (2007) 733-743.
[78] M. Nachman-Clewner, R. St Jules, E. Townes-Anderson, L-type calcium channels in the photoreceptor ribbon synapse: localization and role in plasticity, The Journal of comparative neurology, 415 (1999) 1-16.
[79] S. Broadgate, J. Yu, S.M. Downes, S. Halford, Unravelling the genetics of inherited retinal dystrophies: Past, present and future, Prog Retin Eye Res, 59 (2017) 53-96.
[80] F.P.M. Cremers, C.J.F. Boon, K. Bujakowska, C. Zeitz, Special Issue Introduction: Inherited Retinal Disease: Novel Candidate Genes, Genotype-Phenotype Correlations, and Inheritance Models, Genes, 9 (2018).
[81] J.F. Hejtmancik, S.P. Daiger, Understanding the genetic architecture of human retinal degenerations, Proceedings of the National Academy of Sciences of the United States of America, 117 (2020) 3904-3906.
[82] P.I. Fuller-Carter, H. Basiri, A.R. Harvey, L.S. Carvalho, Focused Update on AAV-Based Gene Therapy Clinical Trials for Inherited Retinal Degeneration, BioDrugs : clinical immunotherapeutics, biopharmaceuticals and gene therapy, 34 (2020) 763-781.
[83] V. Miraldi Utz, R.G. Coussa, F. Antaki, E.I. Traboulsi, Gene therapy for RPE65-related retinal disease, null, 39 (2018) 671-677.
[84] M. Kutluer, L. Huang, V. Marigo, Targeting molecular pathways for the treatment of inherited retinal degeneration, Neural regeneration research, 15 (2020) 1784-1791.
[85] H.P. Scholl, R.W. Strauss, M.S. Singh, D. Dalkara, B. Roska, S. Picaud, J.A. Sahel, Emerging therapies for inherited retinal degeneration, Science translational medicine, 8 (2016) 368rv366.
[86] T.B. O'Neal, E.E. Luther, Retinitis Pigmentosa, StatPearls, StatPearls Publishing Copyright © 2021, StatPearls Publishing LLC., Treasure Island (FL), 2021.
[87] D.T. Hartong, E.L. Berson, T.P. Dryja, Retinitis pigmentosa, Lancet (London, England), 368 (2006) 1795-1809.
[88] M.U. Ali, M.S.U. Rahman, J. Cao, P.X. Yuan, Genetic characterization and disease mechanism of retinitis pigmentosa; current scenario, 3 Biotech, 7 (2017) 251.
[89] S.K. Verbakel, R.A.C. van Huet, C.J.F. Boon, A.I. den Hollander, R.W.J. Collin, C.C.W. Klaver, C.B. Hoyng, R. Roepman, B.J. Klevering, Non-syndromic retinitis pigmentosa, Prog Retin Eye Res, 66 (2018) 157-186.
[90] C. Fuster-García, B. García-Bohórquez, A. Rodríguez-Muñoz, E. Aller, T. Jaijo, J.M. Millán, G. García-García, Usher Syndrome: Genetics of a Human Ciliopathy, International journal of molecular sciences, 22 (2021).
[91] T.P. Dryja, T.L. McGee, E. Reichel, L.B. Hahn, G.S. Cowley, D.W. Yandell, M.A. Sandberg, E.L. Berson, A point mutation of the rhodopsin gene in one form of retinitis pigmentosa, Nature, 343 (1990) 364-366.
[92] S. Ferrari, E. Di Iorio, V. Barbaro, D. Ponzin, F.S. Sorrentino, F. Parmeggiani, Retinitis pigmentosa: genes and disease mechanisms, Current genomics, 12 (2011) 238-249.
[93] M. Danciger, J. Blaney, Y.Q. Gao, D.Y. Zhao, J.R. Heckenlively, S.G. Jacobson, D.B. Farber.
[94] L. Kuehlewein, D. Zobor, K. Stingl, M. Kempf, F. Nasser, A. Bernd, S. Biskup, F.P.M. Cremers, M.I. Khan, P. Mazzola, K. Schäferhoff, T. Heinrich, T.B. Haack, B. Wissinger, E. Zrenner, N. Weisschuh, S. Kohl, Clinical Phenotype of PDE6B-Associated Retinitis Pigmentosa, International journal of molecular sciences, 22 (2021).

[95] S. Marconi, J.T. Stout, PDE6B Mutation-associated Inherited Retinal Disease, International ophthalmology clinics, 61 (2021) 133-142.
[96] N.V. Khramtsov, E.A. Feshchenko, V.A. Suslova, B.E. Shmukler, B.E. Terpugov, T.V. Rakitina, N.V. Atabekova, V.M. Lipkin, The human rod photoreceptor cGMP phosphodiesterase beta-subunit. Structural studies of its cDNA and gene, FEBS letters, 327 (1993) 275-278.
[97] K.M. Nishiguchi, L.S. Carvalho, M. Rizzi, K. Powell, S.M. Holthaus, S.A. Azam, Y. Duran, J. Ribeiro, U.F. Luhmann, J.W. Bainbridge, A.J. Smith, R.R. Ali, Gene therapy restores vision in rd1 mice after removal of a confounding mutation in Gpr179, Nature communications, 6 (2015) 6006.
[98] C. Gargini, E. Terzibasi, F. Mazzoni, E. Strettoi, Retinal organization in the retinal degeneration 10 (rd10) mutant mouse: a morphological and ERG study, The Journal of comparative neurology, 500 (2007) 222-238.
[99] Y. Zhao, K. Feng, R. Liu, J. Pan, L. Zhang, X. Lu, Vitamins and Mineral Supplements for Retinitis Pigmentosa, 2019 (2019) 8524607.
[100] P.G. Limoli, C.S.S. Limoli, M.U. Morales, E.M. Vingolo, Mesenchymal stem cell surgery, rescue and regeneration in retinitis pigmentosa: clinical and rehabilitative prognostic aspects, Restorative neurology and neuroscience, 38 (2020) 223-237.
[101] L.E. Hallum, S.C. Dakin, Retinal Implantation of Electronic Vision Prostheses to Treat Retinitis Pigmentosa: A Systematic Review, Translational vision science & technology, 10 (2021) 8.
[102] C. Liu, Y. Li, M. Peng, A.M. Laties, R. Wen, Activation of caspase-3 in the retina of transgenic rats with the rhodopsin mutation s334ter during photoreceptor degeneration, The Journal of neuroscience : the official journal of the Society for Neuroscience, 19 (1999) 4778-4785.
[103] M.S. Gorbatyuk, T. Knox, M.M. LaVail, O.S. Gorbatyuk, S.M. Noorwez, W.W. Hauswirth, J.H. Lin, N. Muzyczka, A.S. Lewin, Restoration of visual function in P23H rhodopsin transgenic rats by gene delivery of BiP/Grp78, Proceedings of the National Academy of Sciences of the United States of America, 107 (2010) 5961-5966.
[104] A. Comitato, D. Schiroli, M. Montanari, V. Marigo, Calpain Activation Is the Major Cause of Cell Death in Photoreceptors Expressing a Rhodopsin Misfolding Mutation, Molecular neurobiology, 57 (2020) 589-599.
[105] M. Donovan, T.G. Cotter, Caspase-independent photoreceptor apoptosis in vivo and differential expression of apoptotic protease activating factor-1 and caspase-3 during retinal development, Cell death and differentiation, 9 (2002) 1220-1231.
[106] F. Doonan, M. Donovan, T.G. Cotter, Caspase-independent photoreceptor apoptosis in mouse models of retinal degeneration, The Journal of neuroscience : the official journal of the Society for Neuroscience, 23 (2003) 5723-5731.
[107] C.J. Zeiss, J. Neal, E.A. Johnson, Caspase-3 in postnatal retinal development and degeneration, Investigative ophthalmology & visual science, 45 (2004) 964-970.
[108] D. Sanges, A. Comitato, R. Tammaro, V. Marigo, Apoptosis in retinal degeneration involves cross-talk between apoptosis-inducing factor (AIF) and caspase-12 and is blocked by calpain inhibitors, Proceedings of the National Academy of Sciences of the United States of America, 103 (2006) 17366-17371.
[109] A. Comitato, D. Sanges, A. Rossi, M.M. Humphries, V. Marigo, Activation of Bax in three models of retinitis pigmentosa, Investigative ophthalmology & visual science, 55 (2014) 3555-3562.
[110] R.N. Lolley, D.B. Farber, M.E. Rayborn, J.G. Hollyfield, Cyclic GMP accumulation causes degeneration of photoreceptor cells: simulation of an inherited disease, Science (New York, N.Y.), 196 (1977) 664-666.

[111] S.H. Huang, S.J. Pittler, X. Huang, L. Oliveira, E.L. Berson, T.P. Dryja, Autosomal recessive retinitis pigmentosa caused by mutations in the alpha subunit of rod cGMP phosphodiesterase, Nature genetics, 11 (1995) 468-471.
[112] M.E. McLaughlin, M.A. Sandberg, E.L. Berson, T.P. Dryja, Recessive mutations in the gene encoding the beta-subunit of rod phosphodiesterase in patients with retinitis pigmentosa, Nature genetics, 4 (1993) 130-134.
[113] F. Paquet-Durand, V. Marigo, P. Ekström, RD Genes Associated with High Photoreceptor cGMP-Levels (Mini-Review), Advances in experimental medicine and biology, 1185 (2019) 245-249.
[114] V. Ramamurthy, G.A. Niemi, T.A. Reh, J.B. Hurley, Leber congenital amaurosis linked to AIPL1: a mouse model reveals destabilization of cGMP phosphodiesterase, Proceedings of the National Academy of Sciences of the United States of America, 101 (2004) 13897-13902.
[115] S. Sato, I.V. Peshenko, E.V. Olshevskaya, V.J. Kefalov, A.M. Dizhoor, GUCY2D Cone-Rod Dystrophy-6 Is a "Phototransduction Disease" Triggered by Abnormal Calcium Feedback on Retinal Membrane Guanylyl Cyclase 1, The Journal of neuroscience : the official journal of the Society for Neuroscience, 38 (2018) 2990-3000.
[116] S. Orrenius, B. Zhivotovsky, P. Nicotera, Regulation of cell death: the calcium-apoptosis link, Nature reviews. Molecular cell biology, 4 (2003) 552-565.
[117] A. Wenzel, C. Grimm, M. Samardzija, C.E. Remé, Molecular mechanisms of light-induced photoreceptor apoptosis and neuroprotection for retinal degeneration, Prog Retin Eye Res, 24 (2005) 275-306.
[118] D.A. Fox, A.T. Poblenz, L. He, Calcium overload triggers rod photoreceptor apoptotic cell death in chemical-induced and inherited retinal degenerations, Annals of the New York Academy of Sciences, 893 (1999) 282-285.
[119] T. Wang, J. Reingruber, M.L. Woodruff, A. Majumder, A. Camarena, N.O. Artemyev, G.L. Fain, J. Chen, The PDE6 mutation in the rd10 retinal degeneration mouse model causes protein mislocalization and instability and promotes cell death through increased ion influx, J Biol Chem, 293 (2018) 15332-15346.
[120] F. Paquet-Durand, S. Beck, S. Michalakis, T. Goldmann, G. Huber, R. Mühlfriedel, D. Trifunović, M.D. Fischer, E. Fahl, G. Duetsch, E. Becirovic, U. Wolfrum, T. van Veen, M. Biel, N. Tanimoto, M.W. Seeliger, A key role for cyclic nucleotide gated (CNG) channels in cGMP-related retinitis pigmentosa, Human molecular genetics, 20 (2011) 941-947.
[121] W.A. Catterall, Voltage-gated calcium channels, Cold Spring Harbor perspectives in biology, 3 (2011) a003947.
[122] R.R. Fiscus, Involvement of cyclic GMP and protein kinase G in the regulation of apoptosis and survival in neural cells, Neuro-Signals, 11 (2002) 175-190.
[123] A. Deguchi, W.J. Thompson, I.B. Weinstein, Activation of protein kinase G is sufficient to induce apoptosis and inhibit cell migration in colon cancer cells, Cancer Res, 64 (2004) 3966-3973.
[124] L. Liu, H. Li, T. Underwood, M. Lloyd, M. David, G. Sperl, R. Pamukcu, W.J. Thompson, Cyclic GMP-dependent protein kinase activation and induction by exisulind and CP461 in colon tumor cells, The Journal of pharmacology and experimental therapeutics, 299 (2001) 583-592.
[125] E.L. Leung, J.C. Wong, M.G. Johlfs, B.K. Tsang, R.R. Fiscus, Protein kinase G type Ialpha activity in human ovarian cancer cells significantly contributes to enhanced Src activation and DNA synthesis/cell proliferation, Molecular cancer research : MCR, 8 (2010) 578-591.
[126] F. Fallahian, F. Karami-Tehrani, S. Salami, Induction of apoptosis by type Iβ protein kinase G in the human breast cancer cell lines MCF-7 and MDA-MB-468, Cell biochemistry and function, 30 (2012) 183-190.

[127] Y. Wu, M. Yuan, W. Su, M. Zhu, X. Yao, Y. Wang, H. Qian, L. Jiang, Y. Tao, M. Wu, J. Pang, Y. Chen, The constitutively active PKG II mutant effectively inhibits gastric cancer development via a blockade of EGF/EGFR-associated signalling cascades, Therapeutic advances in medical oncology, 10 (2018) 1758834017751635.
[128] M. Park, P. Sandner, T. Krieg, cGMP at the centre of attention: emerging strategies for activating the cardioprotective PKG pathway, Basic research in cardiology, 113 (2018) 24.
[129] E. Vighi, D. Trifunović, P. Veiga-Crespo, A. Rentsch, D. Hoffmann, A. Sahaboglu, T. Strasser, M. Kulkarni, E. Bertolotti, A. van den Heuvel, T. Peters, A. Reijerkerk, T. Euler, M. Ueffing, F. Schwede, H.G. Genieser, P. Gaillard, V. Marigo, P. Ekström, F. Paquet-Durand, Combination of cGMP analogue and drug delivery system provides functional protection in hereditary retinal degeneration, Proceedings of the National Academy of Sciences of the United States of America, 115 (2018) E2997-e3006.
[130] M. Koch, C. Scheel, H. Ma, F. Yang, M. Stadlmeier, A.F. Glück, E. Murenu, F.R. Traube, T. Carell, M. Biel, X.Q. Ding, S. Michalakis, The cGMP-Dependent Protein Kinase 2 Contributes to Cone Photoreceptor Degeneration in the Cnga3-Deficient Mouse Model of Achromatopsia, International journal of molecular sciences, 22 (2020).
[131] Y.L. Deribe, T. Pawson, I. Dikic, Post-translational modifications in signal integration, Nature structural & molecular biology, 17 (2010) 666-672.
[132] N. Kim, D. Chen, X.Z. Zhou, T.H. Lee, Death-Associated Protein Kinase 1 Phosphorylation in Neuronal Cell Death and Neurodegenerative Disease, International journal of molecular sciences, 20 (2019).
[133] A. Roy, J. Groten, V. Marigo, T. Tomar, R. Hilhorst, Identification of Novel Substrates for cGMP Dependent Protein Kinase (PKG) through Kinase Activity Profiling to Understand Its Putative Role in Inherited Retinal Degeneration, International journal of molecular sciences, 22 (2021).
[134] M. Power, S. Das, K. Schütze, V. Marigo, P. Ekström, F. Paquet-Durand, Cellular mechanisms of hereditary photoreceptor degeneration - Focus on cGMP, Prog Retin Eye Res, 74 (2020) 100772.
[135] F. Paquet-Durand, S. Azadi, S.M. Hauck, M. Ueffing, T. van Veen, P. Ekström, Calpain is activated in degenerating photoreceptors in the rd1 mouse, Journal of neurochemistry, 96 (2006) 802-814.
[136] P. Behnen, A. Felline, A. Comitato, M.T. Di Salvo, F. Raimondi, S. Gulati, S. Kahremany, K. Palczewski, V. Marigo, F. Fanelli, A Small Chaperone Improves Folding and Routing of Rhodopsin Mutants Linked to Inherited Blindness, iScience, 4 (2018) 1-19.
[137] V. Shinde, P. Kotla, C. Strang, M. Gorbatyuk, Unfolded protein response-induced dysregulation of calcium homeostasis promotes retinal degeneration in rat models of autosomal dominant retinitis pigmentosa, Cell death & disease, 7 (2016) e2085.
[138] A. Comitato, M.T. Di Salvo, G. Turchiano, M. Montanari, S. Sakami, K. Palczewski, V. Marigo, Dominant and recessive mutations in rhodopsin activate different cell death pathways, Human molecular genetics, 25 (2016) 2801-2812.
[139] M.M. Kunte, S. Choudhury, J.F. Manheim, V.M. Shinde, M. Miura, V.A. Chiodo, W.W. Hauswirth, O.S. Gorbatyuk, M.S. Gorbatyuk, ER Stress Is Involved in T17M Rhodopsin-Induced Retinal Degeneration, Investigative ophthalmology & visual science, 53 (2012) 3792-3800.
[140] W.R. Dayton, W.J. Reville, D.E. Goll, M.H. Stromer, A Ca2+-activated protease possibly involved in myofibrillar protein turnover. Partial characterization of the purified enzyme, Biochemistry, 15 (1976) 2159-2167.
[141] M. Zatz, A. Starling, Calpains and Disease, New England Journal of Medicine, 352 (2005) 2413-2423.

[142] M.A. Smith, R.G. Schnellmann, Calpains, mitochondria, and apoptosis, Cardiovascular research, 96 (2012) 32-37.
[143] R.A. Hanna, R.L. Campbell, P.L. Davies, Calcium-bound structure of calpain and its mechanism of inhibition by calpastatin, 456 (2008) 409-412.
[144] V.M. Machado, A.S. Lourenço, C. Florindo, R. Fernandes, C.M. Carvalho, I.M. Araújo, Calpastatin Overexpression Preserves Cognitive Function Following Seizures, While Maintaining Post-Injury Neurogenesis, Frontiers in Molecular Neuroscience, 10 (2017).
[145] M. Azuma, T.R. Shearer, The role of calcium-activated protease calpain in experimental retinal pathology, Surv Ophthalmol, 53 (2008) 150-163.
[146] L. Araújo Couto, M. Sampaio Narciso, J.N. Hokoç, A.M. Blanco Martinez, Calpain inhibitor 2 prevents axonal degeneration of opossum optic nerve fibers, Journal of neuroscience research, 77 (2004) 410-419.
[147] A. Das, D.P. Garner, A.M. Del Re, J.J. Woodward, D.M. Kumar, N. Agarwal, N.L. Banik, S.K. Ray, Calpeptin provides functional neuroprotection to rat retinal ganglion cells following Ca2+ influx, Brain research, 1084 (2006) 146-157.
[148] V. Marigo, Programmed cell death in retinal degeneration: targeting apoptosis in photoreceptors as potential therapy for retinal degeneration, Cell cycle (Georgetown, Tex.), 6 (2007) 652-655.
[149] F. Paquet-Durand, D. Sanges, J. McCall, J. Silva, T. van Veen, V. Marigo, P. Ekström, Photoreceptor rescue and toxicity induced by different calpain inhibitors, Journal of neurochemistry, 115 (2010) 930-940.
[150] T. Ozaki, T. Yamashita, S. Ishiguro, ERp57-associated mitochondrial μ-calpain truncates apoptosis-inducing factor, Biochimica et biophysica acta, 1783 (2008) 1955-1963.
[151] R.C. McFall, T.W. Sery, M. Makadon, Characterization of a new continuous cell line derived from a human retinoblastoma, Cancer Res, 37 (1977) 1003-1010.
[152] T.W. Reid, D.M. Albert, A.S. Rabson, P. Russell, J. Craft, E.W. Chu, T.S. Tralka, J.L. Wilcox, Characteristics of an established cell line of retinoblastoma, Journal of the National Cancer Institute, 53 (1974) 347-360.
[153] A. Di Polo, D.B. Farber, Rod photoreceptor-specific gene expression in human retinoblastoma cells, Proceedings of the National Academy of Sciences of the United States of America, 92 (1995) 4016-4020.
[154] B.G. Ballios, L. Clarke, B.L. Coles, M.S. Shoichet, D. Van Der Kooy, The adult retinal stem cell is a rare cell in the ciliary epithelium whose progeny can differentiate into photoreceptors, Biology open, 1 (2012) 237-246.
[155] G.C. Demontis, C. Aruta, A. Comitato, A. De Marzo, V. Marigo, Functional and molecular characterization of rod-like cells from retinal stem cells derived from the adult ciliary epithelium, PloS one, 7 (2012) e33338.
[156] F. Giordano, A. De Marzo, F. Vetrini, V. Marigo, FGF and EGF differently affect differentiation of murine retinal stem cells in vitro, (2007).
[157] E. Tan, X.Q. Ding, A. Saadi, N. Agarwal, M.I. Naash, M.R. Al-Ubaidi, Expression of cone-photoreceptor-specific antigens in a cell line derived from retinal tumors in transgenic mice, Investigative ophthalmology & visual science, 45 (2004) 764-768.
[158] Z. Sayyad, K. Sirohi, V. Radha, G. Swarup, 661W is a retinal ganglion precursor-like cell line in which glaucoma-associated optineurin mutants induce cell death selectively, Sci Rep, 7 (2017) 16855.
[159] A.F. Thompson, M.E. Crowe, C.J. Lieven, L.A. Levin, Induction of Neuronal Morphology in the 661W Cone Photoreceptor Cell Line with Staurosporine, PloS one, 10 (2015) e0145270.
[160] L.P. Yang, X.A. Zhu, M.O. Tso, Role of NF-kappaB and MAPKs in light-induced photoreceptor apoptosis, Investigative ophthalmology & visual science, 48 (2007) 4766-4776.

[161] H. Poppe, S.D. Rybalkin, H. Rehmann, T.R. Hinds, X.B. Tang, A.E. Christensen, F. Schwede, H.G. Genieser, J.L. Bos, S.O. Doskeland, J.A. Beavo, E. Butt, Cyclic nucleotide analogs as probes of signaling pathways, Nature methods, 5 (2008) 277-278.
[162] E. Butt, M. Eigenthaler, H.G. Genieser, (Rp)-8-pCPT-cGMPS, a novel cGMP-dependent protein kinase inhibitor, European journal of pharmacology, 269 (1994) 265-268.
[163] E. Vighi, A. Rentsch, P. Henning, A. Comitato, D. Hoffmann, D. Bertinetti, E. Bertolotti, F. Schwede, F.W. Herberg, H.G. Genieser, V. Marigo, New cGMP analogues restrain proliferation and migration of melanoma cells, Oncotarget, 9 (2018) 5301-5320.
[164] D. Hoffmann, A. Rentsch, E. Vighi, E. Bertolotti, A. Comitato, F. Schwede, H.G. Genieser, V. Marigo, New dimeric cGMP analogues reduce proliferation in three colon cancer cell lines, European journal of medicinal chemistry, 141 (2017) 61-72.
[165] M. Quadri, A. Comitato, E. Palazzo, N. Tiso, A. Rentsch, G. Pellacani, A. Marconi, V. Marigo, Activation of cGMP-Dependent Protein Kinase Restricts Melanoma Growth and Invasion by Interfering with the EGF/EGFR Pathway, 142 (2022) 201-211.
[166] A. Tolone, S. Belhadj, A. Rentsch, F. Schwede, F. Paquet-Durand, The cGMP Pathway and Inherited Photoreceptor Degeneration: Targets, Compounds, and Biomarkers, Genes, 10 (2019).
[167] H. Döppler, P. Storz, Regulation of VASP by phosphorylation: consequences for cell migration, Cell adhesion & migration, 7 (2013) 482-486.
[168] A. Tolone, W. Haq, A. Fachinger, A. Rentsch, F.W. Herberg, F. Schwede, F. Paquet-Durand, Retinal degeneration: Multilevel protection of photoreceptor and ganglion cell viability and function with the novel PKG inhibitor CN238, (2021) 2021.2008.2005.455191.
[169] J. Cunha-Vaz, R. Bernardes, C. Lobo, Blood-retinal barrier, European journal of ophthalmology, 21 Suppl 6 (2011) S3-9.
[170] G.A. Peyman, E.M. Lad, D.M. Moshfeghi, Intravitreal injection of therapeutic agents, Retina (Philadelphia, Pa.), 29 (2009) 875-912.
[171] G.A. Ochakovski, T. Peters, S. Michalakis, B. Wilhelm, B. Wissinger, M. Biel, K.U. Bartz-Schmidt, M.D. Fischer, Subretinal Injection for Gene Therapy Does Not Cause Clinically Significant Outer Nuclear Layer Thinning in Normal Primate Foveae, Investigative ophthalmology & visual science, 58 (2017) 4155-4160.
[172] B. Chiang, J.H. Jung, M.R. Prausnitz, The suprachoroidal space as a route of administration to the posterior segment of the eye, Advanced drug delivery reviews, 126 (2018) 58-66.
[173] Y.J. Choi, I.K. Oh, J.R. Oh, K. Huh, Intravitreal versus posterior subtenon injection of triamcinolone acetonide for diabetic macular edema, Korean journal of ophthalmology : KJO, 20 (2006) 205-209.
[174] S.G. Jacobson, G.M. Acland, G.D. Aguirre, T.S. Aleman, S.B. Schwartz, A.V. Cideciyan, C.J. Zeiss, A.M. Komaromy, S. Kaushal, A.J. Roman, E.A. Windsor, A. Sumaroka, S.E. Pearce-Kelling, T.J. Conlon, V.A. Chiodo, S.L. Boye, T.R. Flotte, A.M. Maguire, J. Bennett, W.W. Hauswirth, Safety of recombinant adeno-associated virus type 2-RPE65 vector delivered by ocular subretinal injection, Molecular therapy : the journal of the American Society of Gene Therapy, 13 (2006) 1074-1084.
[175] H. Nikkhah, S. Karimi, H. Ahmadieh, M. Azarmina, M. Abrishami, H. Ahoor, Y. Alizadeh, H. Behboudi, N. Daftarian, M.H. Dehghan, M. Entezari, F. Farrahi, H. Ghanbari, K.G. Falavarjani, M.A. Javadi, R. Karkhaneh, S. Moradian, M.R. Manaviat, M. Mehryar, R. Nourinia, M.M. Parvaresh, A. Ramezani, A.R. Haghi, M. Riazi-Esfahani, M. Soheilian, M. Shahsavari, H.A. Shahriari, Z. Rajavi, S. Safi, A. Shirvani, S. Rahmani, H. Sabbaghi, M. Pakbin, B. Kheiri, H. Ziaei, Intravitreal Injection of Anti-vascular Endothelial Growth Factor Agents for Ocular Vascular Diseases: Clinical Practice Guideline, Journal of ophthalmic & vision research, 13 (2018) 158-169.

[176] E. Himawan, P. Ekström, M. Buzgo, P. Gaillard, E. Stefánsson, V. Marigo, T. Loftsson, F. Paquet-Durand, Drug delivery to retinal photoreceptors, 24 (2019) 1637-1643.
[177] 2 - Modification of drug release, in: M.L. Bruschi (Ed.), Woodhead Publishing2015, pp. 15-28.
[178] S. Laurent, D. Forge, M. Port, A. Roch, C. Robic, L. Vander Elst, R.N. Muller, Magnetic iron oxide nanoparticles: synthesis, stabilization, vectorization, physicochemical characterizations, and biological applications, Chemical reviews, 108 (2008) 2064-2110.
[179] K. Ibrahim, S. Khalid, K. Idrees, Nanoparticles: Properties, applications and toxicities, Arabian Journal of Chemistry, 12 (2019) 908-931.
[180] W.K. Shin, J. Cho, A.G. Kannan, Y.S. Lee, D.W. Kim, Cross-linked Composite Gel Polymer Electrolyte using Mesoporous Methacrylate-Functionalized SiO2 Nanoparticles for Lithium-Ion Polymer Batteries, Sci Rep, 6 (2016) 26332.
[181] J.K. Patra, G. Das, L.F. Fraceto, E.V.R. Campos, M.D.P. Rodriguez-Torres, L.S. Acosta-Torres, L.A. Diaz-Torres, R. Grillo, M.K. Swamy, S. Sharma, S. Habtemariam, H.S. Shin, Nano based drug delivery systems: recent developments and future prospects, Journal of nanobiotechnology, 16 (2018) 71.
[182] M.G. Zariwala, H. Bendre, A. Markiv, S. Farnaud, D. Renshaw, K.M. Taylor, S. Somavarapu, Hydrophobically modified chitosan nanoliposomes for intestinal drug delivery, International journal of nanomedicine, 13 (2018) 5837-5848.
[183] M. Amiri, S. Jafari, M. Kurd, H. Mohamadpour, M. Khayati, F. Ghobadinezhad, O. Tavallaei, H. Derakhshankhah, S. Sadegh Malvajerd, Z. Izadi, Engineered Solid Lipid Nanoparticles and Nanostructured Lipid Carriers as New Generations of Blood-Brain Barrier Transmitters, ACS chemical neuroscience, (2021).
[184] M. Khalkhali, S. Mohammadinejad, F. Khoeini, K. Rostamizadeh, Vesicle-like structure of lipid-based nanoparticles as drug delivery system revealed by molecular dynamics simulations, 559 (2019) 173-181.
[185] C. Chen, X. Zhu, Y. Dou, J. Xu, J. Zhang, T. Fan, J. Du, K. Liu, Y. Deng, L. Zhao, Y. Huang, Exendin-4 Loaded Nanoparticles with a Lipid Shell and Aqueous Core Containing Micelles for Enhanced Intestinal Absorption, Journal of biomedical nanotechnology, 11 (2015) 865-876.
[186] Q. You, M. Sokolov, L. Grigartzik, W. Hintz, B.G.M. van Wachem, P. Henrich-Noack, B.A. Sabel, How Nanoparticle Physicochemical Parameters Affect Drug Delivery to Cells in the Retina via Systemic Interactions, Molecular pharmaceutics, 16 (2019) 5068-5075.
[187] R. Singh, S. Rajaraman, M. Balasubramanian, A Novel Nanoparticle Mediated Selective Inner Retinal Photocoagulation for Diseases of the Inner Retina, IEEE transactions on nanobioscience, 16 (2017) 542-554.
[188] T.L. Fink, P.J. Klepcyk, S.M. Oette, C.R. Gedeon, S.L. Hyatt, T.H. Kowalczyk, R.C. Moen, M.J. Cooper, Plasmid size up to 20 kbp does not limit effective in vivo lung gene transfer using compacted DNA nanoparticles, Gene therapy, 13 (2006) 1048-1051.
[189] H.A. Liu, Y.L. Liu, Z.Z. Ma, J.C. Wang, Q. Zhang, A lipid nanoparticle system improves siRNA efficacy in RPE cells and a laser-induced murine CNV model, Investigative ophthalmology & visual science, 52 (2011) 4789-4794.
[190] A. Koirala, R.S. Makkia, S.M. Conley, M.J. Cooper, M.I. Naash, S/MAR-containing DNA nanoparticles promote persistent RPE gene expression and improvement in RPE65-associated LCA, Human molecular genetics, 22 (2013) 1632-1642.
[191] E.M. Merisko-Liversidge, G.G. Liversidge, Drug nanoparticles: formulating poorly water-soluble compounds, Toxicologic pathology, 36 (2008) 43-48.
[192] S.J. Kang, C. Durairaj, U.B. Kompella, J.M. O'Brien, H.E. Grossniklaus, Subconjunctival nanoparticle carboplatin in the treatment of murine retinoblastoma, Archives of ophthalmology (Chicago, Ill. : 1960), 127 (2009) 1043-1047.

[193] F. Li, B. Hurley, Y. Liu, B. Leonard, M. Griffith, Controlled release of bevacizumab through nanospheres for extended treatment of age-related macular degeneration, The open ophthalmology journal, 6 (2012) 54-58.
[194] S.N. Leow, C.D. Luu, M.H. Hairul Nizam, P.L. Mok, R. Ruhaslizan, H.S. Wong, W.H. Wan Abdul Halim, M.H. Ng, B.H. Ruszymah, S.R. Chowdhury, M.L. Bastion, K.Y. Then, Safety and Efficacy of Human Wharton's Jelly-Derived Mesenchymal Stem Cells Therapy for Retinal Degeneration, PloS one, 10 (2015) e0128973.
[195] J. Cao, X. Shi, D.D. Gurav, L. Huang, H. Su, K. Li, J. Niu, M. Zhang, Q. Wang, M. Jiang, K. Qian, Metabolic Fingerprinting on Synthetic Alloys for Medulloblastoma Diagnosis and Radiotherapy Evaluation, Advanced Materials, 32 (2020) 2000906.
[196] R.H. Müller, M. Radtke, S.A. Wissing, Solid lipid nanoparticles (SLN) and nanostructured lipid carriers (NLC) in cosmetic and dermatological preparations, Advanced drug delivery reviews, 54 Suppl 1 (2002) S131-155.
[197] A.K. Kushwaha, P.R. Vuddanda, P. Karunanidhi, S.K. Singh, S. Singh, Development and evaluation of solid lipid nanoparticles of raloxifene hydrochloride for enhanced bioavailability, BioMed research international, 2013 (2013) 584549.
[198] S. Mukherjee, S. Ray, R.S. Thakur, Solid lipid nanoparticles: a modern formulation approach in drug delivery system, Indian journal of pharmaceutical sciences, 71 (2009) 349-358.
[199] K. Westesen, H. Bunjes, M.H.J. Koch, Physicochemical characterization of lipid nanoparticles and evaluation of their drug loading capacity and sustained release potential, 48 (1997) 223-236.
[200] J.S. Baek, C.W. Cho, Surface modification of solid lipid nanoparticles for oral delivery of curcumin: Improvement of bioavailability through enhanced cellular uptake, and lymphatic uptake, European journal of pharmaceutics and biopharmaceutics : official journal of Arbeitsgemeinschaft fur Pharmazeutische Verfahrenstechnik e.V, 117 (2017) 132-140.
[201] A. Seyfoddin, J. Shaw, R. Al-Kassas, Solid lipid nanoparticles for ocular drug delivery, Drug delivery, 17 (2010) 467-489.
[202] R. Cavalli, M.R. Gasco, P. Chetoni, S. Burgalassi, M.F. Saettone, Solid lipid nanoparticles (SLN) as ocular delivery system for tobramycin, International journal of pharmaceutics, 238 (2002) 241-245.
[203] P.S. Apaolaza, A. Del Pozo-Rodríguez, J. Torrecilla, A. Rodríguez-Gascón, J.M. Rodríguez, U. Friedrich, B.H. Weber, M.A. Solinís, Solid lipid nanoparticle-based vectors intended for the treatment of X-linked juvenile retinoschisis by gene therapy: In vivo approaches in Rs1h-deficient mouse model, Journal of controlled release : official journal of the Controlled Release Society, 217 (2015) 273-283.
[204] Z. Cheng, Y. Li, K. Wang, X. Zhu, P. Tharkar, W. Shu, T. Zhang, S. Zeng, L. Zhu, M. Murray, W. Chrzanowski, F. Zhou, Compritol solid lipid nanoparticle formulations enhance the protective effect of betulinic acid derivatives in human Müller cells against oxidative injury, Exp Eye Res, 215 (2021) 108906.
[205] A. del Pozo-Rodríguez, D. Delgado, M.A. Solinís, A.R. Gascón, J.L. Pedraz, Solid lipid nanoparticles for retinal gene therapy: transfection and intracellular trafficking in RPE cells, International journal of pharmaceutics, 360 (2008) 177-183.
[206] N.J. Kruger, The Bradford method for protein quantitation, Methods in molecular biology (Clifton, N.J.), 32 (1994) 9-15.
[207] A. Swaroop, D. Kim, D. Forrest, Transcriptional regulation of photoreceptor development and homeostasis in the mammalian retina, Nature reviews. Neuroscience, 11 (2010) 563-576.

[208] E. Cuevas, D.L. Holder, A.H. Alshehri, J. Tréguier, J. Lakowski, J.C. Sowden, NRL(-/-) gene edited human embryonic stem cells generate rod-deficient retinal organoids enriched in S-cone-like photoreceptors, Stem cells (Dayton, Ohio), 39 (2021) 414-428.
[209] E.C. Oh, N. Khan, E. Novelli, H. Khanna, E. Strettoi, A. Swaroop, Transformation of cone precursors to functional rod photoreceptors by bZIP transcription factor NRL, Proceedings of the National Academy of Sciences of the United States of America, 104 (2007) 1679-1684.
[210] H. Cheng, T.S. Aleman, A.V. Cideciyan, R. Khanna, S.G. Jacobson, A. Swaroop, In vivo function of the orphan nuclear receptor NR2E3 in establishing photoreceptor identity during mammalian retinal development, Human molecular genetics, 15 (2006) 2588-2602.
[211] Y. Taniguchi, H. Tonai-Kachi, K. Shinjo, Zaprinast, a well-known cyclic guanosine monophosphate-specific phosphodiesterase inhibitor, is an agonist for GPR35, FEBS letters, 580 (2006) 5003-5008.
[212] J.K. Wentworth, G. Pula, A.W. Poole, Vasodilator-stimulated phosphoprotein (VASP) is phosphorylated on Ser157 by protein kinase C-dependent and -independent mechanisms in thrombin-stimulated human platelets, The Biochemical journal, 393 (2006) 555-564.
[213] A. Smolenski, C. Bachmann, K. Reinhard, P. Hönig-Liedl, T. Jarchau, H. Hoschuetzky, U. Walter, Analysis and regulation of vasodilator-stimulated phosphoprotein serine 239 phosphorylation in vitro and in intact cells using a phosphospecific monoclonal antibody, J Biol Chem, 273 (1998) 20029-20035.
[214] H.J. Kim, H.S. Choi, J.H. Park, M.J. Kim, H.G. Lee, R.B. Petersen, Y.S. Kim, J.B. Park, E.K. Choi, Regulation of RhoA activity by the cellular prion protein, Cell death & disease, 8 (2017) e2668.
[215] M. Rolli-Derkinderen, V. Sauzeau, L. Boyer, E. Lemichez, C. Baron, D. Henrion, G. Loirand, P. Pacaud, Phosphorylation of serine 188 protects RhoA from ubiquitin/proteasome-mediated degradation in vascular smooth muscle cells, Circulation research, 96 (2005) 1152-1160.
[216] R.L. Kraus, S. Hering, M. Grabner, D. Ostler, J. Striessnig, Molecular Mechanism of Diltiazem Interaction with L-type Ca²⁺ Channels *, Journal of Biological Chemistry, 273 (1998) 27205-27212.
[217] S.B. Glantz, C.D. Cianci, R. Iyer, D. Pradhan, K.K.W. Wang, J.S. Morrow, Sequential Degradation of αII and βII Spectrin by Calpain in Glutamate or Maitotoxin-Stimulated Cells, Biochemistry, 46 (2007) 502-513.
[218] T. Wang, S.H. Tsang, J. Chen, Two pathways of rod photoreceptor cell death induced by elevated cGMP, Human molecular genetics, 26 (2017) 2299-2306.
[219] G. Wheway, L. Nazlamova, D. Turner, S. Cross, 661W Photoreceptor Cell Line as a Cell Model for Studying Retinal Ciliopathies, Frontiers in genetics, 10 (2019) 308.
[220] D.M. Gamm, L.K. Barthel, P.A. Raymond, M.D. Uhler, Localization of cGMP-dependent protein kinase isoforms in mouse eye, Investigative ophthalmology & visual science, 41 (2000) 2766-2773.
[221] Y. Wu, Q. Cai, W. Li, Z. Cai, Y. Liu, H. Li, J. Pang, Y. Chen, Active PKG II inhibited the growth and migration of ovarian cancer cells through blocking Raf/MEK and PI3K/Akt signaling pathways, Bioscience reports, 39 (2019).
[222] T.R. Tuttle, M.L. Mierzwa, S.I. Wells, S.R. Fox, N. Ben-Jonathan, The cyclic GMP/protein kinase G pathway as a therapeutic target in head and neck squamous cell carcinoma, Cancer letters, 370 (2016) 279-285.
[223] J. Hart, M.F. Wilkinson, M.E. Kelly, S. Barnes, Inhibitory action of diltiazem on voltage-gated calcium channels in cone photoreceptors, Exp Eye Res, 76 (2003) 597-604.

[224] A. Comitato, P. Subramanian, G. Turchiano, M. Montanari, S.P. Becerra, V. Marigo, Pigment epithelium-derived factor hinders photoreceptor cell death by reducing intracellular calcium in the degenerating retina, Cell death & disease, 9 (2018) 560.
[225] J. Kenealey, P. Subramanian, A. Comitato, J. Bullock, L. Keehan, F. Polato, D. Hoover, V. Marigo, S.P. Becerra, Small Retinoprotective Peptides Reveal a Receptor-binding Region on Pigment Epithelium-derived Factor, J Biol Chem, 290 (2015) 25241-25253.
[226] J. Zhao, J. Trewhella, J. Corbin, S. Francis, R. Mitchell, R. Brushia, D. Walsh, Progressive cyclic nucleotide-induced conformational changes in the cGMP-dependent protein kinase studied by small angle X-ray scattering in solution, J Biol Chem, 272 (1997) 31929-31936.
[227] J. Sancho-Pelluz, B. Arango-Gonzalez, S. Kustermann, F.J. Romero, T. van Veen, E. Zrenner, P. Ekström, F. Paquet-Durand, Photoreceptor cell death mechanisms in inherited retinal degeneration, Molecular neurobiology, 38 (2008) 253-269.
[228] A. Rajala, Y. Wang, R.S. Brush, K. Tsantilas, C.S.R. Jankowski, K.J. Lindsay, J.D. Linton, J.B. Hurley, R.E. Anderson, R.V.S. Rajala, Pyruvate kinase M2 regulates photoreceptor structure, function, and viability, Cell death & disease, 9 (2018) 240.
[229] A. Rajala, K. Soni, R.V.S. Rajala, Metabolic and Non-metabolic Roles of Pyruvate Kinase M2 Isoform in Diabetic Retinopathy, Sci Rep, 10 (2020) 7456.
[230] T.J. Wubben, M. Pawar, E. Weh, A. Smith, P. Sajjakulnukit, L. Zhang, L. Dai, H. Hager, M.P. Pai, C.A. Lyssiotis, C.G. Besirli, Small molecule activation of metabolic enzyme pyruvate kinase muscle isozyme 2, PKM2, circumvents photoreceptor apoptosis, Sci Rep, 10 (2020) 2990.
[231] P. Zhu, Q. Yang, G. Li, Q. Chang, PKM2 Is a Potential Diagnostic and Therapeutic Target for Retinitis Pigmentosa, Disease markers, 2021 (2021) 1602797.
[232] E. Zhang, J. Ryu, S.R. Levi, J.K. Oh, C.W. Hsu, X. Cui, T.T. Lee, N.K. Wang, J.R. Lima de Carvalho, S.H. Tsang, PKM2 ablation enhanced retinal function and survival in a preclinical model of retinitis pigmentosa, Mammalian genome : official journal of the International Mammalian Genome Society, 31 (2020) 77-85.
[233] X. Li, Y. Cheng, Z. Wang, J. Zhou, Y. Jia, X. He, L. Zhao, Y. Dong, Y. Fan, X. Yang, B. Shen, X. Wu, J. Wang, C. Xiong, L. Wei, X. Li, J. Wang, Calcium and TRPV4 promote metastasis by regulating cytoskeleton through the RhoA/ROCK1 pathway in endometrial cancer, Cell death & disease, 11 (2020) 1009.
[234] L. Che, J.Y. Song, Y. Lou, G.Y. Li, Analysis from the perspective of cilia: the protective effect of PARP inhibitors on visual function during light-induced damage, International ophthalmology, 40 (2020) 1017-1027.
[235] P.G. Hogan, L. Chen, J. Nardone, A. Rao, Transcriptional regulation by calcium, calcineurin, and NFAT, Genes & development, 17 (2003) 2205-2232.
[236] B. Fiedler, S.M. Lohmann, A. Smolenski, S. Linnemuller, B. Pieske, F. Schroder, J.D. Molkentin, H. Drexler, K.C. Wollert, Inhibition of calcineurin-NFAT hypertrophy signaling by cGMP-dependent protein kinase type I in cardiac myocytes, Proceedings of the National Academy of Sciences of the United States of America, 99 (2002) 11363-11368.
[237] L.V. Gonzalez Bosc, M.K. Wilkerson, K.N. Bradley, D.M. Eckman, D.C. Hill-Eubanks, M.T. Nelson, Intraluminal pressure is a stimulus for NFATc3 nuclear accumulation: role of calcium, endothelium-derived nitric oxide, and cGMP-dependent protein kinase, J Biol Chem, 279 (2004) 10702-10709.
[238] C.A. Bretz, S. Savage, M. Capozzi, J.S. Penn, The role of the NFAT signaling pathway in retinal neovascularization, Investigative ophthalmology & visual science, 54 (2013) 7020-7027.
[239] A.V. Zetterqvist, F. Blanco, J. Öhman, O. Kotova, L.M. Berglund, S. de Frutos Garcia, R. Al-Naemi, M. Wigren, P.G. McGuire, L.V. Gonzalez Bosc, M.F. Gomez, Nuclear factor of

activated T cells is activated in the endothelium of retinal microvessels in diabetic mice, 2015 (2015) 428473-428473.
[240] G. Yu, D.C. Hess, C.V. Borlongan, Combined cyclosporine-A and methylprednisolone treatment exerts partial and transient neuroprotection against ischemic stroke, Brain research, 1018 (2004) 32-37.
[241] A.F. Schinder, E.C. Olson, N.C. Spitzer, M. Montal, Mitochondrial dysfunction is a primary event in glutamate neurotoxicity, The Journal of neuroscience : the official journal of the Society for Neuroscience, 16 (1996) 6125-6133.
[242] F. Ruiz, G. Alvarez, M. Ramos, M. Hernández, E. Bogónez, J. Satrústegui, Cyclosporin A targets involved in protection against glutamate excitotoxicity, European journal of pharmacology, 404 (2000) 29-39.
[243] S.Y. Kim, M.S. Shim, K.Y. Kim, R.N. Weinreb, L.A. Wheeler, W.K. Ju, Inhibition of cyclophilin D by cyclosporin A promotes retinal ganglion cell survival by preventing mitochondrial alteration in ischemic injury, Cell death & disease, 5 (2014) e1105.
[244] N. Yoshida, Y. Ikeda, S. Notomi, K. Ishikawa, Y. Murakami, T. Hisatomi, H. Enaida, T. Ishibashi, Clinical evidence of sustained chronic inflammatory reaction in retinitis pigmentosa, Ophthalmology, 120 (2013) 100-105.
[245] M. Campbell, S.L. Doyle, E. Ozaki, P.F. Kenna, A.S. Kiang, M.M. Humphries, P. Humphries, An overview of the involvement of interleukin-18 in degenerative retinopathies, Advances in experimental medicine and biology, 801 (2014) 409-415.
[246] Q. Xu, N.J. Boylan, J.S. Suk, Y.Y. Wang, E.A. Nance, J.C. Yang, P.J. McDonnell, R.A. Cone, E.J. Duh, J. Hanes, Nanoparticle diffusion in, and microrheology of, the bovine vitreous ex vivo, Journal of controlled release : official journal of the Controlled Release Society, 167 (2013) 76-84.
[247] S. Tavakoli, O.K. Kari, T. Turunen, T. Lajunen, M. Schmitt, J. Lehtinen, F. Tasaka, P. Parkkila, J. Ndika, T. Viitala, H. Alenius, A. Urtti, A. Subrizi, Diffusion and Protein Corona Formation of Lipid-Based Nanoparticles in the Vitreous Humor: Profiling and Pharmacokinetic Considerations, Molecular pharmaceutics, 18 (2021) 699-713.
[248] R. Yang, R.C. Gao, C.F. Cai, H. Xu, F. Li, H.B. He, X. Tang, Preparation of gel-core-solid lipid nanoparticle: a novel way to improve the encapsulation of protein and peptide, Chemical & pharmaceutical bulletin, 58 (2010) 1195-1202.
[249] P. Foroozandeh, A.A. Aziz, Insight into Cellular Uptake and Intracellular Trafficking of Nanoparticles, Nanoscale research letters, 13 (2018) 339.
[250] B. Kong, J.H. Seog, L.M. Graham, S.B. Lee, Experimental considerations on the cytotoxicity of nanoparticles, Nanomedicine (London, England), 6 (2011) 929-941.
[251] C. He, Y. Hu, L. Yin, C. Tang, C. Yin, Effects of particle size and surface charge on cellular uptake and biodistribution of polymeric nanoparticles, Biomaterials, 31 (2010) 3657-3666.
[252] S. Kumari, S. Mg, S. Mayor, Endocytosis unplugged: multiple ways to enter the cell, Cell research, 20 (2010) 256-275.
[253] S. Behzadi, V. Serpooshan, W. Tao, M.A. Hamaly, M.Y. Alkawareek, E.C. Dreaden, D. Brown, A.M. Alkilany, O.C. Farokhzad, M. Mahmoudi, Cellular uptake of nanoparticles: journey inside the cell, Chemical Society reviews, 46 (2017) 4218-4244.
[254] C. Palocci, A. Valletta, L. Chronopoulou, L. Donati, M. Bramosanti, E. Brasili, B. Baldan, G. Pasqua, Endocytic pathways involved in PLGA nanoparticle uptake by grapevine cells and role of cell wall and membrane in size selection, Plant cell reports, 36 (2017) 1917-1928.
[255] S. Belhadj, A. Tolone, G. Christensen, S. Das, Y. Chen, F. Paquet-Durand, Long-Term, Serum-Free Cultivation of Organotypic Mouse Retina Explants with Intact Retinal Pigment Epithelium, Journal of visualized experiments : JoVE, (2020).